Monitoring Oxidation Reactions by Photochemical Techniques

by

Hamdy Saad Sadek El–Sheshtawy

A thesis submitted in partial fulfillment
for the degree of Doctor of Philosophy
in

Chemistry

Approved Thesis Committee:

Prof. Dr. Werner M. Nau
Jacobs University Bremen, Bremen

Prof. Dr. Nikolai Kuhnert
Jacobs University Bremen, Bremen

Dr. Aurica Farcas
"Petru Poni" Institute of Macromolecular Chemistry, Romania

Date of defense: November 7, 2011

School of Engineering and Science

Declaration of Authorship

I, Hamdy El–Sheshtawy, declare that this thesis entitled, “ Monitoring Oxidation Reactions by Photochemical Techniques" and the work presented in it are my own. I confirm that:

- This work was done wholly or mainly while in candidature for a doctoral degree in chemistry at Jacobs University.

- Where I have consulted the published work of others, this is always clearly attributed.

- Where I have quoted from the work of others, the source is always given with the exception of such quotations; this thesis is entirely my own work.

- I have acknowledged all main sources of help.

- Where the thesis is based on work done by myself jointly with others, I have made clear exactly what was done by others and what I have contributed myself.

Signed:

Date:

Yesterday we obeyed kings and bent our necks before emperors. But today we kneel only to truth, follow only beauty, and obey only love.
Khalil Gibran

To my Parents

JACOBS UNIVERSITY

Abstract

PhD Thesis

by Hamdy Saad El–Sheshtawy

This doctoral thesis is devoted to monitor oxidation processes by photochemical techniques. Oxidation reactions play a crucial role in both environmental and biological systems. Therefore, my thesis started with the study of oxygen scavenging of aryl-substituted benzyl radicals. In this part of my work, a combination of experimental techniques (laser-flash photolysis) and theoretical calculations (DFT) was used to elucidate the mechanism of an elementary step in an oxidation process. The effect of substituents on the scavenging rate constants was studied in detail. Solvent effects on the reaction progress, as well as temperature effects were investigated. For the first time, a negative activation energy was observed: the scavenging rate constants of aryl–benzyl radicals in acetonitrile decreased at higher temperature.

In the second part of my thesis, the effect of the solvent on H atom abstractions from C–H donors by oxygen-centered radicals (the cumoxyl radical) and n–π^* excited molecules (2,3-diazabicyclo[2.2.2]oct–2–ene) was investigated. For this, theoretical calculations and experimental results were again combined to rationalize the solvent effects on the H atom abstraction from several C–H donors by the oxygen–centered radicals. The results are compared to those previously reported in the literature for H atom abstraction from O–H donors.

In the last part, I developed a fluorescence-based supramolecular tandem assay to monitor a biologically important oxidation process, namely an enzymatic oxidation. When searching for a macrocyclic receptor (required for tandem assays) for the substrate of peroxidases, namely iodide, I found a novel interaction (halogen bonding) in

supramolecular host–guest complexes associated with cucurbit[*n*]urils (CBs), which is based on the encapsulation of molecular iodine (I_2) inside the nanocavity of CB6. Halogen bonds have been found to play a crucial role in the complex stability in the case of CB6•I_2, while for the CB7•I_2 association complex the hydrophobic effect is dominant. Based on the encapsulation of I_2 into the CB7 cavity, we developed a supramolecular tandem assay for monitoring the activity of peroxidases, namely myeloperoxidase (MPO), lactoperoxidase (LPO), and horseradish peroxidase (HRP). This assay has the advantage of using a small inorganic substrate (I^-), in contrast to the previously employed organic compounds. In addition, the supramolecular tandem assay requires only μM concentrations of the substrate (I^-), such that it overcomes the use of high substrate concentration (needed for other methods), which is known to adversely affect (inhibit) peroxidase activity.

Acknowledgments

I would like to thankfully acknowledge the enormous support, encouragement and guidance of my supervisor, Prof. Dr. Werner M. Nau, who provided me with a diverse playground of projects to develop upon.

I want to thank Prof. Dr. Nikolai Kuhnert and Dr. Aurica Farcas for being kind enough to be committee members for my PhD thesis.

I would also like to thank all members of the Nau research group for providing a stimulating environment, both socially as well as professionally. In particular, I thank Dr. Apurba L. Koner, Indrajit Ghosh for their fruitful discussions regards the wide variety of subjects and instruments in the laboratory.

Special thanks go to Dr. Bassem Bassil for solving extremely complex supramolecular structures and being patient until good results were obtained. I want to also thank Dr. Vanya Uzunova for the ITC measurements, and Dr. Patrice Donfack for Raman spectroscopy measurements.

Also I would like to extend my deepest thankful to Dr. Xiangyang Zhang for the preparation of the substituted dibenzylketones, which have been used during this study.

I acknowledge the kind and generous financial support of the Egyptian Government, DFG, and NanoFun center at Jacobs University.

Finally, to my wife, and our children Ahmed and Ayah, all I can say that I want to express my deep love for you. Your patience, love and encouragement have upheld me, particularly in those many days in which I spent more time with my lab than with you.

Contents

List of Figures:

List of Tables:

Chapter 1

Introduction

Chapter 1

1 Introduction

1.1 Scope of the Thesis and Overview

This thesis is devoted to the study of oxidation reactions in both environmental and biological systems. Oxidation reactions, being one of the most fundamental processes in chemistry, have attracted much interest. They played an important role in the early development on earth, around 2.2 billion years ago, when O_2 appeared in the atmosphere.[1, 2] One of the most important benefits from the presence of oxygen in the atmosphere is the formation of the oxidation product ozone (O_3) in the stratosphere (20–30 km), which protects the earth from harmful UV–C radiation.[3] In the stratosphere region, the high energy of ultraviolet radiation breaks down oxygen molecules (O_2) into oxygen atoms (O), which then react with oxygen molecules to form ozone. Whereas, in the troposphere, ozone formation proceeds through a series of free radical reactions involving volatile organic compounds and oxides of nitrogen (NO_x).[4, 5] The second important aspect is the oxidation of the toxic ferrous ions (Fe^{2+}) in rocks and rivers to the less toxic and insoluble ferric ions (Fe^{3+}), which consume the excess hydroxyl radical ($OH^{\bullet}$) in what we currently know as the Fenton reaction (1876).[6] However, the oxidation process is not beneficial for human beings all the time. The formation of free radicals within cells is responsible for protein and lipids oxidation, and the oxidized forms of proteins and lipids play a major role in aging, oxidative stress, and several pathological conditions.[7, 8]

Therefore, the study of oxidation reactions and their pathways in both the environment and biological systems are of considerable importance, in particular, the development of reliable, economically inexpensive, and sensitive techniques for monitoring oxidation processes and the formation of free radicals. The importance of free radicals as a reactive intermediate species in both environmental and biological systems has intrigued many researchers over the years.[9, 10]

Free radicals play an important role in both environmental and biological systems, mainly due to their high reactivity. They are highly reactive species due to the presence of unpaired electrons, generally centered on an atom. Radicals are most commonly formed by homolytic bond–scission, hydrogen abstraction by other radicals, addition of a radical to an unsaturated molecule, unimolecular decomposition, and electron transfer.[11] In combustion reactions, the unimolecular homolytic bond scission is initiated thermally by providing sufficient heat energy for bond cleavage, whereas in the atmosphere, free radicals are formed as the result of photolytic processes in which high–energy light from the sun is used to break the chemical bonds. However, in biological systems, radicals are frequently formed by electron transfer processes.[12, 13] Due to the presence of a single unpaired electron, radicals are highly reactive and, therefore, short lived. For example, radicals have a high tendency for self–termination through diffusion-controlled processes to form dimers.[14-16]

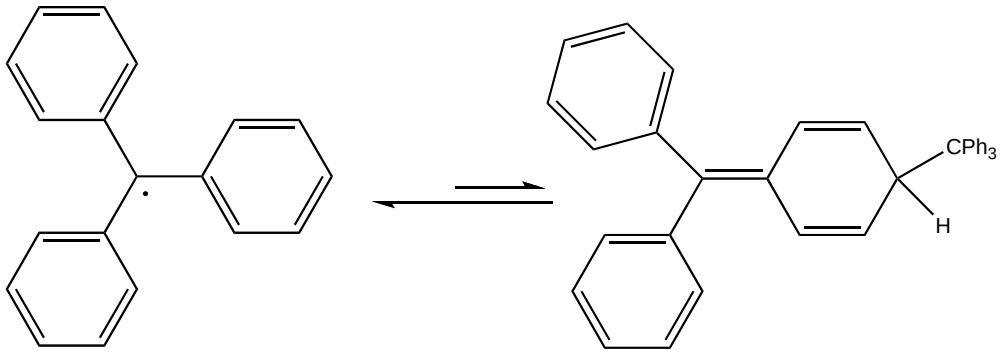

Trityl radical

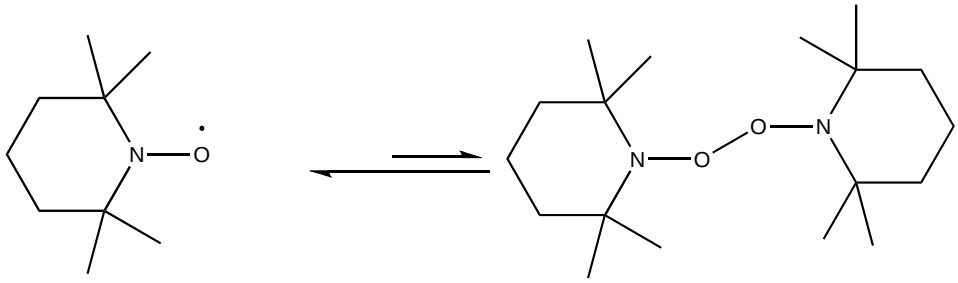

TEMPO

Scheme 1.1: Persistent radicals in equilibrium with their dimers.

However, examples of stable radicals are also known in the literature.[17] The triphenylmethyl radical (trityl radical) can exist in solution in an equilibrium with its

dimer (Scheme 1), which can be observed by the presence of a yellow color at room temperature that disappears in the presence of oxygen.[18] The stability of the triphenylmethyl radical is assigned to the strain in the dimer and the delocalization of the unpaired electron in the radical. Nitroxyl radicals, for example 2,2,6,6-tetramethylpiperidine-N-oxyl (TEMPO), one of the famous persistent radicals, exist in equilibrium because of the weak O–O bond in the dimer (Scheme 1.1).[19, 20] On the other hand, free radicals with short lifetimes, such as the benzyl radical, are well known in the literature and can undergo many follow–up reactions to form stable products.[21, 22]

Although there are much data concerning the initiation, monitoring, and elucidation of different photochemical oxidation processes, some open questions are still in need of investigation. For example, the nature of the intermediates (transition state) during the oxidation process of fuel additives (aromatic hydrocarbons) and the effect of the temperature on the reaction pathway, especially at lower atmospheric conditions, needs more detailed investigation. Therefore, the second chapter in my thesis is concerned with the study of the oxidation of aryl–substituted benzyl radicals as a model for the intermediate radicals in combustion and atmospheric chemistry. Theoretical calculations corroborate the nature of the transition state that helps in drawing a proper mechanism and to understand the questionable effect of solvent and temperature.

Continuing the same line of research, Chapter 3 is dedicated to the study of solvent effects on the H atom abstraction from C–H donors by oxygen centered radicals and n–π^* excited–state molecules, namely the cumoxyl radical and 2,3-diazabicyclo[2.2.2]oct–2–ene (DBO), respectively. For this, theoretical calculations and experimental results are used to rationalize the solvent effects on the H–atom abstraction from several C–H donors by the oxygen–centered radicals in comparison to those observed for O–H donors.

The last chapter in my thesis introduces the possibility to use supramolecular tandem assays, recently developed in our group,[23] to monitor the oxidation of inorganic ions (iodide) by peroxidase enzymes, namely myeloperoxidase (MPO), lactoperoxidase (LPO), and horseradish peroxidase (HRP). The study started with the discovery of the encapsulation of molecular iodine (I_2) inside the macrocyclic hosts cucurbit[*n*]urils (n = 6 and 7), which shows a remarkable change in the photophysical properties of I_2 upon encapsulation. Subsequently, based on the I_2 encapsulation by

CB7, we introduced the possibility to use a simple and small inorganic analyte (I^-) to monitor the activity of peroxidases. Moreover, the study has been extended to elucidate the inhibition of peroxidase by melatonin.

1.2 Environmental Oxidation Reactions

1.2.1 Oxidation Reactions in Combustion Chemistry

Combustion, one of the oldest phenomena discovered by the early human, is commonly known as burning process. Antoine Laurent Lavoisier (1743-1794) was the first to give a proper mechanism for the combustion reactions after the discovery of molecular oxygen by Karl Wilhelm Scheele (1742-1786) and Joseph Priestley (1733–1804). Lavoisier defined combustion as the process by which a material combines with oxygen and heat is produced. The released heat can be used for cooking food, house heating, and, most interestingly, in the steam engine. Denis Papin and Thomas Savery used the idea of using combustion reactions to produce work, first reported by Hero of Alexandria (10-70 AD), to drive a steam engine. The first steam engines employed the combustion of materials; usually coal, to produce heat that was used to boil water. The steam that was produced was then able to move pistons and drive machinery. However, the discovery of new types of fuels (gasoline) and a new type of engine (the internal combustion engine) led to a revolution in modern transportation.

Nowadays, most of the modern engines use hydrocarbons from gasoline, kerosene, and diesel during the combustion process. Aromatic species form a significant percentage of commercial gasoline as well as other fuels used in diesel and aircraft engines to increase the octane rating number.[24, 25] The beneficial components in these fuels consist of aromatics and alkyl–substituted aromatics such as benzene, toluene, as well as, methyl *tert*–butyl ether (MTBE), ethyl *tert*–butyl ether (ETBE), isooctane, and in early times tetraethyl lead. The transformation of alkyl hydrocarbons during the oxidation processes results in toxic species, which have harmful effects on both environment and human health, for example, benzene, toluene, and xylenes are well known for their roles in causing neurological diseases or cancer.[26] In addition, aromatic hydrocarbons are reported to be precursors for polycyclic aromatic

hydrocarbons (PAHs),[27] which are well known for their mutagenic, carcinogenic, and tetratogenic effects.[28]

Aromatic compounds constitute 10–40 % of gasoline and 5–30 % of diesel. This ratio reveals the importance of such species as fuel additives in order to reduce the undesirable autoignition events as engine knock, thereby increasing the fuel octane rating. Therefore, aromatic oxidation decomposition pathways have implications in combustion chemistry in order to improve the ignition process and to maximize the released power and minimize volatile organic compounds (VOC). Being one of the most important fuel additives, toluene has attracted much attention; therefore, it will be used as a model in the following sections.

At the high temperatures found under combustion conditions, toluene oxidation proceeds by H atom abstraction.[29, 30] There are two pathways for the radical initiation in toluene oxidation, the first channel is the abstraction of a H atom from the toluene phenyl ring, and secondly, the abstraction of a H atom from the methyl group mounted on the phenyl ring; however the dissociation energy of the C–H bond of the phenyl group (112.9 kcal mol)[31] is much higher than the corresponding dissociation energy of the methyl C–H bond (89.8 kcal mol^{-1}).[31] Therefore, the emphasis of the toluene oxidation has been placed on the stabilized benzyl radical and not the methylphenyl radical. It should be noted that, although the benzyl radical formation is dominant in toluene oxidation, the methylphenyl radical is still formed during the combustion reaction even at low temperatures.[32]

The decomposition of toluene is an important initiation step in the oxidation of toluene at moderate to high temperatures (>1200 K).[33, 34] the decomposition occurs either by fission of C–H bonds in the methyl group (Equation 1) or by cleavage of the C–C bond, which connects the methyl and the phenyl groups (Equation 2).

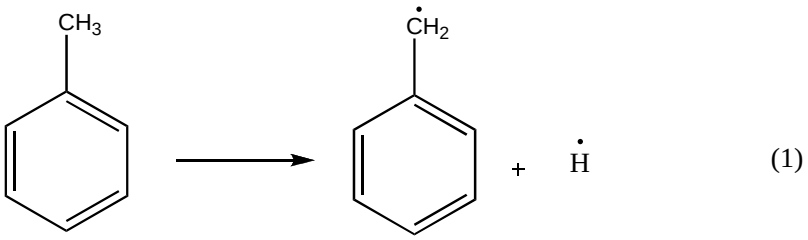

(1)

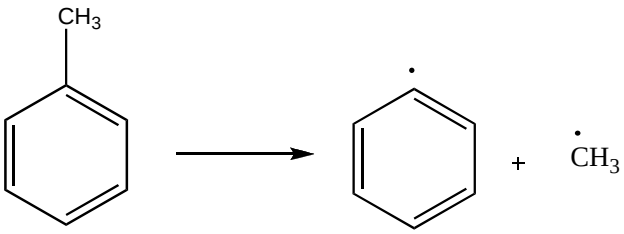

(2)

In addition, high temperature toluene oxidation has been shown to be sensitive to the reaction with molecular oxygen, where oxygen abstracts an H atom from the methyl group and a benzyl radical is formed (equation 3).[29, 30, 35]

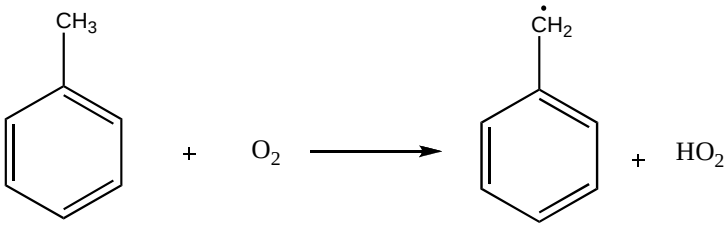

(3)

1.2.2 Oxidation Reactions in Atmospheric Chemistry

Large amounts of small volatile hydrocarbon molecules in the atmosphere are released by anthropogenic and biogenic sources.[36, 37] In particular, aromatic hydrocarbons (AHCs) are considered an important set of volatile organic compounds, as they account for 20 – 40% of the total non-methane hydrocarbons (NMHC).[38, 39] The average distribution of AHCs in urban air is benzene (21%), toluene (36%), ethylbenzene (9%), *m*/*p*-xylene (15%), *o*-xylene (7%), 4-ethyltoluene (4%), 1,2,4-trimethylbenzene (6%), and 1,3,5- trimethylbenzene (2%).[40] The fate of emitted hydrocarbons depends largely on their reactivity with reactive radicals such as $OH^{\bullet}$. The oxidation products are the main constituents of volatile gases and organic pollution such as ozone, aldehydes, epoxides, and peroxyacetyl nitrate. They are the main sources of photochemical smog in urban areas.[37, 41]

The oxidation process is initiated by free radical formation, alkyl radicals are formed from the direct reaction of the parent alkane with hydroxyl or NO_3 radicals, for example (Equations 4 and 5).[42]

$$OH^{\bullet} + RH \longrightarrow R^{\bullet} + H_2O \quad (4)$$

$$NO_3^{\bullet} + RH \longrightarrow R^{\bullet} + HNO_3 \quad (5)$$

Unsaturated hydrocarbons are generally degraded by the addition of OH and NO_3 radicals to the C=C double bond (Equations 6 and 7).

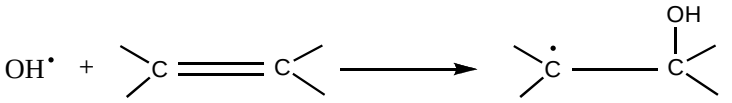

(6)

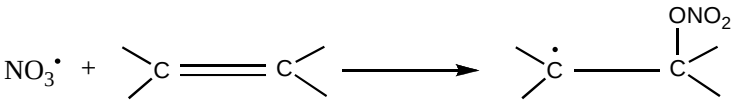

(7)

The first step of the troposphere degradation of aromatic hydrocarbons is the reaction with •OH radicals. The reaction of •OH radicals with toluene mainly proceeds by reversible addition, leading to hydroxycyclohexadienyl radical formation at normal atmospheric temperatures, whereas at high temperature ($T \geq 400$ K), the abstraction of an H atom from the methyl group to form a benzyl radical is the main determining factor (Scheme 1.2).[43-45]

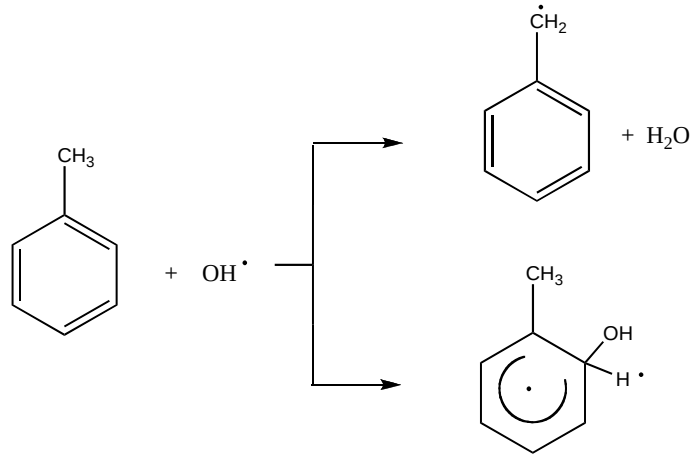

Scheme 1.2: Schematic representation of toluene oxidation mechanisms.

1.2.3 The Benzyl Radical as a Model for Combustion and Atmospheric Radical Reactions

The benzyl radical ($C_6H_5CH_2$•), the prototype for an aromatic molecular radical, plays an important role in both combustion and atmospheric chemistry because of its involvement as an intermediate during toluene and other aromatic radical reactions.[46] Additionally, the benzyl radical has been reported as a powerful stimulant for the spontaneous ignition of diesel fuel.[46, 47] Therefore, much work has been done focusing on the electronic structures, the radical stability, and characterization of this radical. The starting point was in 1955, after the development of the flash photolysis technique, when G. Porter studied the formation of benzyl radicals, which give a weak absorption band in the visible region and a strong band in the near–ultraviolet.[48]

Due to the resonance effect, the benzyl radical is considered more stable than other radicals, for example, than the methyl, ethyl, and phenyl radicals.[49] At low temperatures, the benzyl radical tends to terminate by self–combination forming a stable dibenzyl product,[50] whereas at higher temperature the benzyl radical decomposes by losing an additional H atom and a C_7H_6 fragment is observed.[51, 52] The termination process of the benzyl radical to dibenzyl has been reported to occur very fast, with a rate constant close to the diffusion limit.[15, 50]

Time–resolved fluorescence spectroscopy measurements of benzyl, monomethylbenzyl and dimethylbenzyl radicals were performed at low temperature, and the fluorescence lifetime of these radicals was observed to be very long (10^{-7} – 10^{-6} s), which can be attributed to the methyl substitutents.[53] Researchers have been interested to study the substituents effect of various groups to stabilize radicals. In 1937, Louis P. Hammett introduced for the first time the substituent constant (σ). This substituent constant correlates the effects of *para* and *meta* substituents of benzene rings on the reaction rate, as well as on the equilibrium constant. Subsequently, a number of scales specific for radical reactions have been developed. For example, based on the electron spin resonance spectra of *para* and *meta* substituted benzyl radicals, Dust and Arnold[54] developed a substituent constant (σ_α•) for radical reactions from the benzylic α–hydrogen hyperfine coupling constant. The σ_α• constant reflects the component of energy that may be attributed to spin delocalization in substituted benzyl radicals in comparison to the unsubstituted radicals according to

equation 8.

$$\sigma_{\alpha}\bullet = 1 - \text{hfc } \alpha\text{–}H_x / \text{ hfc } \alpha\text{–}H_0 \qquad (8)$$

They concluded that *para* substituents are radical stabilizing groups, except for fluorine, whereas *meta* substituents act as destabilizing groups for the benzyl radical.[54] Fisher *et al*.[55] studied the effect of *meta* substituents (Me, H, Br, NO_2, and CN) on the bromination rates of *m*–cyanotoluenes. Among the *meta* substituents, Br, NO_2, and CN were found to destabilize the intermediate benzyl radical system, while the methyl substituent had a stabilizing effect. Adam *et. al*.[56] introduced a *ΔD* scale ($\Delta D = D_H - D_X$, where *D* is a measure of spin–spin separation), which is based on the effects of substituents (*meta* and *para*) in monosubstituted benzyl–type triplet di-radicals **1** and symmetrically disubstituted triplet diradicals **2** on the spin delocalization at the radical site (Figure 1.1).

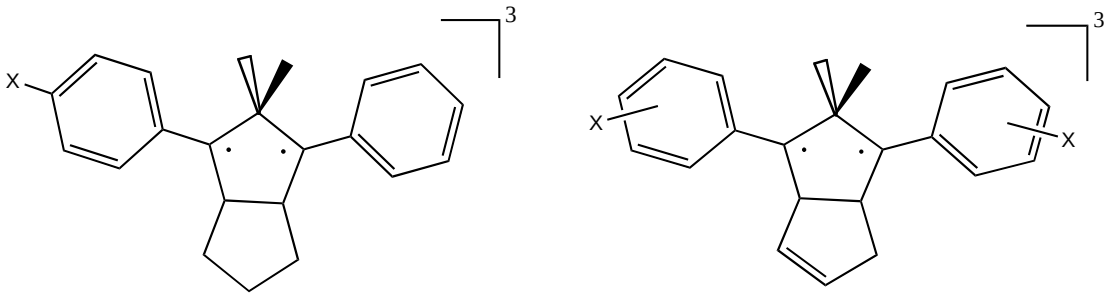

1 **2**

Figure 1.1: Mono–and–di substituted benzyl–type triplet diradicals used for the Δ*D* scale.

Positive values were found for spin–accepting substituents (*p*–CF_3, *p*–CN, *p*–NO_2, and *p*–NH_2), while negative values were observed for spin donating substituents (*p*–F, *p*–OCOMe, and *p*–OH). All *meta* substituents were found to give negative values. A good correlation between the *ΔD* scale and the hyperfine coupling constants, as a measure of the α spin densities, and the radical–stabilizing energy of cumyl radicals was obtained.

From the previous discussion, the benzyl radical and its derivatives are produced as a reactive intermediate in both combustion and atmospheric chemistry. Therefore, monitoring the radical scavenging by molecular oxygen is an important

task, which helps to formulate proper mechanisms for oxidation processes. Hence, Chapter II in this thesis is concerned with the study of the scavenging rate constants for aryl-substituted benzyl radicals by molecular oxygen. The effects of temperature and solvent effect are also discussed in detail.

1.3 Oxidation Reactions in Biological Systems

1.3.1 An Overview

All aerobic organisms need oxygen to produce energy in mitochondria. The prerequisite for O_2 obscures the fact that it is a toxic gas and that aerobes survive only because they have adapted by developing antioxidant defenses.[57, 58] Unlike most of the elements, molecular oxygen is found in the triplet ground state. This has led to the presence of a kinetic energy barrier for the oxidation of biological molecules, which are normally present in the ground state. Therefore, in living organisms, enzymes that decrease the activation barrier between molecular oxygen and the substrate are in high demand. This process occurs by taking advantage of free radical formation in bond activation or molecular rearrangement.

Hydrogen peroxide (H_2O_2) and the superoxide anion radical ($O_2^{\bullet -}$) are considered important intermediates during the triplet oxygen reduction to water in biological systems. These reactive intermediates are known to cause severe damage to tissue and DNA, but they can be efficiently removed by several enzymes such as superoxide dismutase,[59] catalase,[60] and peroxidases.[61, 62] In my Ph.D thesis, I have studied peroxidase–mediated oxidation reactions for halides. Therefore, the discussion will be restricted to peroxidases.

Peroxidases, ubiquitously found in plants, microorganisms, and animals, play a key role in enzymatic detoxification of reactive oxygen species (ROS) in living organisms. They are divided into two main classes, superfamily I, which is comprised of most types of plant (e.g., horseradish peroxidase, HRP), fungal, and bacterial enzymes that have the same helical fold but differ in their three–dimensional structure.[63, 64] Superfamily II mammalian peroxidases are comprised of thyroid peroxidase (TPO), myeloperoxidase (MPO), and lactoperoxidase (LPO). The prosthetic heme group in heme peroxidases, unlike plant and fungal enzymes, is

covalently linked to the protein.[65] This linkage is responsible for the high stability of the heme core and for the peculiar values of redox potentials that account for the ability of theses enzymes to oxidize inorganic ions such as SCN^-, Br^-, I^-, and Cl^-.[66, 67] Heme peroxidases catalyze two general types of reactions; the first is the one–electron abstraction reaction from a substrate to yield a radical product. This reaction is responsible for the oxidation of most organic substrates, for example, the conversion of guaiacol to the guaiacol radical.[68, 69] The second reaction is the two–electron oxidation reaction, which is mainly based on the conversion of halides (X^-) to hypohalides (HOX).[70] The oxidation process by heme peroxidases, especially in the one–electron oxidation, occurs through formation of a reactive intermediate the so–called "Compound **I**".

1.3.2 Mechanism of Compound I Formation in Heme Peroxidases

Inorganic substrates such as SCN^-, Br^-, Cl^-, and I^- are oxidized through the formation of the reactive intermediate Compound **I**.[69, 71] The initial step in this process starts by the reaction of the enzyme with hydrogen peroxide to form Compound **I**, the oxidant of halide ions.[72] Compound **I** formation starts by the binding of hydrogen peroxide (an essential co–factor) to the ferric atom with the concurrent donation of a proton to the histidine residue from the α oxygen atom (i.e., the oxygen atom bound to the heme iron) (Scheme 1.3).[73] The positively charged ganidinum side chain of arginine stabilizes the negative charge on the β oxygen atom (i.e., the oxygen atom not bound to the heme iron). The transfer of a proton from histidine to the β oxygen atom results in the heterolytic cleavage of the O–O bond and the formation of H_2O and Compound **I**. The formed intermediate, Compound **I**, has two electrons less than the native enzyme, one electron from the oxidation of Fe(III) in the native enzyme to the Fe(IV) to give the oxy–ferryl (Fe^{IV}=O) intermediate, and the second from a porphyrin (Por) to give the porphyrin π–cation radical.

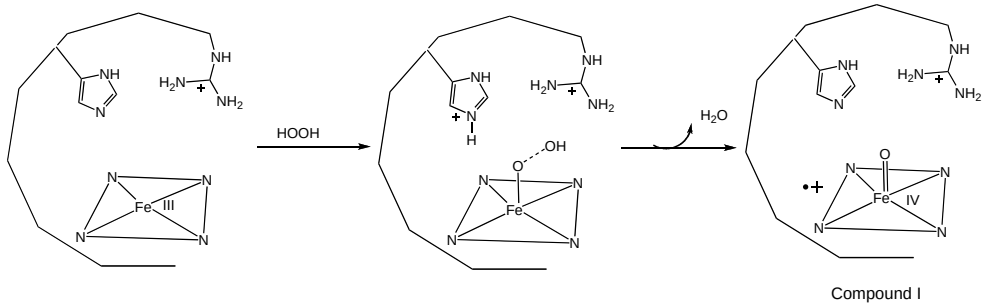

Scheme 1.3: Schematic presentation of Compound **I** formation. The radical cation is delocalized over the porphyrin (not shown).

The overall oxidation–reduction reaction for Compound **I** formation is given by Equation 9:[74]

$$PorFe^{III} + H_2O_2 \longrightarrow {}^{\bullet+}PorFe^{IV}{=}O + H_2O \qquad (9)$$

In this redox reaction, the reduction of hydrogen peroxide to water is coupled with the oxidation of the ferric ion.[75] The absorption spectrum of Compound **I** is different from the native enzyme. For example, MPO gives a collection of peaks at 430, 570, 620, 690 nm with two shoulders at 370 and 496 nm while MPO Compound **I** shows the same soret band at 430 nm with a 50% lower extinction coefficient (ε) and shifted peaks at 572 and 625 nm.[66, 76] For Compound **I** formation, peroxidases need different H_2O_2 concentrations. An equimolar concentration of H_2O_2 is needed for the formation of Compound **I** in LPO,[77, 78] HRP, and TPO,[78] whereas MPO needs a 10–fold excess of H_2O_2 to produce Compound **I**.[76] This has been attributed to the catalytic activity of MPO, in other words, MPO Compound **I** has the ability to convert H_2O_2 to molecular oxygen (O_2),[79, 80] such that high H_2O_2 concentrations are needed.

1.3.3 Halide Oxidation by Heme Peroxidases

Halide oxidation by peroxidases through formation of Compound **I** plays a vital role in the biosynthesis of thyroid hormones[81, 82] as well as in the immune defense system[83] through the formation of the iodonium ion (I^+) and hypohalous acids (XOH), respectively. The key step in this process, as we pointed out (see

above), is the formation of Compound **I**, which has two electrons less than the native enzyme. Compound **I** oxidizes halide ions by a single two–electron oxidation step, (i.e., $2I^- \rightarrow I_2 + 2e^-$) in contrast to the two one–electron oxidation reaction of organic substrates.[84] The iodide ion (I^-) has been extensively studied as a model for the oxidation of halides by peroxidase. In this thesis, the iodide ion will be used as a representative for halide ions.

The process starts by the reaction of the native enzyme (E) with hydrogen peroxide (H_2O_2) to form Compound **I** (EO).[69] In the presence of iodide, the hypoiodous complex is formed (equations 10–12).[69] This complex subsequently reacts with excess iodide to yield molecular iodine. In the presence of high concentrations of iodide, triiodide (I_3^-) is formed, which is the basis for monitoring the enzyme activity spectrophotometrically by using the triiodide band at 353 nm.[85-87]

$$E + H_2O_2 \longrightarrow EO \xrightarrow{I^-} [EOI]^- \longrightarrow E + IO^- \qquad (10)$$

$$IO^- + I^- + H^+ \longrightarrow I_2 + OH^- \qquad (11)$$

$$I_2 + I^- \longrightarrow I_3^- \qquad (12)$$

However, spectrophotometric methods need a high concentration of the substrate (I^-) in order to form a stable product (I_3^-), but high concentrations of the substrate inhibit the activity of peroxidases.[88, 89] The assay which I have developed herein (Chapter 4) requires much lower iodide concentrations.

1.3.4 Defense Mechanisms Based on Halogen Oxidation

Living organisms respond to the attack of pathogens by the production of reactive oxygen species (ROS) such as superoxide anion radicals ($O_2^{\bullet -}$) and hydrogen peroxide (H_2O_2).[69, 90] Then, H_2O_2 is subsequently used by peroxidases to produce the hypohalous acid to deactivate pathogens (Equations 13 and 14).

$$H^+ + X^- + H_2O_2 \longrightarrow HOX + H_2O \qquad (13)$$

$$HOX + O_2^{\bullet -} \longrightarrow {}^{\bullet}OH + O_2 + X^- \qquad (14)$$

Hypohalous acids (HOX) are then converted to hydroxyl radicals ($OH^{\bullet}$), which together cause their biocidal activity.

Myeloperoxidase (MPO) is present in high concentration in the granules of leucocytes and monocytes. It is released during phagocytosis and is believed to play a major role in the killing of microorganisms and the inactivation of viruses. MPO oxidizes most of the halide ions, with preference to chloride because of its the high concentration in the plasma (100–140 mM),[91] and the resulting hypohalous acids have strong biocidal activity.[69] However, Klebanoff has pointed out that despite the high concentration of chloride present in plasma, iodide is much more effective in antimicrobial systems.[92] Lactoperoxidase (LPO), a constituent of milk, saliva and tears, also plays an important role in the antimicrobial defense.[75] LPO oxidizes iodide, chloride, bromide, and thiocyanate ions to the analogous hypohalous acids. In addition, horseradish peroxidase (HRP) (superfamily I) has been reported to have a strong effect on tumor cells.[93, 94]

In summary, oxidation processes are very important in biological systems, in particular, for the antimicrobial defense mechanism. Peroxidases themselves have little bactericidal effect, however, the reaction of peroxidases (for example MPO) with H_2O_2 in the presence of halides (Cl^-, Br, I^-) or pseudohalide (SCN^-) ions generates hypohalous acids: hypochlorous acid (HOCl), hypobromous acid (HOBr), hypoiodous acid (HOI), and hypothiocyanous acid (HOSCN).[95-97] These oxidants are widely believed to be responsible for the anti–bactericidal activity.

We developed (Chapter 4) a sensitive and inexpensive supramolecular tandem assay to monitor the activity of different classes of peroxidases (superfamily I and superfamily II). In addition, our developed assay requires the substrate (I^-) concentration to be only in the micromolar range (μM). This advantage overcomes the use of high concentrations of the substrate, which is reported to inhibit the peroxidase activity.

References

[1] B. Halliwell, *Plant Physiol.* **2006**, *141*, 312.
[2] D. E. Canfield, *Annu. Rev. Earth Planet. Sci.* **2005**, *33*, 1.
[3] E. S. Rubin, *Introduction to Engineering & the Environment*, 1st ed., McGraw–Hill, **2001**.
[4] J. H. Seinfield, S. Panids, *Atmospheric Chemistry and Physics*, John Wiley and Sons: New York, **1998**.
[5] X. Tang, S. R. Wilson, K. R. Solomon, M. Shao, S. Madronich, *Photochem. Photobiol. Sci.* **2011**, *10*, 280.
[6] E. Neyens, J. Baeyens, *J. Hazard. Mater.* **2003**, *98*, 33.
[7] B. S. Berlett, E. R. Stadtman, *J. Biol. Chem.* **1997**, *272*, 20313.
[8] S. Linton, M. J. Davies, R. T. Dean, *Exp. Gerontol.* **2001**, *36*, 1503.
[9] R. Poli, *Eur. J. Inorg. Chem.* **2011**, 1513.
[10] L. Tebben, A. Studer, *Angew. Chem.-Int. Edit.* **2011**, *50*, 5034.
[11] R. A. Moss, M. S. Platz, J. M. Jones, *Reactive Intermediate Chemistry*, John Wiley & Sons, Inc., Hoboken, New Jersey, **2004**.
[12] K. H. Cheeseman, T. F. Slater, *Br. Med. Bull.* **1993**, *49*, 481.
[13] V. A. Selivanov, T. V. Votyakova, V. N. Pivtoraiko, J. Zeak, T. Sukhomlin, M. Trucco, J. Roca, M. Cascante, *PLoS Comput. Biol.* **2011**, *7*, DOI: 10.1371/journal.pcbi.1001115.
[14] S. Hashimoto, H. Seki, T. Masuda, M. Imamura, M. Kondo, *Int. J. Radiat. Biol.* **1981**, *40*, 31.
[15] A. M. Mayouf, H. Lemmetyinen, J. Koskikallio, *J. Photoch. Photobio. A* **1993**, *70*, 215.
[16] S. Nishida, T. Nada, M. Terazima, *Biophys. J.* **2004**, *87*, 2663.
[17] R. G. Hicks, *Org. Biomol. Chem.* **2007**, *5*, 1321.
[18] M. Gomberg, *J. Am. Chem. Soc.* **1900**, *22*, 757.
[19] R. Braslau, *J. Org. Chem.* **1995**, *60*, 6191.
[20] J. M. Fukuto, M. D. Bartberger, A. S. Dutton, N. Paolocci, D. A. Wink, K. N. Houk, *Chem. Res. Toxicol.* **2005**, *18*, 790.
[21] M. Ueda, E. Kondoh, Y. Ito, H. Shono, M. Kakiuchi, Y. Ichii, T. Kimura, T. Miyoshi, T. Naito, O. Miyata, *Org. Biomol. Chem.* **2011**, *9*, 2062.
[22] A. Egorov, S. Matyukhova, I. Kocherova, A. Novikova, A. Anisimov, *Russ. J. Gen. Chem.* **2009**, *79*, 444.
[23] A. Hennig, H. Bakirci, W. M. Nau, *Nat. Methods* **2007**, *4*, 629.
[24] E. A. Smolenskii, G. V. Vlasova, A. L. Lapidus, *Dokl. Phys. Chem.* **2004**, *397*, 145.
[25] G. da Silva, J. W. Bozzelli, *Combust. Flame* **2010**, *157*, 2175.
[26] C. T. Chiou, D. W. Schmedding, M. Manes, *Environ. Sci. Technol.* **1982**, *16*, 4.
[27] M. Frenklach, *Phys. Chem. Chem. Phys.* **2002**, *4*, 2028.
[28] L. C. Marr, T. W. Kirchstetter, R. A. Harley, A. H. Miguel, S. V. Hering, S. K. Hammond, *Environ. Sci. Technol.* **1999**, *33*, 3091.
[29] M. A. Oehlschlaeger, D. F. Davidson, R. K. Hanson, *Combust. Flame* **2006**, *147*, 195.
[30] P. Dagaut, G. Pengloan, A. Ristori, *Phys. Chem. Chem. Phys.* **2002**, *4*, 1846.
[31] S. J. Blanksby, G. B. Ellison, *Acc. Chem. Res.* **2003**, *36*, 255.
[32] G. da Silva, C.-C. Chen, J. W. Bozzelli, *J. Phys. Chem. A* **2007**, *111*, 8663.

[33] R. A. Eng, A. Gebert, E. Goos, H. Hippler, C. Kachiani, *Phys. Chem. Chem. Phys.* **2002**, *4*, 3989.
[34] K. Luther, J. Troe, K. M. Weitzel, *J. Phys. Chem.* **1990**, *94*, 6316.
[35] J. L. Emdee, K. Brezinsky, I. Glassman, *J. Phys. Chem.* **1992**, *96*, 2151.
[36] C. N. Hewitt, *Reactive Hydrocarbons in the Atmospher*, Academic Press, London, **1999**.
[37] W. L. Chameides, R. W. Lindsay, J. Richardson, C. S. Kiang, *Science* **1988**, *241*, 1473.
[38] K. Sexton, H. Westberg, *Atmos. Environ.* **1984**, *18*, 1125.
[39] V. A. Isidorov, I. G. Zenkevich, I. B. V, *Atmos. Environ.* **1983**, *17*, 1347.
[40] H. B. Singh, L. J. Salas, B. K. Cantrell, R. M. Redmond, *Atmos. Environ.* **1985**, *19*, 1911.
[41] J. Zhang, P. J. Lioy, Q. He, *Environ. Sci. Technol.* **1994**, *28*, 146.
[42] R. Atkinson, *Atmos. Environ. Part A* **1990**, *24*, 1.
[43] K. Brezinsky, *Prog. Energy Combust. Sci.* **1986**, *12*, 1.
[44] T. Seta, M. Nakajima, A. Miyoshi, *J. Phys. Chem. A* **2006**, *110*, 5081.
[45] F. P. Tully, A. R. Ravishankara, R. L. Thompson, J. M. Nicovich, R. C. Shah, N. M. Kreutter, P. H. Wine, *J. Phys Chem.* **1981**, *85*, 2262.
[46] P. Q. E. Clothier, D. Shen, H. O. Pritchard, *Combust. Flame* **1995**, *101*, 383.
[47] W. M. Davis, S. M. Heck, H. O. Pritchard, *J. Chem. Soc., Faraday Trans.* **1998**, *94*, 2725.
[48] G. Porter, F. J. Wright, *T. Faraday. Soc.* **1955**, *51*, 1469.
[49] M. Szwarc, *Discuss. Faraday Soc.* **1947**, *2*, 39.
[50] R. F. C. Claridge, H. Fischer, *J. Phys. Chem.* **1983**, *87*, 1960.
[51] M. Braunukhoff, P. Frank, T. Just, *Ber. Bunsen-Ges. Phys. Chem.* **1990**, *94*, 1417.
[52] M. A. Oehlschlaeger, D. F. Davidson, R. K. Hanson, *J. Phys. Chem. A* **2006**, *110*, 6649.
[53] T. Okamura, K. Obi, I. Tanaka, *Chem. Phys. Lett.* **1974**, *26*, 218.
[54] J. M. Dust, D. R. Arnold, *J. Am. Chem. Soc.* **1983**, *105*, 1221.
[55] T. H. Fisher, S. M. Dershem, M. L. Prewitt, *J. Org. Chem.* **1990**, *55*, 1040.
[56] W. Adam, H. M. Harrer, F. Kita, W. M. Nau, *Pure Appl. Chem.* **1997**, *69*, 91.
[57] G. P. Trueba, G. M. Sanchez, A. Giuliani, *Front. Biosci.* **2004**, *9*, 2029.
[58] M. Valko, C. J. Rhodes, J. Moncol, M. Izakovic, M. Mazur, *Chem.-Biol. Interact.* **2006**, *160*, 1.
[59] I. Fridovich, *Annu. Rev. Biochem.* **1995**, *64*, 97.
[60] R. J. DeJong, L. M. Miller, A. Molina-Cruz, L. Gupta, S. Kumar, C. Barillas-Mury, *Proc. Natl. Acad. Sci. USA* **2007**, *104*, 2121.
[61] T. Kawano, *Plant Cell Rep.* **2003**, *21*, 829.
[62] R. P. Brandes, *Cardiovasc. Res.* **2011**, *91*, 1.
[63] H. B. Dunford, *Heme peroxidases*, John Wiley & Sons, New York, **1999**.
[64] K. G. Welinder, J. M. Mauro, L. Norskovlauritsen, *Biochem. Soc. Trans.* **1992**, *20*, 337.
[65] R. Fenna, J. Zeng, C. Davey, *Arch. Biochem. Biophys.* **1995**, *316*, 653.
[66] P. G. Furtmüller, U. Burner, C. Obinger, *Biochemistry* **1998**, *37*, 17923.
[67] I. M. Kooter, N. Moguilevsky, A. Bollen, N. M. Sijtsema, C. Otto, R. Wever, *J. Biol. Inorg. Chem.* **1997**, *2*, 191.
[68] C. Capeillere-Blandin, *Biochem. J.* **1998**, *336*, 395.
[69] M. Morrison, G. R. Schonbaum, *Annu. Rev. Biochem.* **1976**, *45*, 861.
[70] M. Nakamura, S. Nakamura, *Free Radical Biol. Med.* **1998**, *24*, 537.

[71] A. N. P. Hiner, E. L. Raven, R. N. F. Thorneley, F. Garcia-Canovas, J. N. Rodriguez-Lopez, *J. Inorg. Biochem.* **2002**, *91*, 27.
[72] J. N. Rodriguez-Lopez, D. J. Lowe, J. Hernandez-Ruiz, A. N. P. Hiner, F. Garcia-Canovas, R. N. F. Thorneley, *J. Am. Chem. Soc.* **2001**, *123*, 11838.
[73] T. L. Poulos, J. Kraut, *J. Biol. Chem.* **1980**, *255*, 8199.
[74] J. Arnhold, E. Monzani, P. G. Furtmüller, M. Zederbauer, L. Casella, C. Obinger, *Eur. J. Inorg. Chem.* **2006**, 3801.
[75] P. G. Furtmüller, M. Zederbauer, W. Jantschko, J. Helm, M. Bogner, C. Jakopitsch, C. Obinger, *Arch. Biochem. Biophys.* **2006**, *445*, 199.
[76] J. E. Harrison, T. Araiso, M. M. Palcic, H. B. Dunford, *Biochem. Biophys. Res. Commun.* **1980**, *94*, 34.
[77] P. G. Furtmüller, W. Jantschko, G. Regelsberger, C. Jakopitsch, J. Arnhold, C. Obinger, *Biochemistry* **2002**, *41*, 11895.
[78] H. Kohler, A. Taurog, H. B. Dunford, *Arch. Biochem. Biophys.* **1988**, *264*, 438.
[79] H. Iwamoto, T. Kobayashi, E. Hasegawa, Y. Morita, *J. Biochem.* **1987**, *101*, 1407.
[80] A. J. Kettle, C. C. Winterbourn, *Biochemistry* **2001**, *40*, 10204.
[81] A. Virion, D. Deme, J. Pommier, J. Nunez, *Eur. J. Biochem.* **1981**, *118*, 239.
[82] A. Virion, J. Pommier, D. Deme, J. Nunez, *Eur. J. Biochem.* **1981**, *117*, 103.
[83] K. Suzuki, E. Muso, W. M. Nauseef, *Jpn. J. Infect. Dis.* **2004**, *57*, S1.
[84] A. Butler, M. Sandy, *Nature* **2009**, *460*, 848.
[85] T. Hosoya, I. Sato, Y. Hiyama, H. Yoshimura, H. Niimi, O. Tarutani, *J. Biochem.* **1985**, *98*, 637.
[86] C. D. Murphy, R. M. Moore, R. L. White, *J. Appl. Phycol.* **2000**, *12*, 507.
[87] M. Huwiler, H. Kohler, *Eur. J. Biochem.* **1984**, *141*, 69.
[88] R. P. Magnusson, A. Taurog, M. L. Dorris, *J. Biol. Chem.* **1984**, *259*, 197.
[89] A. Taurog, D. E. Gamble, *Fed. Proc.* **1966**, *25*, 347.
[90] M. A. Torres, J. D. G. Jones, J. L. Dangl, *Plant Physiol.* **2006**, *141*, 373.
[91] S. Oka, Y. Sibazaki, S. Tahara, *Anal. Chem.* **1981**, *53*, 588.
[92] S. j. Klebanoff, W. L. Green, *J. Clin. Invest.* **1973**, *52*, 60.
[93] R. A. Clark, S. J. Klebanoff, A. B. Einstein, A. Fefer, *Blood* **1975**, *45*, 161.
[94] D. L. Lefkowitz, K. Mills, A. Castro, S. S. Lefkowitz, *J. Leukocyte Biol.* **1991**, *50*, 615.
[95] S. j. Klebanoff, *J. Bacteriol.* **1968**, *95*, 2131.
[96] M. J. Davies, C. L. Hawkins, D. I. Pattison, M. D. Rees, *Antioxid. Redox Signaling* **2008**, *10*, 1199.
[97] A. J. Kettle, C. C. Winterbourn, *Redox Report* **1997**, *3*, 3.

Chapter 2

Oxygen Scavenging of Aryl–Substituted Benzyl Radicals

Chapter 2

2. Oxygen Scavenging of Aryl–Substituted Benzyl Radicals

Corresponds to:

El–Sheshtawy H. S., Nau W. M., "Oxygen Scavenging of Aryl–Substituted Benzyl Radicals",in preparation.

– Supporting information correspond to this chapter are collected in **Appendix I**.

2.1 Introduction

Oxidation reactions play a crucial rule in both combustion and atmospheric chemistry, in particular the reaction of carbon centered radicals with molecular oxygen to produce alkylperoxy radicals.[1, 2] Organic peroxy radicals (RO_2•) are critical reaction intermediates in both the low temperature combustion[3, 4] (T < 700 K) and in the atmospheric oxidation[5-7] of organic compounds. The mechanism of low-temperature combustion of hydrocarbons begins with the abstraction of a hydrogen atom from the fuel (RH) by a hydroxyl radical (OH•) or any other reactive radical to form an alkyl radical (R•). The alkyl radical then reacts with molecular oxygen to form an alkyl peroxy radical (RO_2•) (Equation 1).[8]

$$R\bullet + O_2 \rightleftharpoons RO_2\bullet \qquad (1)$$

The interest to study oxidation reactions of aromatic compounds can be traced back to the use of toluene and benzene as desirable constituents or additives in transportation fuels.

Moreover, aromatic hydrocarbon radicals have attracted much attention because they are formed by the photochemical oxidation of alkylbenzenes in polluted air. Finally, benzyl or substituted benzyl radicals are thought to be important intermediates in the formation of benzaldehyde and benzyl nitrate, which contribute to photochemical smog formation.[9-11]

Benzyl radical scavenging by molecular oxygen has attracted particular interest, especially in the gas phase. Ebata *et al*.[12] investigated the scavenging rate constants of the parent benzyl radicals by molecular oxygen by flash photolysis. This value was reported to be 0.99×10^9 $M^{-1}s^{-1}$, which is in good agreement with the value reported by Nelson *et al*.[13] In their study, the authors reported the quenching rate constant to be independent on the studied temperature range (298–373 K). In contrast, Elmaimouni *et al*.[14] reported a variation of the quenching rate constants of the benzyl radical by molecular oxygen with temperature. Fenter and co–workers[15] studied the association reaction of the benzyl radical with oxygen as a function of temperature as well as pressure in a buffer gas. They observed that the reaction is independent on both pressure and temperature. This result was in agreement with the work of Ebata[12] and Nelson[13] but in contrast with the result obtained by Elmaimouni.[14] Recently, Murakami *et al*.[16] have conducted theoretical investigations on the effect of temperature on the oxygenation rate constant of benzyl radicals. As the temperature was varied from 300–500 K, there was an increase in the oxygenation rate constant, whereas in higher temperature ranges (700–1500 K), the rate constant deviated and showed inverse temperature dependence.

Liquid phase autoxidation involving benzyl radicals has attracted less interest compared to the gas phase despite its importance in the oxidative degradation of organic materials and living organisms.[17, 18] Maillard *et al*.[19] have studied the oxygenation rate constant of benzyl radicals in different solvents. They pointed out that the rate constant is slower in low viscosity solvents than expected for diffusion–controlled reactions. The authors further reported the rate constant to be independent on polarity and polarizability of the solvent. On the other hand, Tokumura *et al*[20] reported a substituent–dependent correlation of the quenching rate constants of different *p*–X–substituted benzyl radicals (X = H, CH_3, F, Cl, Br, CN, NO_2, OCH_3, and OCH_2Ph) with oxygen in *n*–hexane.

Despite the previous work, the data available on the solvent effect, the

temperature dependence, and substituent effect on benzyl radical reactivity in the liquid phase are still scarce. Therefore, my work was devoted to the study of quenching rate constants of different aryl–substituted benzyl radicals (*p*–MeO, *p*-Me, H, *p*–Cl, and *p*–CF_3) in *n*–hexane and acetonitrile over a sizable temperature range (Scheme 2.1, and Appendix 1). Our results are supported by quantum chemical calculation using density functional theory (DFT) at the B3LYP hybrid level of theory and a 6–311G (2d,p) basis set.

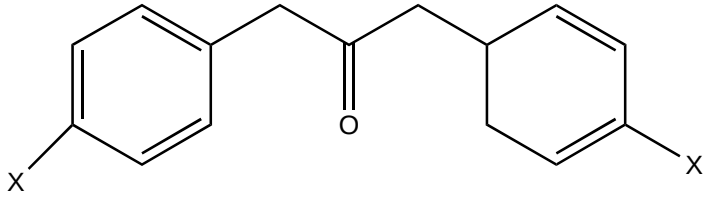

X = OCH_3, CH_3, H, Cl and CF_3

Scheme 2.1: Structures of dibenzylketones employed as aryl–substituted benzyl radical precursors.

2.2 Oxygen Scavenging Rate Constants

Upon 308-nm laser pulse irradiation of *p*–X–dibenzyl ketones derivatives (X = OCH_3, CH_3, H, Cl and CF_3) in the presence of different oxygen concentrations (Appendix 1) in *n*–hexane and in acetonitrile, the corresponding substituted benzyl radicals gave a transient absorbance signals at around 314 nm.[20-22] All signals exhibited a mono–exponential decay for the differently substituted benzyl radicals as shown in Figure 2.1. Under these conditions, the scavenging rate constants follow Equation 2:

$$k_{obs} = k_0 + k_{Ox}[O_2] \qquad (2)$$

where k_{obs} is the measured first–order rate constant for the radical, k_0, which includes all kinetically first–order decay processes other than the reaction with oxygen, and k_{Ox} refers to the forward reaction between oxygen and the studied radicals. The observed rate

constants were plotted against the oxygen concentration to afford the k_{OX} values from the slope (see inset in Figure 2.1). Table 2.1 shows the scavenging rate constants of substituted benzyl radicals at different temperatures (288–325 K) in *n*–hexane and in acetonitrile.

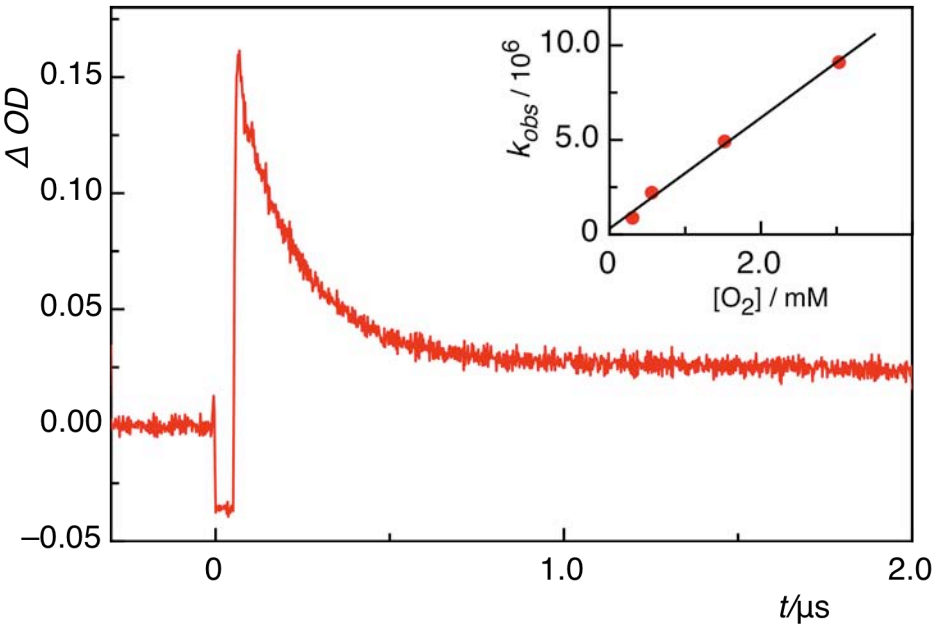

Figure 2.1: Transient absorption decay traces, observed at 314 nm, for the parent benzyl radical after 308-nm laser photolysis in acetonitrile saturated with 1.31 mM oxygen at 298 K. The Inset shows the plot of the oxygenation rate *versus* the oxygen concentration in acetonitrile.

Table 2.1: Scavenging rate constants of aryl–substituted benzyl radicals (in 10^9 $M^{-1}s^{-1}$) by molecular oxygen at different temperatures (K) in *n*–hexane and acetonitrile.

substituents	solvent	Temperature / K				
		288	298	308	318	328
p–OCH_3	*n*–hexane	2.72	2.76	2.92	2.74	–
	acetonitrile	4.84	4.48	4.37	3.97	3.78
p–CH_3	*n*–hexane	2.29	2.29	2.30	2.28	–
	acetonitrile	3.28	3.10	2.96	2.77	2.57
p–H	*n*–hexane	1.97	2.19	2.1	2.12	–
	acetonitrile	3.14	2.99	2.84	2.63	2.34
p–Cl	*n*–hexane	1.80	1.85	1.84	1.82	–
	acetonitrile	2.96	2.80	2.74	2.50	2.26
p–CF_3	*n*–hexane	1.50	1.45	1.43	1.43	–
	acetonitrile	2.83	2.71	2.59	2.29	1.79

The obtained scavenging rate constants for electron–donating groups (*p*–OCH_3 and *p*–CH_3) showed higher values than those for the unsubstituted benzyl radical, whereas the electron–withdrawing groups (*p*–Cl and *p*–CF_3) showed lower values. These results are in a good agreement with the reported trends by Tokamoura *et al*.[20] except for the rate constant values of *p*–OCH_3 and *p*–CH_3: Our results show a higher value for *p*–OCH_3 than *p*–CH_3, which is in contrast to the reported data.

The scavenging rate constant trend (*p*–OCH_3 > *p*–CH_3 > H > *p*–Cl > *p*–CF_3) has been supported by quantum chemical calculations performed using B3LYP density functional theory and the 6-311G(2d,p) basis set. Table 2.2 shows that the C---O–O bond dissociation energies (BDEs) of the peroxyl radicals support the experimental trend as the values reveal lower BDEs for the electron donating groups (*p*–OCH_3 and *p*–CH_3) and higher values for electron–withdrawing groups (*p*–Cl and *p*–CF_3) relative to the parent compound (toluene). Consequently, higher scavenging rate constants are expected for the

former groups and lower values for the latter. The optimized transition state (TS) geometries (Figure 2.2) of the substituted radicals show that the radicals with electron–donating substituents have TS structures, in which the reactants (*p*–X–benzyl radical and oxygen) approach together in a faster rate (i.e., already at a longer distance) with respect to electron withdrawing groups. Consequently, the radicals with electron–donating groups are expected to combine faster with oxygen than with the electron–withdrawing substituted radicals.

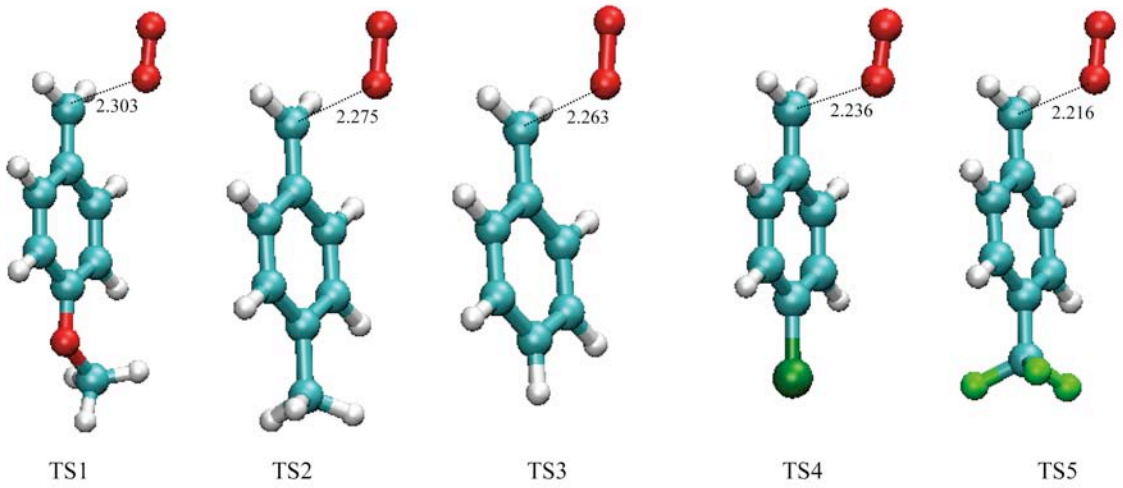

Figure 2.2: Optimized transition-state geometries of the substituted benzyl radicals (*p*–OCH_3: TS1, *p*–CH_3: TS2, *p*–H: TS3, *p*–Cl: TS4, *p*–CF_3: TS5), calculated using the UB3LYP level of theory and the 6–311G(2d,p) basis set, in the gas phase.

Table 2.2: Calculated Mulliken atomic charges in the aryl-substituted benzyl radicals and the transition states for peroxyl radical formation. The C–OO bond distance (*r*) for aryl–substituted benzyl radicals transition state are also tabulated.

substituent	BDE [a] /kcal	r [b] /Å	Mulliken atomic charges [b] /|e|				μ/D
			δ (C1)	δ(C2)	δ(O1)	δ(O2)	
p–OCH_3	−22.41	2.303	−0.2021	−0.12792	−0.06402	−0.08945	0.232
p–CH_3	−22.34	2.275	−0.1908	−0.11958	−0.05994	−0.08362	0.214
p–H	−22.32	2.263	−0.1848	−0.11550	−0.05764	−0.07978	0.205
p–Cl	−21.66	2.236	−0.1835	−0.11546	−0.05807	−0.07632	0.203
p–CF_3	−21.35	2.216	−0.1725	−0.10785	−0.05573	−0.07097	0.19

[a] Values calculated by single-point calculations (CBS–QB3//B3LYP/6–311G(2d,p). [b] Values determined after the optimizations at the B3LYP/6–311G(2d,p) level of theory.

Our scavenging rate constant values suggest that electron–donating substituent stabilize the incipient benzylperoxy radicals, while electron–withdrawing substituents destabilized them. This demonstrates that a polar substituent effect is a dominant factor in the scavenging of substituted benzyl radicals by oxygen. A linear correlation of log (k_X/k_H) *versus* the Hammet σ values (σ_{pol})[23] applies in both *n*-hexane (n = 5, r = 0.97) (Figure 2.3) and acetonitrile (n = 5, r = 0.76).

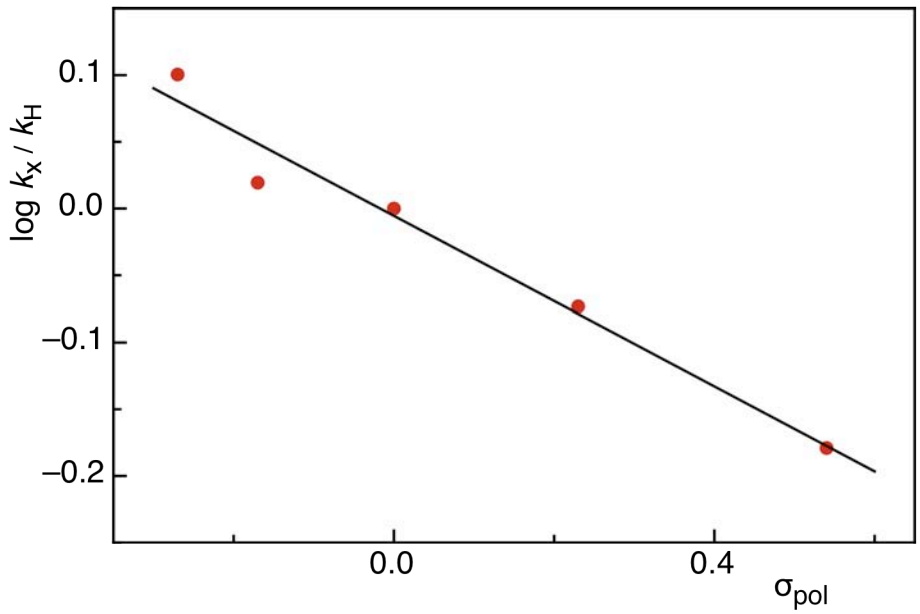

Figure 2.3: Hammet relationship for kinetics of oxygen scavenging by the aryl–substituted benzyl radical in *n*-hexane.

The dominance of a polar substituent effect on the scavenging rates suggests that the kinetics of the scavenging process should be correlated with the reaction enthalpy, *i.e.* the bond dissociation enthalpy (BDE) of the formed C–OO bond. The experimental heat of enthalpy for the scavenging of the unsubestituted benzyl radical by oxygen has been determined to be –21.8 kcal/mol by Fenter *et. al*.[15] and –20 kcal/mol by Elmaimouni *et. al*.[14] We calculated a value of –22.32 kcal/mol (see Table 2) from the relative energy for the scavenging of the parent benzyl radical by oxygen using the CBS–QB3 level of theory. The value (–22.32 kcal/mol) for the parent benzyl radical, calculated both in this work and by Murakami *et. al*.[16], is in good agreement with the experimental values obtained by Fenter *et. al*.[15] and Elmaimouni *et al*.[14] Interestingly, the C–OO bond dissociation energy for the radicals with electron donating groups (CH_3 and OCH_3) is *higher* than those for the the radicals with electron withdrawing groups (Cl and CF_3). This result supports the idea that electron–donating substituents strengthen the formed bond, while electron withdrawing substituents weaken it, in agreement with the experimentally observed trend of the rate constants (Table 2.2).

2.3 Solvent Effect on the Scavenging Rate Constants

The effects of the solvent polarity on the reaction rate of the radicals have attracted the attention of many researchers (see also Chapter 3 of this thesis).[24, 25] Despite this interest, little work has been done on the solvent effect on the oxygenation rate of benzylic radicals. To the best of our knowledge, the only work was done by Maillard *et al.*[19] studying the effect of solvents on the oxygenation rate constant of carbon centered radicals. In this study, we measured the oxygen scavenging of aryl–substituted benzyl radicals in two different solvents (*n*–hexane and acetonitrile), at different temperatures ranging from 288 to 328 K. The resulting scavenging rate constants showed that with higher solvent polarity, there is an increase in the oxygenation rate constant (Figure 2.4), which is in consistent with the reported results. The scavenging rate constant in acetonitrile was twice as large as that in *n*-hexane (Table 2.1). The same trend is also observed for the other substituted benzyl radicals.

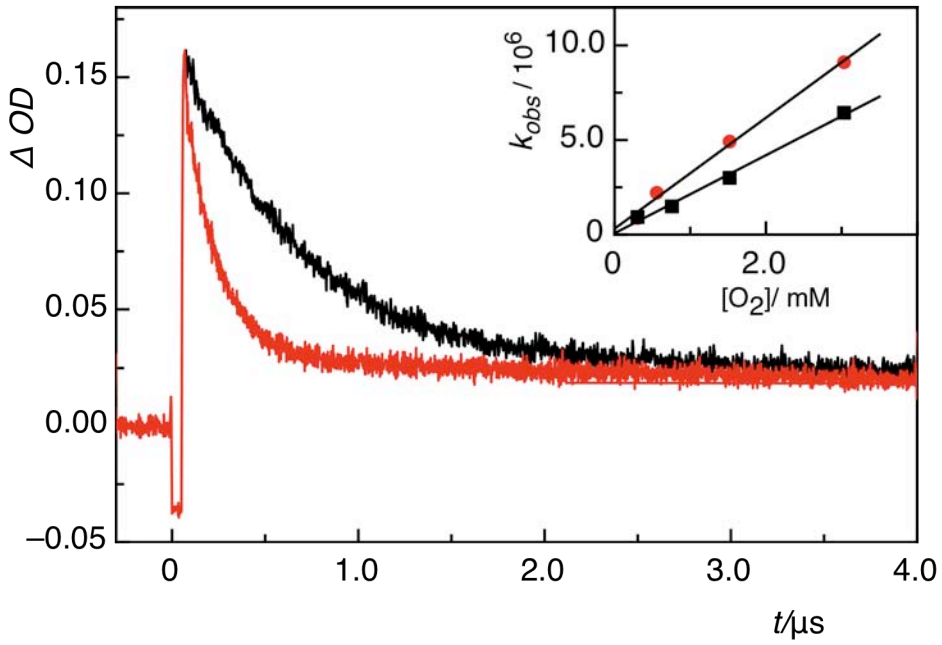

Figure 2.4: Transient decay traces of benzyl radicals, observed at 314 nm after 308-nm laser photolysis in acetonitrile (red) and in *n*-hexane (black) saturated with comparable oxygen concentration at 298 K. The inset shows the plot of the observed rate constants *versus* the oxygen concentration in acetonitrile (●) and *n*–hexane (■).

An increase in the scavenging rate constants in polar solvents has been reported previously for the unsubstitued benzyl radical.[20] Our results confirm that this solvent effect not only apply for the unsubstituted benzyl radical, but also for substituted derivatives. The origin of solvent effects can be interpreted by its influence on the charge distribution between the carbon atom (C2) and the two oxygen atoms in the transition state (benzylperoxy radical) as shown in Scheme 2. Initially, we observed a development of a negative charge on the benzyl carbon atom (C1) as shown in Table 2.2. This negative partial charge was distributed over the two oxygen atoms upon their approach to the benzyl radicals to form a C–OO bond. In the transition state structure, the benzylic carbon atom (C2) is carrying less partial negative charge than in the initial carbon atom (C1). This difference between the partial negative charge formed on C2 and the negative charge on both oxygen atoms is more stabilized by polar solvents than by non–polar solvents. Moreover, the calculated bond dipole μ (C–OO) for the electron–donating substituents is higher than that for the electron–withdrawing substituents with respect to the parent benzyl radical (Table 2.2).

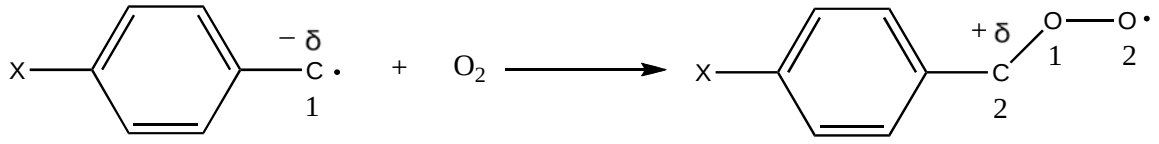

Scheme 2.2: Charge distribution on the transition state of substituted benzyl radicals.

In other words, oxygen scavenging involves a significant amount of charge transfer (from the benzyl fragment to the peroxy group), which is facilitated in polar solvents. It should be noted that a similar charge distribution argument (changes in molecular dipole moments) has also been used before to deduce the solvent effect on the decarbonylation of the phenacetyl radicals.[21]

2.4 Temperature Effect on the Scavenging Rate Constants

Several authors have reported temperature effects on the scavenging rate constant of unsubstituted benzyl radical.[12-15] Although, Elmaimouni *et. al.*[14] reported a temperature dependence on the scavenging rate constant for the unsubstituted benzyl radical, Ebata,[12] Nelson,[13] and Fenter[15] found that the scavenging rate constant in the gas phase is temperature-independent. On the other hand, no work has been done on the effect of temperature on the scavenging rate constant of benzyl radical and its derivatives by oxygen in the liquid phase. Therefore, the scavenging rate constants of aryl–substituted benzyl radical over a sizable temperature range (288–328 K) were measured in *n*-hexane and in acetonitrile. The transient decay signals monitored at 314 nm for the unsubstituted benzyl radical in acetonitrile display a significant decrease in the decay rate with increasing temperature (Figure 2.5) in acetonitrile only.

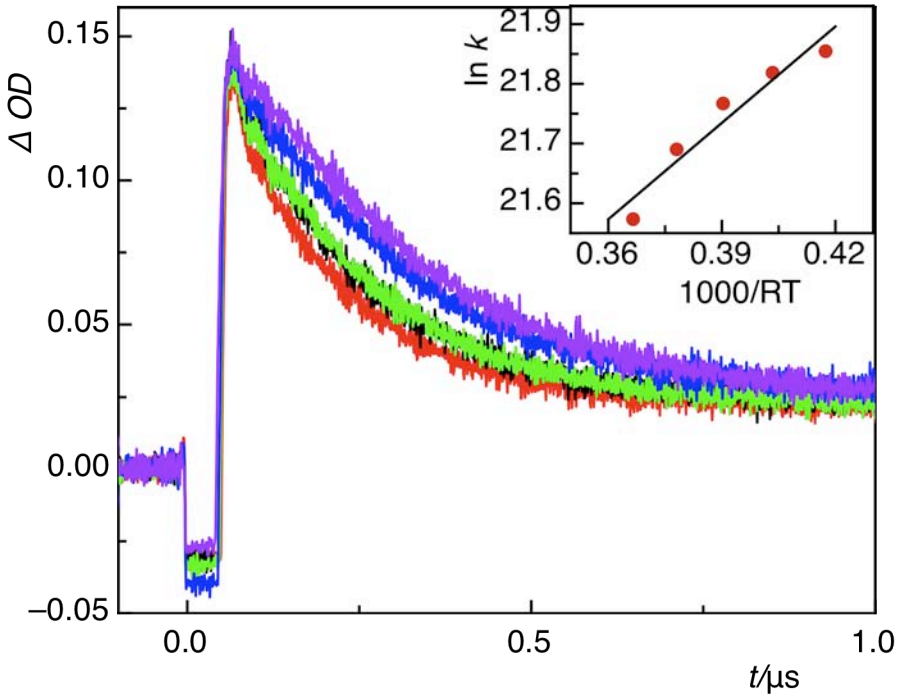

Figure 2.5: Transient absorption decay traces of benzyl radical at 314 nm after a 308 nm laser pulse in acetonitrile, saturated with comparable oxygen concentration at different temperatures. The inset shows an Arrhenius plot of the measured rate constants over a temperature range from 288 to 318 K.

Table 2.1 shows the effect of temperature on the scavenging rate constants of the investigated substituted benzyl radicals. The studied substituted benzyl radicals (*p*–OCH_3, *p*–CH_3, H, *p*–Cl, *p*–CF_3) showed a sizable change of the scavenging rate constants in acetonitrile (polar solvent) with temperature, however no significant change of the rate constants was observed in *n*–hexane under the same conditions.

The insensitivity of the scavenging rates on temperature of the substituted benzyl radicals with oxygen in *n*–hexane is in agreement with the result of Ebata,[12] Nelson,[13] and Fenter,[15] who performed measurements in the gas phase. Hence, the scavenging rates are not affected by the small change in polarity between the gas phase and non–polar solvents (*n*–hexane). Interestingly, aryl–substituted benzyl radicals exhibited a decrease in the oxygen–scavenging rate constants in acetonitrile with an increase in the temperature. Accordingly, Arrhenius plots for the measured rate constants provided a *negative* activation energy, which ranged from −1.14 to −1.05 kcal/mole for *p*–CF_3 and *p*–OCH_3 respectively (Table 2.3). Negative activation energies have been occasionally reported before for different systems,[26] which were interpreted either by a pre–complex formation[27, 28] or by the Houk model.[29, 30] In the Houk model, the association reactions have zero or close to zero enthalpic barriers but may develop significant free energy barriers due to the decrease in entropy occurring as the two molecules unit to form a single product. The location of the transition state (maximum ΔG) is then determined by the point along the reaction coordinate at which the decrease in the ΔH term overcomes the increase in the $-T\Delta S$ term. Clearly, since the magnitude of the $-T\Delta S$ term is temperature dependent, higher temperatures will move the position of the transition state further towards the product and result in a higher value of ΔG. This model has been used to interpret the negative activation energy for the addition of carbenes to alkenes[29-31] and the reactivity of singlet oxygen towards furans and indoles.[32]

Table 2.3: Calculated activation energies ($\Delta H^{\#}$), and Arrhenius activation energies (E_a), and pre–exponential factors (ln A) for the scavenging of substituted benzyl radicals by molecular oxygen.[a]

substituents	$\Delta H^{\#}$ (kcal/mol)	E_a (kcal/mol)	ln A $M^{-1}s^{-1}$
p–OCH_3	0.083	–1.14	8.81
p–CH_3	0.343	–1.11	8.67
p–H	0.559	–1.10	8.65
p–Cl	1.187	–1.08	8.61
p–CF_3	1.58	–1.05	8.55

[a] Values calculated at B3LYP/6–311G(2d,p) level.

Alternatively, negative activation energies have been interpreted in terms of the formation of an exothermic complex, which undergoes competitive collapse to the starting materials and products. Examples are the cycloaddition of tetracyanoethylene and 9,10–dimethylanthracene, the cycloaddition of phenylchlorocarbene and alkenes, the reaction of triplet fluorenylidene with olefins.[27, 28] To investigate the potential energy surface for oxygen scavenging of the substituted benzyl radicals, we performed a potential energy surface scan at the B3LYP density functional theory with the 6–311G(2d,p) basis set. Along the reaction coordinate, there was only one maximum energy structure (TS), which indicates the absence of a stable pre-complex formation, at least along the investigated reaction coordinate.

Potential energy surfaces for all the substituted benzyl radicals showed that oxygen approaches the benzyl radicals with a small positive change in the enthalpy (ΔH) (Figure 2.6, and Appendix 1). On the other hand, significant changes in both the free energy (ΔG) and the $-T\Delta S$ values were observed. The ΔG curves show that the free energy maxima correspond to small positive ΔH values, i.e., there is a small positive activation energy in the order (*p*–OCH_3 < *p*–CH_3 < *p*–H < *p*–Cl < *p*–CF_3) in the gas phase. The ΔG maximum is the energy, which corresponds to the energy of the transition state. Moreover, the potential energy curves showed an increase in the $-T\Delta$S values for

all substituted benzyl radicals, i.e., the value of ΔS decreases along the reaction coordinate (from right to left) due to the formation of a tight transition state and, ultimately, the peroxyl radical product (two reactants give one product).

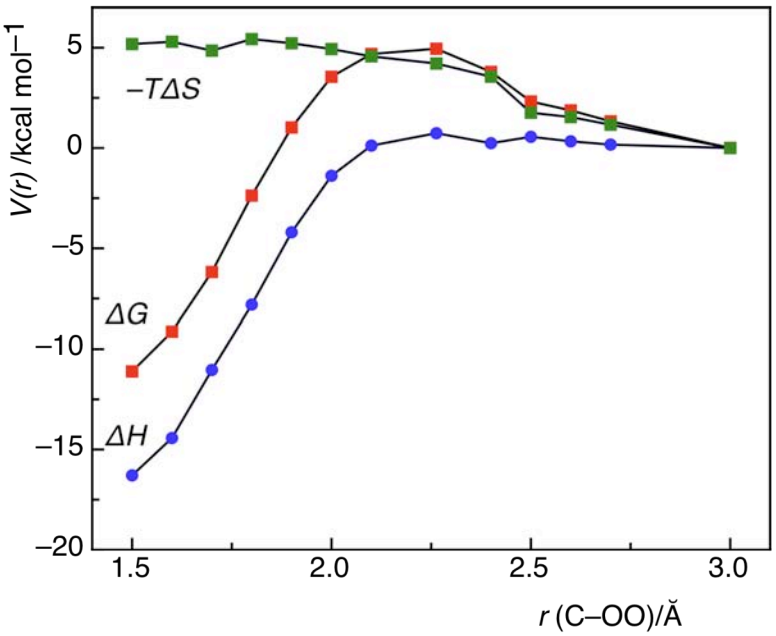

Figure 2.6: Potential energy profile for the unsubstituted benzyl radical, calculated by using the UB3LYP level of theory and the 6–311G(2d,p) basis set.

The small positive enthalpic barrier ($\Delta H^{\#}$), where $\Delta H^{\#} = E_a - RT$, observed along the potential energy surface supports the insignificant change of the scavenging rates of substituted benzyl radicals with temperature, both in the gas phase and in *n*–hexane. Although our calculations show a small energy barrier in ΔH and TS (maximum of ΔG), we cannot exclude that a similar situation as in Houk model applies in case of acetonitrile as solvent. Note that our calculations refer to the gas phase, whereas, the negative activation energy was observed in acetonitrile, a polar solvent. Solvation effects may be significant and could be responsible for the negative activation energy. Unfortunately, efforts to optimize the reaction coordinate by applying solvation models similar to those used in Chapter 3 for hydrogen atom abstraction reactions, did not meet with success, which precluded a more detailed computational investigation on the origin of the peculiar solvent effect.

References

[1] S. W. Benson, *J. Am. Chem. Soc.* **1965**, *87*, 972.
[2] S. W. Benson, P. S. Nangia, *Acc. Chem. Res.* **1979**, *12*, 223.
[3] S. Q. Wang, D. L. Miller, N. P. Cernansky, H. J. Curran, W. J. Pitz, C. K. Westbrook, *Combust. Flame* **1999**, *118*, 415.
[4] H. J. Curran, P. Gaffuri, W. J. Pitz, C. K. Westbrook, *Combust. Flame* **1998**, *114*, 149.
[5] P. D. Lightfoot, R. A. Cox, J. N. Crowley, M. Destriau, G. D. Hayman, M. E. Jenkin, G. K. Moortgat, F. Zabel, *Atmos environ A-Gen* **1992**, *26*, 1805.
[6] G. J. Frost, G. B. Ellison, V. Vaida, *J. Phys. Chem. A* **1999**, *103*, 10169.
[7] T. J. Wallington, P. Dagaut, M. J. Kurylo, *Chem. Rev.* **1992**, *92*, 667.
[8] E. N. Sharp, P. Rupper, T. A. Miller, *Phys. Chem. Chem. Phys.* **2008**, *10*, 3955.
[9] B. Bohn, *J. Phys. Chem. A* **2001**, *105*, 6092.
[10] J. P. Killus, G. Z. Whitten, *Atmos. Environ.* **1982**, *16*, 1973.
[11] F. Caralp, V. Foucher, R. Lesclaux, T. J. Wallington, M. D. Hurley, *Phys. Chem. Chem. Phys.* **1999**, *1*, 3509.
[12] T. Ebata, K. Obi, I. Tanaka, *Chem. Phys. Lett.* **1981**, *77*, 480.
[13] H. H. Nelson, J. R. McDonald, *J. Phys. Chem.* **1982**, *86*, 1242.
[14] L. Elmaimouni, R. Minetti, J. P. Sawerysyn, P. Devolder, *Int. J. Chem. Kinet.* **1993**, *25*, 399.
[15] F. F. Fenter, B. Noziere, F. Caralp, R. Lesclaux, *Int. J. Chem. Kinet.* **1994**, *26*, 171.
[16] Y. Murakami, T. Oguchi, K. Hashimoto, Y. Nosaka, *J. Phys. Chem. A* **2007**, *111*, 13200.
[17] F. R. Mayo, *Acc. Chem. Res.* **1968**, *1*, 193.
[18] K. U. Ingold, *Acc. Chem. Res.* **1969**, *2*, 1.
[19] B. Maillard, K. U. Ingold, J. C. Scaiano, *J. Am. Chem. Soc.* **1983**, *105*, 5095.
[20] K. Tokumura, T. Ozaki, H. Nosaka, Y. Saigusa, M. Itoh, *J. Am. Chem. Soc.* **1991**, *113*, 4974.
[21] X. Y. Zhang, W. M. Nau, *J. Phys. Org. Chem.* **2000**, *13*, 634.
[22] R. F. C. Claridge, H. Fischer, *J. Phys. Chem.* **1983**, *87*, 1960.
[23] L. P. Hammett, *J. Am. Chem. Soc.* **1937**, *59*, 96.
[24] Y. P. Tsentalovich, L. V. Kulik, N. P. Gritsan, A. V. Yurkovskaya, *J. Phys. Chem. A* **1998**, *102*, 7975.
[25] D. V. Avila, C. E. Brown, K. U. Ingold, J. Lusztyk, *J. Am. Chem. Soc.* **1993**, *115*, 466.
[26] A. A. Gorman, G. Lovering, M. A. J. Rodgers, *J. Am. Chem. Soc.* **1979**, *101*, 3050.
[27] N. J. Turro, G. F. Lehr, J. A. Butcher, R. A. Moss, W. Guo, *J. Am. Chem. Soc.* **1982**, *104*, 1754.
[28] P. C. Wong, D. Griller, J. C. Scaiano, *Chem. Phys. Lett.* **1981**, *83*, 69.
[29] K. N. Houk, N. G. Rondan, J. Mareda, *J. Am. Chem. Soc.* **1984**, *106*, 4291.
[30] K. N. Houk, N. G. Rondan, *J. Am. Chem. Soc.* **1984**, *106*, 4293.
[31] P. S. Skell, M. S. Cholod, *J. Am. Chem. Soc.* **1969**, *91*, 7131.
[32] A. A. Gorman, G. Lovering, M. A. J. Rodgers, *J. Am. Chem. Soc.* **1979**, *101*, 3050.

Chapter 3

Solvent Polarity Affects H–Atom Abstractions from C– H Donors

Chapter 3

3. Solvent Polarity Affects H–Atom Abstractions from C–H Donors

Corresponds to:

El–Sheshtawy H. S., Pischel U., Nau W. M., "Solvent Polarity Affects H Atom Abstractions from C–H Donors, *Org. Lett.* **2011**, 13, 2694–2697. **(Appendix II)**

3.1 Introduction

Alkoxyl ($RO^{\bullet}$) radicals are important intermediates in the (photo)chemical pathway for the tropospheric oxidation of aliphatic and aromatic volatile organic compounds.[1, 2] They are the primary products of homolytic cleavage of a wide variety of precursors such as peroxides,[3] nitrates,[4] nitrites,[5] hyponitrites,[6, 7] and hypohalites.[8] In the atmosphere, RO• radicals are formed by two ways: the first root is the reaction of small peroxy radicals with NO according to Equation 1. This reaction can only occur at high NO_x levels, while at low levels the peroxy radicals recombine under elimination of molecular oxygen to form the corresponding alkoxyl radicals (Equation 2).

$$RO_2^{\bullet} + NO \longrightarrow RO^{\bullet} + NO_2 \qquad (1)$$

$$2\ RO_2^{\bullet} \longrightarrow 2\ RO^{\bullet} + O_2 \qquad (2)$$

Under atmospheric conditions, the fate of alkoxyl radicals takes place through three different competing reactions: (1) the decomposition of the radical to the corresponding carbonyl compound, (2) the reaction with molecular oxygen, which is dominant, and (3) the isomerization process (intramolecular H–atom transfer).[9, 10] Therefore, during the photochemical degradation of volatile organic

compounds, the relative contribution of these competing reaction routes of the alkoxyl radicals determines, to a large extent, the photochemical products.

3.1.1 Intramolecular H–Atom Transfer (Isomerization)

If the alkoxyl radicals have an H atom at the 4th position relative to the alkoxy O atom, one plausible degradation root for these radicals occurs by an isomerization by 1,4 hydrogen atom shift. This process occurs via a six–member transition state to form 4–hydroxyalkyl radicals (Scheme 3.1).[2] The smallest alkoxy radical prone to the 1,4 H atom shift is the 1–butoxyl radical. Although most of the rate constants of the isomerization processes for several alkoxyl radicals have been reported, mostly relative to their scavenging rate by molecular oxygen,[9, 11] there are several theoretical data concerning the isomerization process for alkoxy radicals.[12, 13]

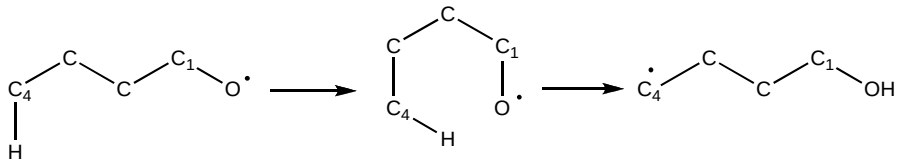

Scheme 3.1: Proposed transition state in alkoxy radical isomerization.

3.1.2 Solvent Effect on Intermolecular H–Atom Transfer

Hydrogen–atom abstraction (H abstraction) reactions, particularly by alkoxyl radicals have attracted considerable interest due to their importance in biological and chemical processes.[14-17] Radical reactions are known to have a small and in some cases negligible solvent effect. This is in contrast to ionic reactions, which are highly sensitive to the environment. However, the hydrogen abstractions from phenols by alkoxyl radicals are exceptional.[18] In detail, the hydrogen atom abstractions from phenols by alkoxyl radical proceed with lower rate constants especially in hydrogen–bond–donating solvents. This has been attributed to the reactivity of the substrate (XOH) towards the radical, influenced by the solvent (S) (Scheme 3.2). This was shown to be the result of deactivation of the substrate towards the radical by acting as hydrogen–bond donor to hydrogen-bond-accepting (HBA) solvent. The hydrogen bonded XOH---S species is unreactive towards the radical and the reaction proceeds

only with the free (non-hydrogen-bonded) substrate XOH. Therefore, the net result is a lower rate of hydrogen–atom transfer from the hydrogen–atom donors to the radical in the hydrogen–bonding accepting solvents.

While kinetic solvent effects (KSEs) for phenols and amines (hydrogen donors) and hydroxyl radicals (H–abstracting species) in protic solvents are pronounced and well documented in the literature,[18, 19] the effect of solvent polarity on the H atom abstraction by carbon-centered radicals from C–H donors is still under controversial discussion.[19] Unlike the H atom abstraction from O–H donors by alkoxyl radicals, which shows a significant solvent effect, the H–atom abstraction from C–H donors has been claimed to be solvent-polarity independent.[18] This is surprising, since the reactivity of molecules is quite affected by the surrounding environment.[20] For charged molecules, where the interaction with the solvent is pronounced, the influence of the solvent on chemical reactions is very large, particularly for ionic reactions. Only in case of radical reactions, there is a debate whether the solvent effect is significant, for example, the lower rate constant of O–H atom abstraction by radicals in polar solvents, or insignificant, such as claimed for some H–atom abstractions from C–H by alkoxyl radicals.[21]

The first example of a solvent effect on an H atom abstraction from C–H bond by oxygen centered radicals has been reported by Sakurai and Hosomi.[22] They reported a slower rate constant of H atom abstraction by the oxygen-centered *tert*–butoxyl radical from C–H donors (toluene) in polar solvents. However, the claim of solvent-polarity independent H atom abstraction rate constant remained in the literature.[18, 19]

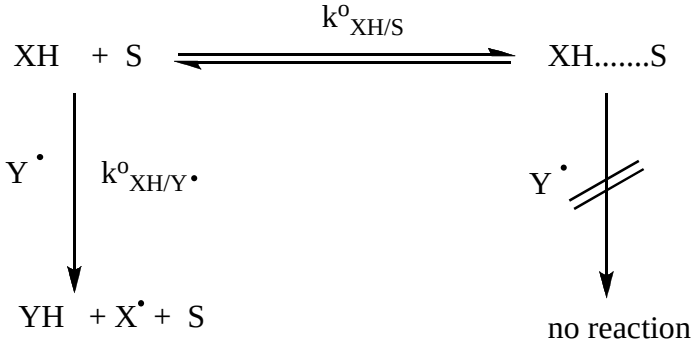

Scheme 3.2: Kinetic solvent effect (KSE) for hydrogen atom abstraction from O–H bonds (phenols) proposed by Ingold.[18]

In 2007, Nau *et al* [21] have reported two comprehensive experimental data sets, which led to the conclusion that there is small, but significant effect of the solvent polarity on the rate constant of H atom abstractions from C–H donors. In addition, the solvent effect can become even larger for specific reactive intermediates relative to the gas phase. The slower reaction rate with increasing solvent polarity was confirmed for both *tert*–butoxyl and cumyloxyl radicals as hydrogen acceptors as well as for n,π*-excited 2,3–diazabicyclo[2.2.2]oct–2-ene (DBO), a model for the persistent 2,2–diphenyl–1–picrylhydrazyl radical (DPPH).

The effect of slower rate constants with increasing solvent polarity the so–called "inverted KSE" as compared to that for electron transfer, where faster reactions in polar solvents are common, has been used by Lanzalunga and co–workers as an indicator to unravel mechanistic details of DPPH scavenging by *N*,*N*–dimethylaniline derivatives.[15] Moreover, the observed KSEs in the intramolecular hydrogen abstractions from benzylic C–H by alkyl radicals gives another example of dominance KSEs.[16]

Although several data sets on solvent effects, spanning more than one order of magnitude variation in rate constants, have become available, the notion that H–atom abstractions from C–H donors show no environmental dependence has persisted in the chemical literature. Recently, Bietti and Salamone, have again claimed the absence of KSEs on the H atom abstraction reaction from 1,4–cyclohexadiene by cumyloxyl radicals.[19] Therefore, in this work, we are further supporting the existence of KSEs on H atom abstractions from C–H donors experimentally and, for the first time, through high–level theoretical calculations.

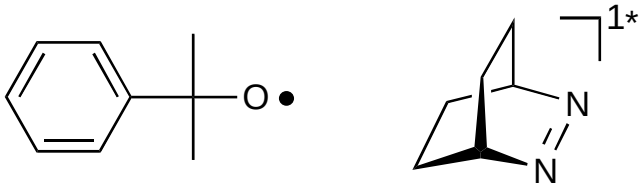

Scheme 3.3: Structures of the hydrogen-abstracting species, the cumyloxyl radical and singlet–excited DBO.

The aim of this work is to validate and reproduce the previously reported data by our group for the persistence of the KSE.[21] In order to do so we selected the same hydrogen abstracting species (the cumyloxyl radical and DBO, cf. Scheme 3.3) and the same sets of hydrogen donors. In addition, we used a binary solvent mixture to

allow the continuous variation of solvent polarity. We selected acetonitrile (CH_3CN) and ethylacetate (EtOAc), because (*i*) these two non–viscous solvents are miscible in all proportions, (*ii*) the intrinsic lifetime ($t_0 = 1/k_0$) of the hydrogen–abstracting species is comparable in these two solvents (620 *versus* 670 ns for singlet–excited DBO, and 0.97 *versus* 1.20 μs for cumyloxyl radicals in EtOAc and CH_3CN, respectively), thereby minimizing artifacts from measurements on different instrumental time scales and/or quencher concentrations, (*iii*) they differ significantly in solvent polarity ($E_T(30)$ = 38.1 for EtOAc and 45.6 for CH_3CN),[20] (*iv*) their polarizability are comparable (refractive index, n_D = 1.372 for EtOAc and 1.344 for CH_3CN),[20] and (*v*) they are both *aprotic* and possess essentially the same hydrogen-bond acceptor properties (β_2^H = 0.45 for EtOAc and 0.44 for CH_3CN);[23] variations of the latter have been held responsible for the inverted KSE in H atom abstractions from phenols.[23-25]

Cumyloxyl radicals were generated by laser flash photolysis at 308 nm from dicumylperoxide in aerated solution and monitored at 485 nm (maximum absorption peak).[26] The transient decays (Figure 3.1) were fitted according to monoexponential functions at different hydrogen donor concentrations, [HD]. The observed rate constants (k_{obs}) were plotted with respect to [HD] according to Equation 3,

$$k_{obs} = k_0 + k_H[HD] \qquad (3)$$

and the hydrogen abstraction rate constant (k_H) values were determined from the slope (cf. inset in Figure 3.1). On the other hand, the fluorescence lifetime decays of singlet-excited DBO (λ_{exc} = 373 nm) in deaerated solution was monitored at 450 nm by time correlated single-photon counting. The monoexponential decays (Figure 3.2) afforded the fluorescence lifetime in the absence (τ_0) and presence (τ) of hydrogen donor. The data were plotted according to Equation 4,

$$\tau_0/\tau = 1 + k_H\tau_0[HD] \qquad (4)$$

where the slope of the fitted date in Equation 4 provided the k_H values (cf. inset in Figure 3.2).

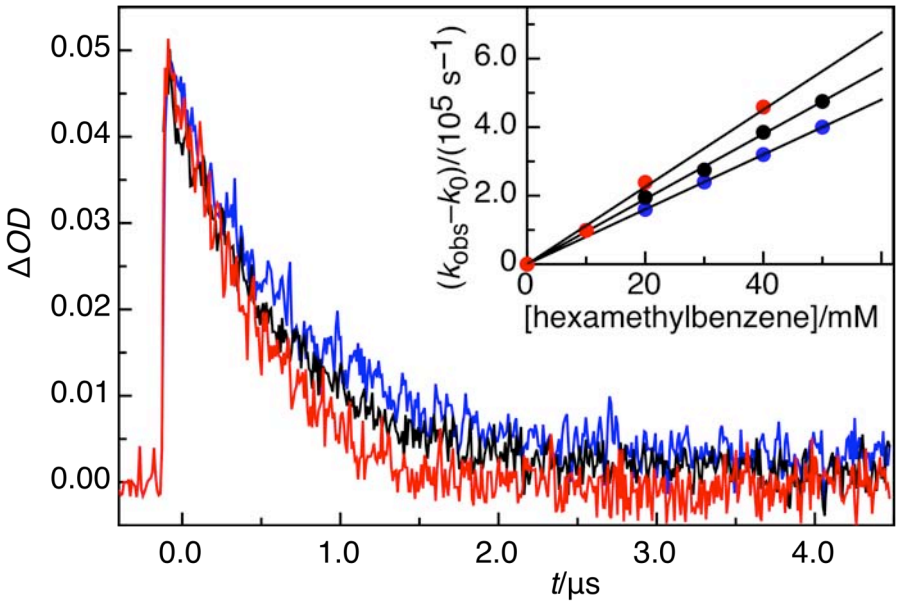

Figure 3.1: Transient absorption decays of cumyloxyl radicals in aerated CH_3CN (blue), EtOAc/CH_3CN (50/50, black), and EtOAc (red) in the presence of hexamethylbenzene (40 mM). The inset shows the corresponding kinetic plots.

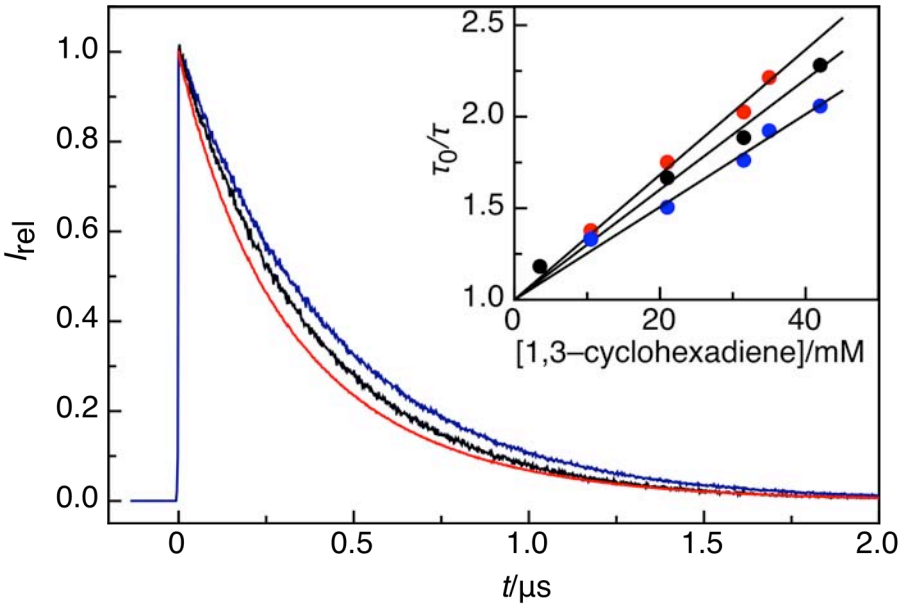

Figure 3.2: Fluorescence lifetime decays of DBO in deaerated CH_3CN (blue), EtOAc/CH_3CN (50/50, black), and EtOAc (red) in the presence of 1,3–cyclohexadiene (31 mM). The inset shows the corresponding kinetic Stern–Volmer plots.

Table 3.1: Scavenging Rate Constants for Cumyloxyl Radicals

Scavenger	k_H/ (10^7 $M^{-1}s^{-1}$)[a]	
	EtOAc	CH_3CN
1,4-cyclohexadiene	6.5	6.2
2,5-dihydrofuran	6.5	6.0
Tetrahydrofuran	0.72	0.55
hexamethylbenzene	1.1	0.80

[a] Error ± 5%; data reproducibility ±10%.

The determined H atom abstraction rate constants (k_H) from several H–donors by both the cumyl radical and DBO in acetonitrile and ethylacetate are listed in Tables 3.1 and 3.2. The data reveals a slower H–atom abstraction by the cumyloxyl radical and DBO in acetonitrile than in the less polar ethylacetate. The systematic dependence obtained upon continuous variation of the solvent polarity (Figure 3.3 and 50/50 entries in Table 3.2) provides further circumstantial evidence. Chemical intuition suggests that any chemical reaction is sensitive to the medium.[20] For H abstractions from C–H bonds the effects are small, but in favor of a higher reactivity in nonpolar solvents. Recently, we have attributed the KSE to a selective stabilization of the reactants.[21, 27]

Table 3.2: Fluorescence Quenching Rate Constants for DBO

quencher	k_q/ (10^7 $M^{-1}s^{-1}$)[a]		
	EtOAc	EtOAc/CH_3CN (50/50)	CH_3CN
1,3–cyclohexadiene	5.5	4.3	3.6
1,4–cyclohexadiene	2.4	2.0	1.8
2,3–dihydrofuran	1.8	1.4	1.2
2,5–dihydrofuran	2.3	1.9	1.5
hexamethylbenzene	2.2	1.7	1.4

[a] Error ± 5%; data reproducibility ±10%.

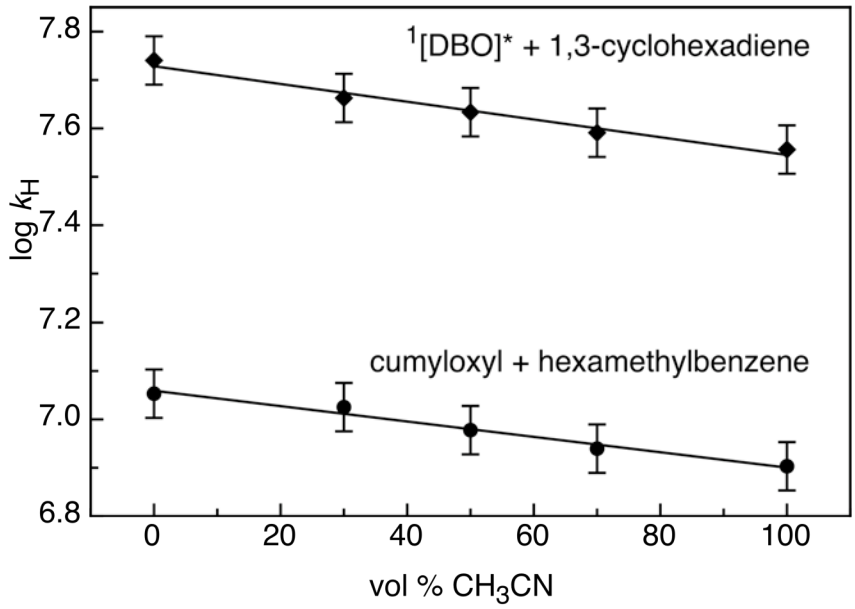

Figure 3.3: Plots of log *k versus* the composition of a binary EtOAc/CH_3CN mixture.

In order to support our experimental results, we have performed high-–level quantum–chemical calculations, which were most conveniently accessible for the ground–state reactions of the cumyloxyl radical. We selected density–functional theory (UB3LYP) due to its known robust performance for treating radical reactions.[28, 29] A high basis set (6–311++G**) was chosen to achieve high accuracy; in particular, diffuse functions are known to be indispensable to reproduce solvation effects, and those for H were included since this atom is being transferred.[28, 30]

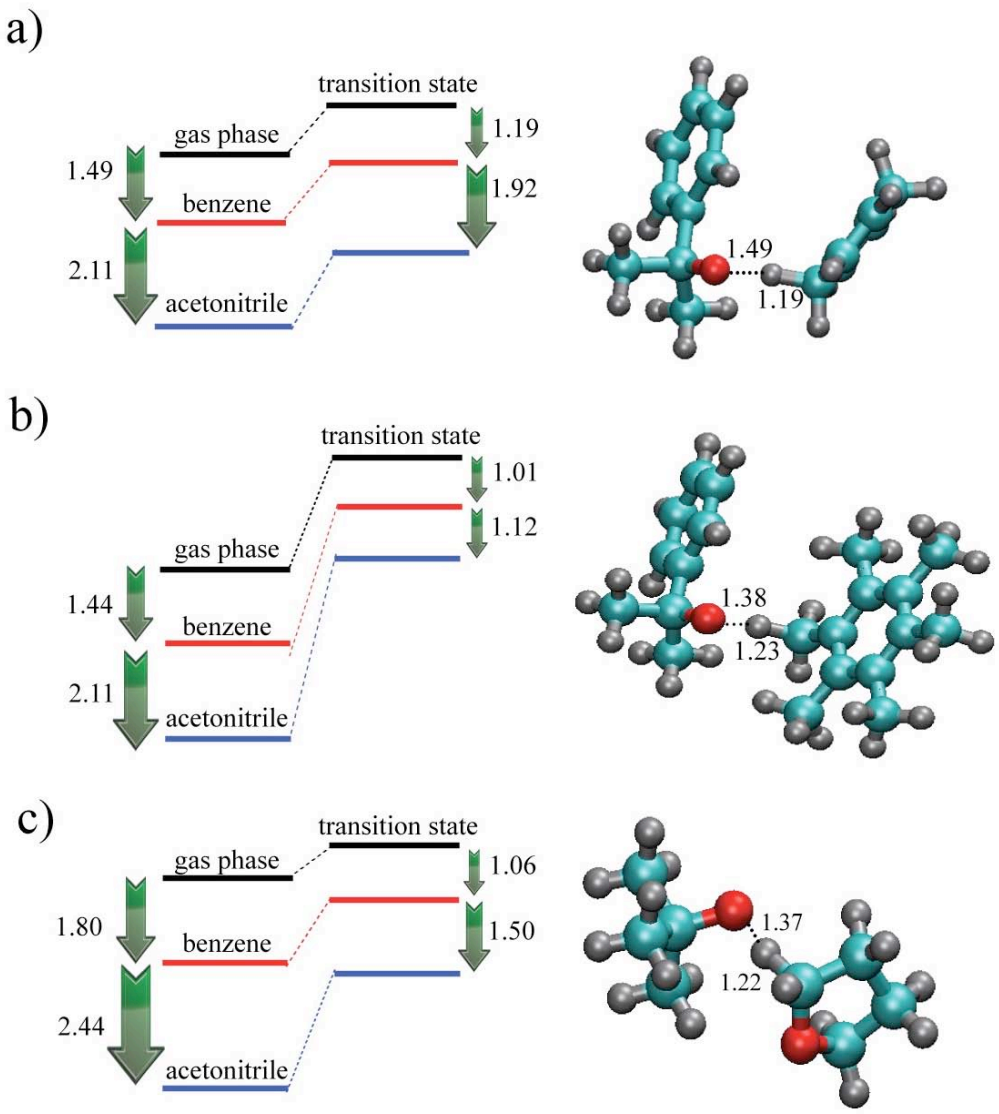

Figure 3.4: Optimized (B3LYP/6–311++G**) transition–state structures and solvation energies of the reactants and the transition state for the scavenging of the cumyloxyl radical by a) 1,4–cyclohexadiene and b) hexamethylbenzene as well as c) for the scavenging of the *tert*–butoxyl radical by tetrahydrofuran.

The transition states for H–atom abstraction in the gas phase were optimized (Figure 3.4) and their identity verified through the occurrence of a single imaginary frequency (that for stretching along the O---H---C coordinate for H abstraction). The resulting activation enthalpies in the gas phase are shown in Table 3.3. Solvation energies were calculated by a continuum description of the solvent based on the self–consistent restricted field (SCRF) method; the polarized continuum model (PCM)[28, 30] with a UAHF cavity was employed. Values were obtained (including geometry optimization at the stationary points) for nonpolar benzene ($E_T(30)$ = 34.3)[20] and

polar acetonitrile (Table 3.3), two solvents for which also a significant amount of experimental reactivity data exists.

Table 3.3: Calculated Activation Enthalpies[a] for Cumyloxyl Radical Scavenging in Different Solvents

Scavenger	calc. $E_a^{\ddagger}$/(kcal mol^{-1})		
	gas phase	benzene	acetonitrile
1,4-cyclohexadiene	1.42	1.72	1.91
2,5-dihydrofuran	1.28	1.77	2.23
tetrahydrofuran	2.59 [1.16][b]	2.98 [1.90][b]	4.08[2.25][b]
hexamethylbenzene	2.86	3.29	4.29

[a] UB3LYP/6–311++G** level of theory; values include thermal enthalpy corrections at 298.15K as well as zero–point energy (ZPE) corrections. [b] Values for the *tert*–butoxyl radical are given in brackets.

Experimental activation energies for C–H abstractions are scarce and limited to the *tert*–butoxyl radical, mostly in nonpolar benzene/di–*tert*–butyl peroxide (1/2) solution.[10, 31-33] The absolute order–of–magnitude agreement between calculated values and reported experimental activation energies (e.g., 2.5 and 3.5 kcal mol^{-1} for tetrahydrofuran and toluene) were nevertheless gratifying to observe. The calculated solvation effects are compelling in that they reveal without a single exception an increase in activation enthalpy upon going from the gas phase to benzene to acetonitrile. Most importantly, the close inspection of the solvation energies for each hydrogen donor reveals invariably larger values for the reactants than the transition states (Figure 3.4 and Appendix III). The reactants do therefore experience a selective stabilization by the (polar) solvent, which accounts adequately for the observed trend in absolute activation energies as well as rate constants.

A comparative calculation for H abstraction from tetrahydrofuran by the extensively investigated *tert*–butoxyl radical,[10, 31, 34] revealed the same trends in activation energies (Table 3.3) and solvation effects (Figure 3.4c). The theoretical findings do therefore fully support our originally tentative explanation based on the Kirkwood continuum model.[20, 21, 27] The trend of the calculated activation enthalpies is fully consistent with the observed lower reactivity towards H abstraction in polar solvents (inverted effect). Also the order of magnitude of the solvent effects is well

reproduced: if one assumes constant pre–exponential factors for a particular H donor, the absolute variation of the activation energies in dependence on the medium would correspond to about a factor of 2–5 difference between the different media (*ca.* 0.5–1 kcal mol^{-1}). Theoretical predictions and experimental measurements expose therefore jointly that kinetic solvent effects on H abstractions by alkoxyl radicals from C–H donors are small, but significant, and, whenever observed, they are inverted. The effects, which originate from a selective stabilization of the reactants, become more obvious in protic solvents with phenolic H donors,[24, 35, 36] but they are offset only in exceptional cases, in which a specific solvation of the transition state competes.[37]

References

[1] R. Atkinson, E. S. C. Kwok, J. Arey, S. M. Aschmann, *Faraday Discuss.* **1995**, *100*, 23.
[2] R. Atkinson, *Int. J. Chem. Kinet.* **1997**, *29*, 99.
[3] O. M. Zarechnaya, I. A. Opeida, A. F. Dmitruk, *Russ. J. Organ. Chem.* **2001**, *37*, 1405.
[4] A. Matsunaga, P. J. Ziemann, *Proc. Nat. Acad. Sci. USA* **2010**, *107*, 6664.
[5] M. D. Paredes, R. Alonso, *J. Org. Chem.* **2000**, *65*, 2292.
[6] G. D. Mendenhall, L. C. Stewart, J. C. Scaiano, *J. Am. Chem. Soc.* **1982**, *104*, 5109.
[7] D. V. Avila, K. U. Ingold, A. A. Di Nardo, F. Zerbetto, M. Z. Zgierski, J. Lusztyk, *J. Am. Chem. Soc.* **1995**, *117*, 2711.
[8] A. Padwa, *J. Org. Chem.* **2009**, *74*, 6421.
[9] P. Devolder, *J. Photochem. Photobiol. A-Chem.* **2003**, *157*, 137.
[10] M. Finn, R. Friedline, N. K. Suleman, C. J. Wohl, J. M. Tanko, *J. Am. Chem. Soc.* **2004**, *126*, 7578.
[11] A. Heiss, K. Sahetchian, *Int. J. Chem. Kinet.* **1996**, *28*, 531.
[12] M. A. Ferenac, A. J. Davis, A. S. Holloway, T. S. Dibble, *J. Phys. Chem. A* **2003**, *107*, 63.
[13] O. Kysel, S. Budzak, M. Medved, P. Mach, *Polym. Degrad. Stabil.* **2011**, *96*, 660.
[14] G. Hörner, A. Lewandowska, G. L. Hug, B. Marciniak, *J. Phys. Chem. C* **2009**, *113*, 11695.
[15] E. Baciocchi, A. Calcagni, O. Lanzalunga, *J. Org. Chem.* **2008**, *73*, 4110.
[16] C. B. DeZutter, J. H. Horner, M. Newcomb, *J. Phys. Chem. A* **2008**, *112*, 1891.
[17] G. Litwinienko, A. L. J. Beckwith, K. U. Ingold, *Chem. Soc. Rev.* **2011**, *40*, 2157.
[18] G. Litwinienko, K. U. Ingold, *Acc. Chem. Res.* **2007**, *40*, 222.
[19] M. Bietti, M. Salamone, *Org. Lett.* **2010**, *12*, 3654.
[20] C. Reichardt, *Solvents and Solvent Effects in Organic Chemistry*, 3rd ed., Wiley-VCH, Weinheim, Germany, **2003**.
[21] A. L. Koner, U. Pischel, W. M. Nau, *Org. Lett.* **2007**, *9*, 2899.
[22] H. Sakurai, A. Hosomi, *J. Am. Chem. Soc.* **1967**, *89*, 458.

[23] P. A. MacFaul, K. U. Ingold, J. Lusztyk, *J. Org. Chem.* **1996**, *61*, 1316.
[24] D. W. Snelgrove, J. Lusztyk, J. T. Banks, P. Mulder, K. U. Ingold, *J. Am. Chem. Soc.* **2001**, *123*, 469.
[25] M. F. Nielsen, K. U. Ingold, *J. Am. Chem. Soc.* **2006**, *128*, 1172.
[26] D. V. Avila, K. U. Ingold, A. A. Di Nardo, F. Zerbetto, M. Z. Zgierski, J. Lusztyk, *J. Am. Chem. Soc.* **1995**, *117*, 2711.
[27] W. M. Nau, U. Pischel, *Angew. Chem. Int. Ed.* **1999**, *38*, 2885.
[28] V. Thavasi, R. P. A. Bettens, L. P. Leong, *J. Phys. Chem. A* **2009**, *113*, 3068.
[29] A. K. Chandra, T. Uchimaru, *J. Phys. Chem. A* **2000**, *104*, 9244.
[30] Y. Wang, X. Cheng, X. Yang, X. Yang, *J. Solut. Chem.* **2006**, *35*, 869.
[31] P. K. Das, M. V. Encinas, S. Steenken, J. C. Scaiano, *J. Am. Chem. Soc.* **1981**, *103*, 4162.
[32] V. Malatesta, J. C. Scaiano, *J. Org. Chem.* **1982**, *47*, 1455.
[33] S. Li, W. Y. Fan, *Chem. Phys. Lett.* **2006**, *427*, 276.
[34] C. Aliaga, D. R. Stuart, A. Aspée, J. C. Scaiano, *Org. Lett.* **2005**, *7*, 3665.
[35] R. E. Galian, G. Litwinienko, J. Pérez-Prieto, K. U. Ingold, *J. Am. Chem. Soc.* **2007**, *129*, 9280.
[36] M. Salamone, G. Anastasi, M. Bietti, G. A. DiLabio, *Org. Lett.* **2011**, *13*, 260.
[37] S. Mitroka, S. Zimmeck, D. Troya, J. M. Tanko, *J. Am. Chem. Soc.* **2010**, *132*, 2907.

Chapter 4

Catalytic Oxidation of Iodide by Peroxidases: A Supramolecular Tandem Assay for Monitoring Peroxidase Activity

Chapter 4

4. Catalytic Oxidation of Iodide by Peroxidases: A Supramolecular Tandem Assay for Monitoring Peroxidase Activity

4.1 Supramolecular Host–Guest Assemblies

Supramolecular chemistry has emerged as an important research area in chemistry and offered an interdisciplinary contact between biology and material science.[1] Nobel laureate (1987) Jean–Marie Lehn, defined supramolecular chemistry as the "chemistry beyond molecules", where non–covalent forces and spatial arrangements between interacting individual molecules play a major role in the formation of these entities.[2-4] In contrast to traditional molecular chemistry, where molecules interact or combine through bond breaking or bond formation, supramolecular chemistry deals with non–covalent interactions between molecules. Among noncovalent forces, electrostatic interactions (ion–ion, ion–dipole, and dipole–dipole), π–π stacking interactions, cation–π interactions, van der Waals forces, hydrophobic interactions, hydrogen bonding, and halogen bonding are common examples. Unlike covalent interactions, these modes of binding are weak and usually reversible, a property which is crucial for biological processes, such as cellular recognition, ion transport, antibody–antigen interactions, enzymatic catalysis, and DNA replication.[2, 5] In my Ph.D thesis, some of these interactions, for example, hydrogen and halogen bonds that are related to my work will be discussed in detail,.

4.2 Driving Forces for Host–Guest Interactions

4.2.1 Hydrogen Bond

Hydrogen bond (HB) is a non–covalent interaction in which hydrogen atom is shared between a donor (D) and an acceptor (A) and the D–H–A angle is close to 180° (Scheme 4.1–a).

a)

HB: D–H – – –A

b)

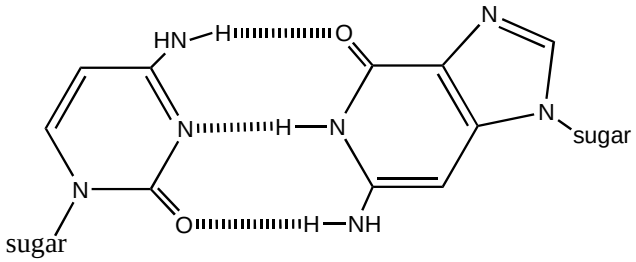

cytosine (C) guanine (G)

Scheme 4.1: a) illustration of a hydrogen bond, and b) a representative model for two DNA pairs held together by hydrogen bonds.

The strength of the HB (4–120 kJ Mol^{-1}) is comparable to that of electrostatic interactions. The importance of HB in supramolecular chemistry is well documented in the literature.[6-8] Perhaps the most important example of HB is the self–assembly of two DNA helical strands held together by HB to form a helical structure (Scheme 4.1–b).[9] Another example of host–guest assembly is the resistance of the anti–tuberculosis drug isoniazid to acylation by forming HB with the oxygen atoms of the carbonyl group existing on the portal of CB*n*, for example, Cucurbit[6]uril and Cucurbit[7]uril.[10]

4.2.2 Halogen Bond

In analogy to HB, halogen bond (XB) is formed by a non–covalent interaction where the halogen atom (X) is shared between a donor (D) and an acceptor (A) (Scheme 4.2–a).

a) b)

XB : D – X – – – – A

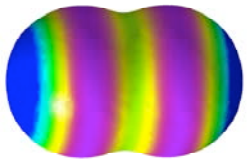

Scheme 4.2: a) representative model for halogen bond, and b) an electrostatic potential map of iodine calculated with B3LYP/3-21G* level, which shows a positive pole at the extreme sides of the molecule (blue).

The halogen atom (X) can be chlorine, bromine, or iodine and the donor (D) can be oxygen, nitrogen or even another halogen atom. XB is a directional bond and the angle D–X–A is close to 180° and the X–A distance is shorter than the sum of the van der Waals radii of the involved atoms, for example, Cl---O is 3.27 Å, Br---O is

3.37 Å, I---O is 3.50 Å, N---I is 3.53 Å, I---S is 3.78 Å.[11] However, halogen bond is more sensitive to steric hindrance than hydrogen bond is, because of the larger and more polarizable halogen atom compared to hydrogen atom.[12] The recognition of halogen bond was first reported by Benesi and Hildebrand for the interaction of iodine with aromatic hydrocarbons, which was known, at that time, as charge–transfer complexes.[13] Later, it was Hassel in his Nobel prize (1970) speech who pointed out the importance of halogen atom in directing self–assembly phenomena.[14]

The origin of XB stems from the unequal distribution of the partially negative charge on the covalent C–X bond, which results on the positive region of the halogen atoms, referred as σ–hole that increases in the order of Cl < Br < I (Scheme 4.2–b). The strength of XB increases with the electron withdrawing nature of the atom attached to the halogen atom, for example, C(sp)–X > $C(sp^2)$– X > $C(sp^3)$–X. The halogen bond has been reported to play a vital role in crystal engineering,[15-17] enzyme inhibitors,[18] and recently in directing molecular confirmation of DNA.[19]

The extensive studies exploring the driving forces responsible for host–guest interactions and the increasing understanding towards the mechanisms of complexation, have allowed supramolecular chemistry to mimic the weak non–covalent interactions and molecular recognition processes, which are ubiquitous in living biological systems. Therefore, the efforts have been directed towards carefully designed artificial receptor (host) molecules, which are capable to selectively recognize the substrate (guest) molecules. The corner stone in supramolecular host–guest chemistry was the discovery of crown ethers by Pederson .[20, 21] Subsequently, many artificial receptors have been reported, for example cyclodextrins, calixarenes, and recently cucurbiturils. In my thesis, I have worked mainly with the new class of macrocyclic receptors, the cucurbituril family; therefore, I will give a brief introduction about the cucurbiturils focusing on their physical properties.

4.3 Cucurbiturils

Unlike most macrocycles, cucurbit[*n*]urils (CB*n*) are highly symmetric and rigid molecules. In 1900, Rusche under the supervision of Behrend was the first to successfully synthesize a CB sample, which was later investigated for its physical properties and interaction with some inorganic compounds and dyes by Meyer in his Ph.D thesis supervised by Behrend.[22, 23] In 1980, Mock reinvestigated the product compound (white powder), which was synthesized by Behrend, and revealed the CBs cyclic structure.[24] The structure had six glycoluril units connected by methylene bridges (CB6). The dramatically expanded use of CBs as a nanocontainers starts after the preparations of the CBs analogues (*n* = 5, 6, 7, 8, and 10) independently by Kim[25] and Day.[26] In 2004, our group also reported an improved CB7 synthesis procedure (Appendix III).[27]

Cucurbituril resembles a barrel container, with a cavity volume and accessible *via* two portals controlling the barrel entrance. CBs are cyclic methylene–bridged glycoluril oligomers. The glycoluril units (*n*) are repeated and connected together with methylene groups in order to form CB*n* (n = 5, 6, 7, 8, and 10) homologues. CBs are relatively poorly soluble in water; however the solubility increases in concentrated aqueous acid solutions or in the presence of metal ions.[28] CBs are accessible through two carbonyl–lined portals carrying a partial negative charge (Scheme 4.3). The presence of the negative charges on the portals rationalizes the popularity of CBs as a cation–receptor macrocycles. Not only the CBs portals control the preferential guest binding, but the cavity properties regarding the volume size also plays an effective role. The inner cavity volume of CBs has been calculated by different methodologies using a blocking group (graphene–like) to seal the CBs cavity.[29] Among these methods, the inner cavity volume, in which the blocking group penetrates to the plane defined by the portal oxygen nuclei of different CBs is recommended. Note that the cavity volume of the CBs was found to increase dramatically with increasing the number of glycoluril units (Table 4.1).

Table 4.1: Volume and some important physical properties of cucurbiturils

CB*n*	Molecular weight	V [Å^3][29]	Number of H_2O in the cavity[29]	Solubility (mM)[28]
CB5	830	68	2	20–30
CB6	996	142	4	0.018
CB7	1163	242	8	20–30
CB8	1329	367	12	<0.01
CB10	1661	691	-	<0.05

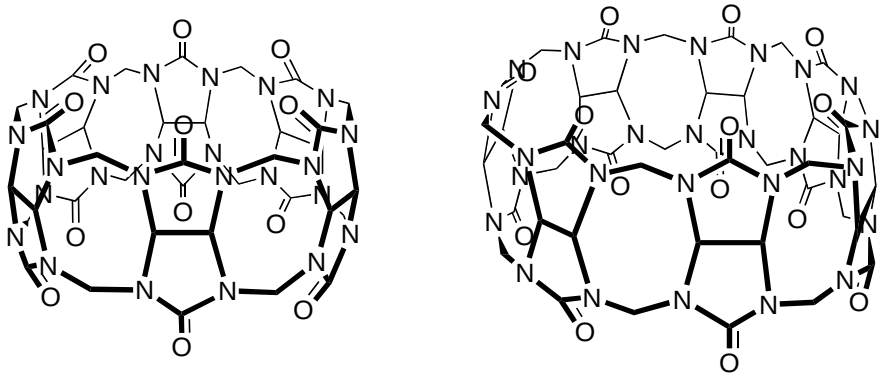

cucurbit[6]uril (CB6) cucurbit[7]uril (CB7)

Scheme 4.3: Chemical structures of cucurbit[6]uril and cucurbit[7]uril.

However, the increase in cavity volume is not always corresponding to an increase in the binding between the guest and the host. The relation between the volume of the guest divided by the volume of the host cavity, which is known as packing coefficient, *PC*, is crucial in binding affinities. Generally, "the 55% solution" proposed by Rebek[30] is associated with the highest binding affinities. The proposed percentage was successfully applied for capsules self–assembly[31, 32] and other closed cavities hosts.[33-35] Recently, the "the 55% solution" role was also transferred to cucurbiturils.[29]

Another important physical property of CBs is their hydrophobic nature. The tendency of the molecules to escape from the solvent, particularly water, to the less polar environment and less polarizable medium is known as hydrophobic effect.

Although, the hydrophobic effect is not a real force, however, it plays an important role in biosystems, for example protein folding and in lipids-bilayer structures. Cucurbiturils are able to accommodate a number of water molecules depending on the cavity size, for example, CB5 houses two water molecules; CB6, four; CB7, eight: that of CB8, twelve (Table 4.1). Upon addition of the guest to an aqueous solution of CBs, the hydrophobic guest tends to replace the high–energy water molecules from the CBs cavities.

In conclusion, despite the poor solubility in water and organic solvents,[28, 36] their exceptional properties and their distinct noncovalent interactions helped different CBs to be used in catalysis,[37] drug delivery,[38, 39] and enzyme assays.[40-43]

4.4 Iodine by the Barrel–On the Macrocyclic Recognition of an Element

Corresponds to:
El–Sheshtawy H. S., Bassil B., Gesing T. M., Kortz U., Nau W. M., "Iodine by the Barrel–On the Macrocyclic Recognition of an Element", in preparation.

— Supporting information correspond to this chapter are collected in **Appendix III**.

4.4.1 Molecular Iodine Binding with Cucurbit[*n*]urils

Molecular iodine (I_2) is known to undergo hydrolysis in aqueous solutions.[44] The most predominant species are I_2, I_3^-, and I^-, which have extinction coefficient values of 740 M^{-1}, 25.000 M^{-1}, 12.600 M^{-1} at 460 nm, 350 nm, and 226 nm respectively.[45-47] In addition, I_2 has an additional absorption band at 353 nm with an extinction coefficient of 35 M^{-1}.[47]

Upon adding successive amounts of CB*n* (*n* = 6 and 7) to I_2 solution, the 460 nm peak exhibits a bathochromic shift to 485 and 517 nm for CB6 (in the presence of 0.1 M Na_2SO_4) and CB7, respectively. The resulting CBs•I_2 complexes showed a hypochromic (by 20% for CB6 and 18% for CB7) and bathochromic shift (25 nm for CB6 and 57 nm for CB7) (Figure 4.1). The shift for CB7 is spectacular, switching between the two extreme characteristic colors of iodine, namely from yellow–brown to violet (Figure 4.1, photograph). The change in the color is equivalent to the change from a lone–pair donating to nonpolar solvents. The hypochromic shift by CB7 could be reverted by the addition of a competitive molecule (1–adamantanecarboxlic acid) (Appendix III). The peak shift is followed by a concurrent decrease of the 350 nm peak till its disappearance at the maximum concentration of both CB7 and CB6 (Figure 4.1), which indicates the inclusion of molecular iodine into CBs cavities. The fading of the band at 350 nm clearly shows that CB*n* suppress the formation of I_3^- in contrast to cyclodextrins, which shows a higher affinity towards I_3^- than to I_2, for example, α–cyclodextrin (Appendix III).

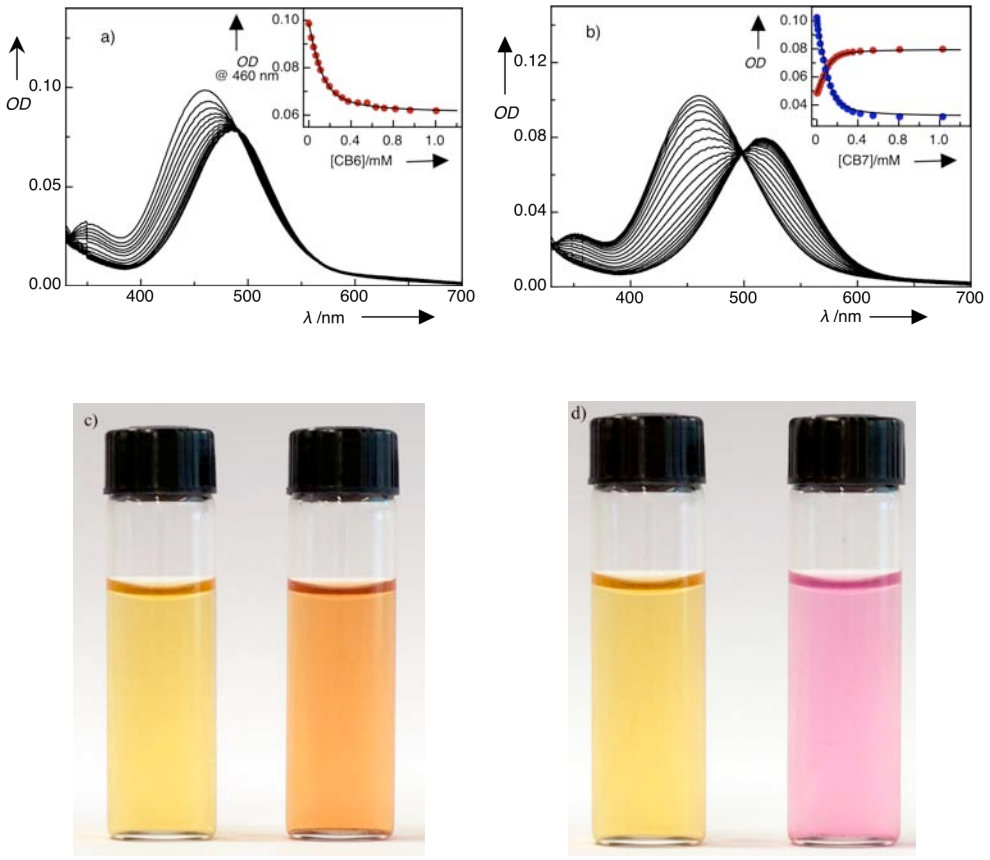

Figure 4.1: UV-Vis titrations of iodine (0.1 mM) upon addition of a) CB6 and b) CB7 in aqueous solution (0.1 M Na_2SO_4 for CB6). The insets show the titration curves fitted according to 1:1 binding model. The visible color change (photograph) of iodine in the absence (left vial) and presence of hosts (right vial) for c) CB6 and d) CB7 complexes.

The solution color change (yellow to violet) and the red shift of the 460 nm band supports Cram′s famous hypothesis that the inner space of such molecular container compounds behave as a new phase of matter.[48] From the change of the optical density of I_2 at 460 nm, the binding constant of CB7•I_2 complex $(5.6 \pm 0.9) \times 10^4$ M^{-1} in aqueous solution (pH 3.3) was obtained. In the case of CB6•I_2 the experiment was performed in 0.1 M Na_2SO_4 due to solubility limitations and the binding is $(2.4 \pm 0.14) \times 10^4$ M^{-1} assuming 1:1 host-guest complexation (Table 4.2). Isothermal titration calorimetry (ITC) was employed for the determination of the complex stoichiometry and binding with CBs, which proved to be 1:1, and of the binding constants values in Table 4.2. Surprisingly, the ITC data reveals I_2 binding values by CB6 in H_2O $(1.35 \pm 0.1 \times 10^6$ $M^{-1})$, which are among the largest observed for neutral guest binding[29, 49]and among the largest ones observed for supramolecular receptors for iodine in general, being reached only by α–CD•I_2 complexes.[50-52] The formation

of a 1:1 inclusion complex was independently corroborated by displacement experiments with guests and fluorescent dye (DAPI), which are well known to form inclusion complexes with CB7 (Appendix III).

Data in Table 4.2 reveals that the host–guest complexation between iodine and CBs are enthalpically–driven due to the hydrophobic effect,[29, 53] accompanied with entropic penalty due to the loss of conformational degrees of freedom. In the CB7 host, the iodine guest is less confined than in CB6, therefore the observed entropy is more favorable (Table 4.2). The results measured in the presence of salts (0.1 M Na_2SO_4) always show lower binding constants due to the influence of ions, which often act as competitors for the cucurbituril macrocycles.[40, 41, 54]

Furthermore, mass spectrometry has been used to provide evidence for the encapsulation of molecular iodine with CB6 in presence of Cs^+ ions. The m/z peaks at 630.9 and 757.9 clearly shows the presence of the CB6•2Cs^+ and CB6•I_2•2Cs^+ species respectively (Appendix III). The addition of either CB5 or CB8 to I_2 solution did not cause any change in the UV–Vis spectra, which suggest that these macrocycles were either too small or too large to effectively bind. *Ab initio* (HF/3–21G*) calculations, with fixing geometry of the highly symmetric CBs and only I_2 left to optimize, shows that iodine encapsulation inside CB6 favors the axial conformation by –13.5 kcal mol^{-1}. For the CB7•I_2 complex the axial conformation is favorable by only –2.4 kcal mol^{-1}. Interestingly, the single point calculations (with higher level) on the same optimized structures (MP2/3–21G*//HF/3–21G*) predict the axial form of CB6•I_2 to be thermoneutral (+0.04 kcal mol^{-1}) with the equatorial geometry, a small energy difference, which could be easily tipped in favor of the axial orientation by the additional halogen–bonding interactions with a water molecule as they are expected in aqueous solution. In contrast, the single point calculations (MP2/3-21G*//HF/3-21G*) on CB7•I_2 optimized structures show that equatorial conformations are favorable (–3.6 kcal mol^{-1}) (Figure 4.2 and Appendix III).

Table 4.2: Stability constants (K_a), and thermodynamic values for the complex formation between iodine and CBs at pH 3.3.

Host	K_a/ (M^{-1})		ΔG°/ (kJ mol^{-1})	ΔH°/ (kJ mol^{-1})	TΔS°/ (kJ mol^{-1})
	UV	ITC[a]			
CB*n*•I_2 in H_2O					
CB6	–	$(1.35\pm0.11)\times10^6$	−34.86 (± 0.20)	−64.81 (± 3.41)	−29.65 (± 3.25)
CB7	$(5.6\pm0.9)\times10^4$	$(1.00\pm0.01)\times10^5$	−28.45 (± 0.02)	−31.49 (± 1.27)	−2.88 (± 1.29)
CB*n*•I_2 in 0.1 M Na_2SO_4					
CB6	$(2.4\pm0.14)\times10^4$	$(1.04\pm0.33)\times10^4$	−22.79 (± 0.81)	−33.39 (± 1.77)	−10.43 (± 2.57)
CB7	$(5.39\pm0.28)\times10^3$	$(5.55\pm0.78)\times10^4$	−21.29 (± 0.35)	−17.17 (± 1.58)	4.23 (± 0.37)

[a] Mean values measured at 25 °C in aqueous solution, error given as standard deviation (±1σ); for the CB6 titrations dilution is neglected due to low dilution signal.

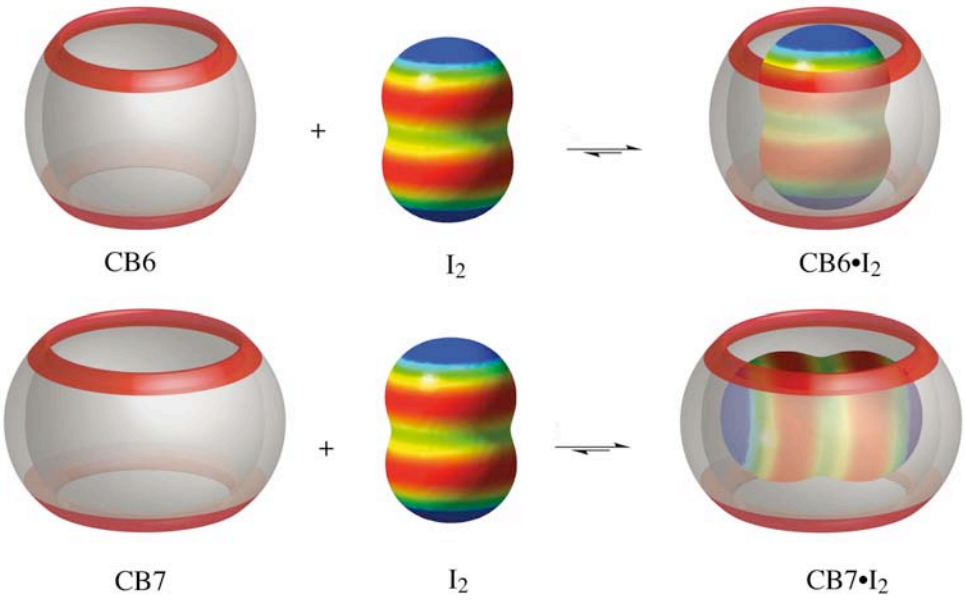

Figure 4.2: Encapsulation of iodine in CB6 and CB7. The schematic host representation shows the carbonyl rims in red. The charge distribution of iodine is shown in the form of calculated electrostatic potential maps at the van der Waals surface (B3LYP/3–21G* level of theory) showing σ–hole with electron deficiency (blue) at the poles of the dihalogen and electron rich equators (red).

The packing coefficients, considering molecular volumes of 71 $Å^3$ for I_2 and 68, 142, 242, and 367 $Å^3$ for the inner cavities of the homologues CBs, amount to 104% for CB5, 50% for CB6, 29% for CB7 and 19% for CB8, which nicely rationalize the trend in complex statiometry and affinity; ideally, about 55% of a macrocycle cavity should be packed to optimize enthalpy, while balancing the entropic factors (Table 4.1 and (Appendix III).[29] The packing of CB6•I_2 complex is therefore essentially ideal, while for the CB7•I_2 complex can be optimized by an equatorial co-conformation of the guest.

Now, the question arises concerning the driving forces behind the encapsulation of the neutral guest (I_2) inside the CBs. Apparently, it is not the electrostatic interaction, as neither I_2 nor CBs are charged, rather it is the quadrupole interaction and the hydrophobic effect, which drives the complexation process.[29] As we discussed earlier (section 4.3), CBs cavities contain a certain number of high-energy-water molecules, 4 molecules inside CB6 and 8 in case of CB7, which can be replaced by the highly polarizable molecular iodine molecule (non classical hydrophobic effect).[29, 53] In addition, optical spectroscopy and crystallographic data (see below) show that the complex of CB6 experience a special type of halogen bonding.

4.4.2 Halogen Bond in CB6•I_2Crystal Structure

A single crystal of CB6•I_2 suitable for X–ray was obtained by the slow evaporation strategy. 7.5 mg of CB6 (1.5 mmole) was dissolved in 5 ml 0.1 M cesium chloride and an organic layer of 8 mg iodine (3.14 mmole) dissolved in ethylether left in contact for two days. A brownish CB6•I_2 crystal suitable for the X–ray characterization was obtained.

Figure 4.3 shows the x–ray crystal structure of CB6•I_2 (see CIF file in Appendix III), which reveals that I_2 fits completely inside CB6. Interestingly, the structure has a water molecule at the lower CB6 rim with strong interaction with I_2, the H_2O---I_2 bond length is 3.11 Å which is much shorter than the sum of van der Waals radii of both O (1.52 Å) and I (1.98 Å) and the I–I---O bond angle is 178°. The I_2 molecule completely immersed inside the CB6 cavity adapts the axial position with

a tilting angle of 12.9° from CB6 axes leans towards three carbonyl portals, keeping the strong interaction with the H_2O molecule.

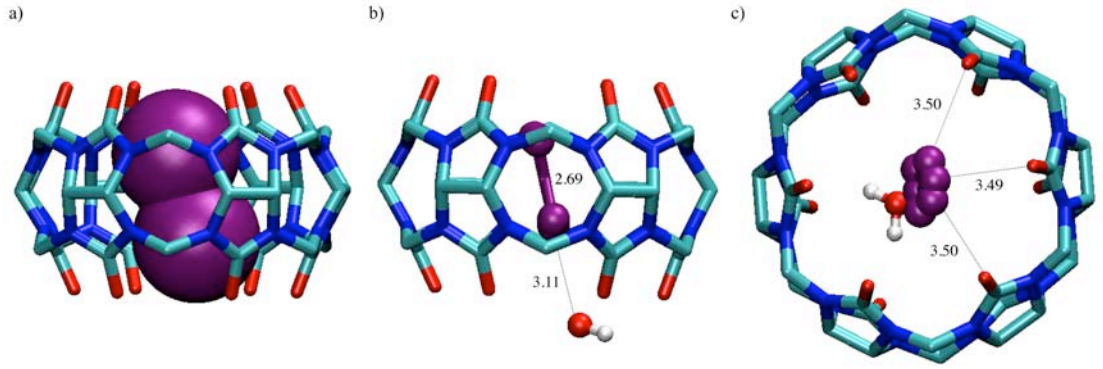

Figure 4.3: View of the crystal structure of the CB6•I_2 complex, showing a) the van der Waals surface of iodine inside the CB6 cavity, b) the halogen bonding with a water molecule near the lower portal, c) the halogen bonding with the carbonyl oxygen at the upper portal.

Carbonyl oxygen atoms have two sources as an electron donor for halogen bond; one is the n electron and the second is the sp^2–hybridized electrons in the π orbital. The halogen bond between H_2O---I_2 is a prototype of the interaction between the n electrons from the heteroatom (O or N) and halogens in terms of the bond angle I–I---O (178°) and the bond length (3.11 Å).[55, 56]

However, molecular iodine interacts with the carbonyl oxygen atoms (70%) at the upper portal and two symmetrically disordered positions for the iodine molecule (each 15%) is observed (see Figure 4.3). The bond distance between iodine and the carbonyl atom is 3.49 Å (70%), which lies at the upper end of the O----I halogen bonds (3.50–3.54 Å), but is very similar to the value of 3.4 Å found in several protein–iodine interactions.[55, 57] For example, the halogen bond in the complex of 3,5–diiodosalicylic acid and human serum albumin (I----C=O) is 3.46 Å, which has been considered to stabilize the structure.[58] The other symmetrically disordered iodine positions (each 15%), are interacting similarly with comparable bond lengths (3.50 Å), confirming the tendency of the upper iodine pole to interact with the carbonyl oxygen π orbital lobes.

Recently, there has been an increasing interest of the halogen bond in biological systems, where on one hand, mainly carbonyl groups serve as donor sites, and on the other hand, the π orbital of the carbonyl group is involved.[59, 60] The evidence has been reported recently by the ability of halogen atom to form both hydrogen bond and halogen bond.[60, 61] Such special type of orthognality has been

referred to as *h*X–bonds. The driving force for such an interaction is that halogen bonding can take place with the carbonyl system while simultaneously involving the lone electron pairs in an orthogonal hydrogen bonding. Hence the *h*X–bonds most likely prefer the occurrence in protic solvents. The halogen bond between CB6 carbonyl groups and I_2 perfectly matches the ideal dihedral angle requirement for carbonyl oxygen π halogen bonds (N–C=O---I dihedral angle is 87–91°).[60] The linearity of the halogen bond slightly deviates from the hydrogen bond (the O---X–X bond angle is 131 – 148° compared to 180° in HB), but this value still falls within the known range of such halogen bonds observed in biological systems.[55, 60, 62] In particular, it is known that the last angle can show substantial deviations in confined structured media.[60, 62] Hence, the interaction between iodine and the carbonyl groups at the upper portal of CB6 in Figure 5 establishes the first non–biological analogue of such *h*X–bond in presence of water molecule.[60]

4.4.3 Iodine as Solvatochromic Probe for Polarizability Inside Cucurbit[*n*]uril Cavity

Solvatochromic probes based on changes in absorption, fluorescence and phosphorescence have the potential to be used for determining polarity and polarizability of solvents, as well as the inner cavities of nano–containers, which are not accessible by direct spectroscopic methods.[29] The change in the fluorescence and absorption bands of dyes, such as Rhodamine 6G, upon encapsulation has been used to determine the CB7 polarity (ca. 48),[63] which is much similar to that of *n*–octanol ($E_T(30)$= 48.1)[64] and much less than that of water (E_T (30)= 63.1).[64] Curcumin has been used as a solvatochromic probe to asses the polarity inside the smaller homologue CB6 and revealed a value of (E_T (30)= 39), also less than water.[65]

Nau *et. al.*[66] have explored the polarizability inside CB7 and have given a detailed explanation for the extremely low value obtained, based on the structure of the macrocycle.[66] As the CBs consist of glycolurils units connected together with methylene groups, the optimized structures show that thes methylene C–H bonds are pointed outside the CBs cavity. Hence there is no electron density inside the cavity, which gives the low polarizability inside the CBs cavities.[29, 66] As a result, molecules that are totally immersed inside CBs cavities experience an extremely low polarizable

environment close to the gas phase. Using the exceptionally long fluorescence lifetime of 2,3–diazabicyclo[2.2.2]oct–2–ene (DBO), 1 μs, the polarizability inside CB7 has been measured (0.12), a value lower than the value of perfluoreohexane (0.159), the lowest non–polarizable solvent.[66]

However, the quality of the reported polarity and polarizability values inside CBs depend largely on the guest confinement inside the host and specific complexation of certain regions of the guest.[29]As we discussed in section 4.3, CB6 and CB7 have a large cavity volume, which are large enough to completely accommodate the I_2 molecule and perhaps completely eliminate the direct contact with the solvent (H_2O). Therefore, I_2 could be used as a solvatochromic probe to evaluate the polarizability inside CB6 and CB7 cavities.

The spectral data for iodine in different environments are compiled in Table 4.3. The data reveals that both the extinction coefficient at the maximum as well as the oscillator strength of the electronic transition is suppressed in both CB6 and CB7. The electronic transition becomes less probable inside the macrocyclic cavities. The extinction coefficient of the visible absorption band of iodine increases systematically with increasing refractive index/polarizability of the solvent (Table 4.3).

Table 4.3: Photophysical properties of iodine in different environments at 298 K

environment	λ_{max} [a] [nm]	ε [$M^{-1}cm^{-1}$]	f [b] [10^{-2}]	n_D [c]	P [d]
Yellow-brown solutions					
water	460[e]	701 740[f]	1.546	1.333	0.206
CB6	485[g]	592	1.057	–	0.088[h]
violet solutions					
gas phase	523	710[i]	1.093	1.000	0.00
CB7	517[g]	607	1.004	1.187	0.120
perfluorohexane	522	757	1.158	1.252	0.159
n-hexane	522	913 (940)	1.365	1.375	0.229
n-heptane	522	910 (910)[j,k]	1.352	1.388	0.235
nonane	523	1108	1.249	1.407	0.246
chloroform	512	882	1.359	1.446	0.267
carbon tetrachloride	517	892 (930)[j]	1.447	1.460	0.279
benzene	502	1110 (1150)[j]	1.792	1.501	0.295
carbon disulfide	520	1250 (1120)[j]	2.102	1.628	0.355
diiodomethane	493	1632	3.220	1.748	0.404

[a] From ref.[67], unless stated otherwise; our own experimental values were the same, within ± 1 nm error. [b] Oscillator strength of the visible transition, $f = 4.32 \times 10^{-9} \int_{400nm}^{800nm} \varepsilon(\tilde{\nu}) d\tilde{\nu}$, with ε in $M^{-1}cm^{-1}$ and $\tilde{\nu}$ in cm^{-1}; for carbon disulfide and diiodomethane, which showed the onset of a second band near 400 nm, the short-wavelength portion of the visible absorption band between 430-400 nm was extrapolated by a Gaussian fit. [c] From ref.[64], at 293 K. [d] $P = (n^2-1)/(n^2+2)$. [e] From ref.[47] [f] From ref.[47] [g] The data for the host-guest complexes were recorded under conditions of quantitative (99.9%) complexation (0.1 mM I_2 and 1.2 mM CB6/CB7). [h] Interpolated values. [i] The gas phase spectrum was recorded in vacuum at 298 K, since the gas-phase spectra show pressure- and temperature-dependent shapes above 500 nm. The spectrum has been normalized with the absorption cross section at 500 nm.[68] [j] From ref.[13] [k] From ref.[69]

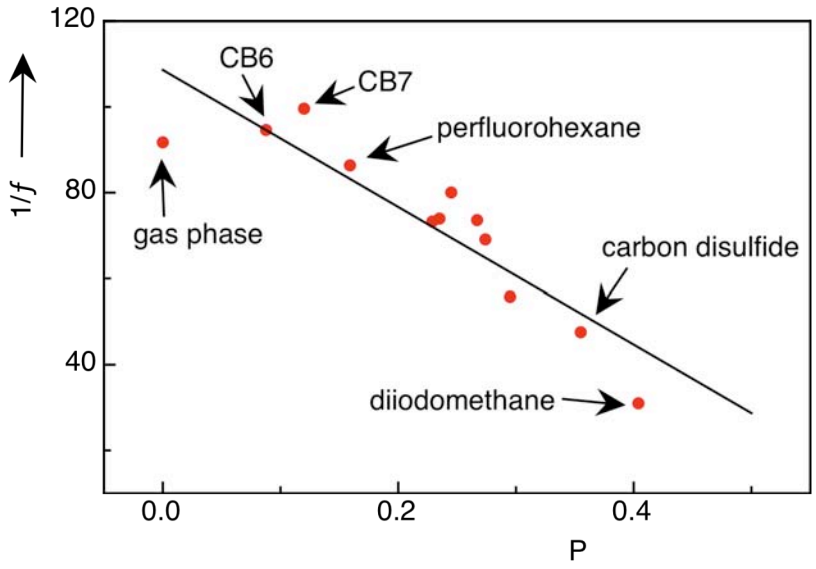

Figure 4.4: linear correlation of the inverse oscillator strength ($1/f$) of I_2 and the polarizability of the environment.

A linear correlation between the solvent polarizability and the inverse of the oscillator strength ($1/f = 108 - 160\ P$, $n = 10$, r = 0.91, Figure 4.4) has been obtained. By employing this equation, we can interpolate a very low polarizability for the CB6 cavity (0.088), the value that is slightly lower than CB7 polarizability (0.12). Such a correlation has been observed for the n,π^* transition of a bicyclic azoalkane and biacetyl.[66] The very low extinction coefficients of the CB7•I_2 and CB6•I_2 complexes can therefore be partially rationalized in terms of the low polarizability of the CBs microenvironment, which has been previously revealed for other solvatochromic probes by absorption and fluorescence.[66, 70] However, the correlation with the polarizability cannot account for the fact that the oscillator strength of iodine inside CBs falls below that of the gas phase. The hypochromic shift of iodine upon encapsulation by CB6 and CB7 (see section 4.4.1) can therefore be qualitatively but not quantitatively rationalized. The specific macrocyclic architecture appears to exert an additional, yet unknown effect in lowering the oscillator strength far below expectation.

The absorption maximum of iodine (Table 4.3) clearly does not depend on polarizability because it remains the same in microenvironments of lowest (gas phase, perfluorohexane) and highest (carbon disulfide) refractive index. It presents only an indirect measure of the polarity of its microenvironment. Rather, it signals the electron–donor strength of the solvent and presence of basic and nuclophilic sites (oxygen and nitrogen lone pairs or aryl π systems).[67, 71] The color of the yellow–

brown iodine solutions is therefore due to the formation of (halogen–bonded) solvent•I_2 complexes.[72] Iodine immersed in CB7 retains its violet color and the absorption band lies at 517 nm, which is similar to (520 ± 3) absorption band in the gas phase and in non–dipolar non–electron-donating solvents, such as alkanes, perfluoroalkanes, CCl_4 and CS_2. Therefore, one can conclude that iodine immersed inside CB7 is not involved in halogen bonding. In the smaller CB6, the absorption maximum of I_2 is similar to that observed in ethers and benzene (450–505 nm). Therefore, it can be confirmed that iodine maintains some degree of halogen bonding in the CB6 complex, although less pronounced than in bulk water (460 nm).

4.4.4 Raman Spectroscopy of Iodine Encapsulated Inside Cucurbit[*n*]urils Cavity

Corresponds to:
El–Sheshtawy H. S., Donfack P., Materny A., Nau W. M., "Raman Spectroscopy of Iodine Molecules Trapped in Cucurbiturils", in preparation.

The confinement of matter on the nanometer scale materials is not only of great interest to fundamental research in physics and chemistry, but is also important for nanotechnology and biotechnology.[73, 74] One example is the alignment of a one-dimensionally ordered chain of water molecules inside nanotubes, where the hydrophobic channels of the carbon nanotube are filled with water. The encapsulation of water molecules inside the carbon nanotube channels is reflected in the change of the phase transition lifetime of the nanotubes between the filled state (τ = 247 ps) and the empty state (τ = 2065 ps).[75] Another example is the synthesis of nanowires by encapsulating molecular iodine within the channels of different zeolites.[76]

In the preceding sections, I have provided evidence that iodine has the ability to displace the high–energy water molecules of CBs cavities to form stable inclusion complexes. Moreover, the alignment of encapsulated iodine depends on the nanocontainer volume and the stabilizing intermolecular interactions. Both spectroscopic methods and theoretical calculations proved the axial orientation of iodine inside CB6 and the equatorial orientation inside CB7 (section 4.4.1). Here, we are interested to study the change of the molecular properties of iodine inside CBs; in particular, we are investigating the physical constants of iodine by probing its molecular vibrations using Raman spectroscopy as a sensitive structure-dependent technique.

The Raman spectra of molecular iodine dissolved in different aqueous solutions show mainly the fundamental (υ = 0→1) Raman mode of the I_2 stretching vibration ($\nu_{I\text{---}I}$) at approximately 203–205 cm^{-1} (Figure 4.5 and 4.6, red). The first overtone can be hardly observed because of the low signal-to-noise ratio. However, molecular I_2 encapsulated inside the CBs cavities possesses a very strong fundamental vibration mode, in addition, a large number of vibrational overtones (4–6) were

observed. Figure 4.5 and 4.6 shows the Raman spectra of CB6•I_2, and CB7•I_2 in different aqueous solutions. In fact, upon addition of CBs to aqueous solution of I_2, the inclusion complexes (CBs•I_2) are formed and the observed Raman overtones of I_2 are shifted. A number of overtone progressions were resolved (υ = 4–6), and all modes were assigned to the molecular vibration of I_2. The concentration of molecular iodine was always kept low (300–500 μM), in order to suppress the contribution from triodide (I_3^-). Therefore, no Raman vibration has been detected at 112 and its overtone 224 and 336 cm^{-1}, which would correspond to I_3^-.[77]

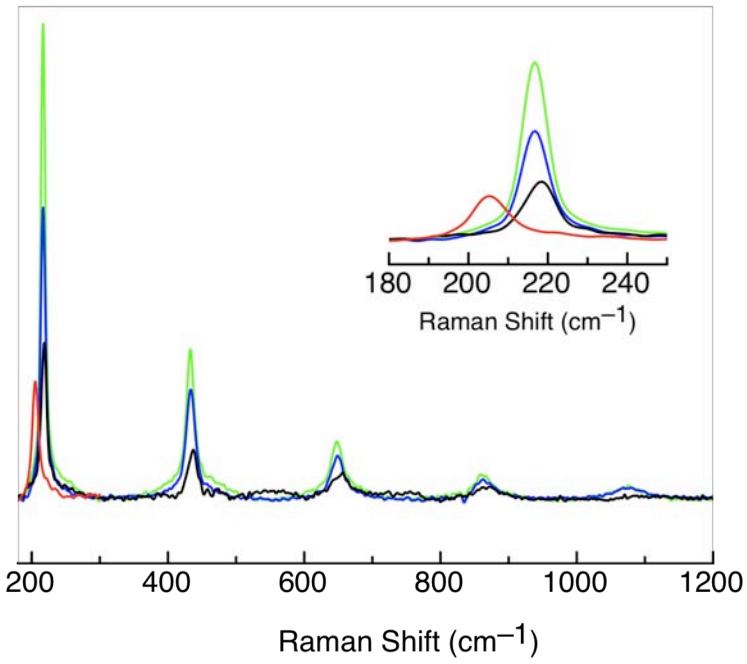

Figure 4.5: Raman spectra of 0.3 mM I_2 (red) and the inclusion complex of 0.3 mM I_2 with 3 mM CB6 dissolved in 0.1 M CsCl (green), 0.1 M RuCl (blue), and 0.1M Na_2SO_4 (black). The inset shows a magnified region for clarity.

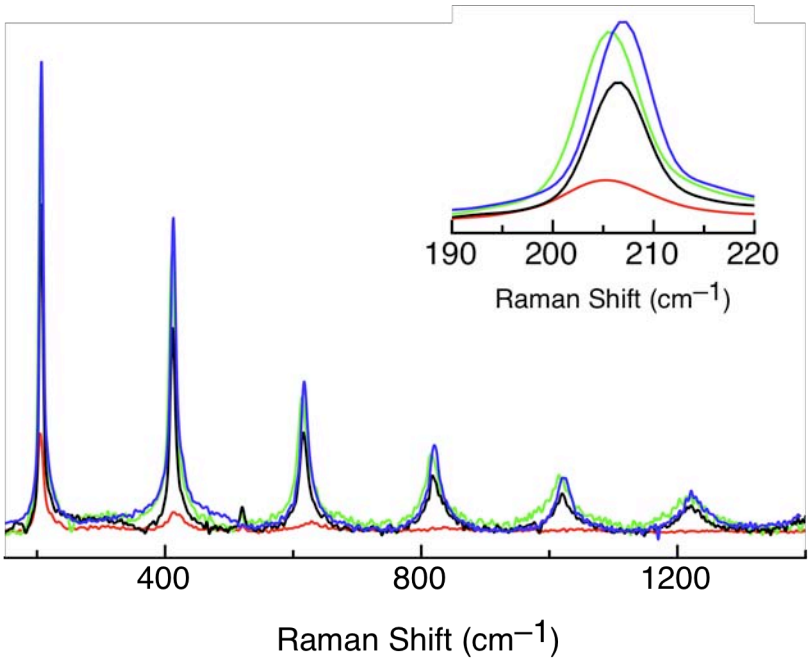

Figure 4.6: Raman spectra of 0.3 mM I_2 (red) and the inclusion complex of 0.3 mM I_2 with 2.5 mM CB7•I_2 in 0.1 M CsCl (green), and 0.1M Na_2SO_4 (black). The inset shows a magnified region for clarity.

Molecular oscillators exhibit a shift in the wave numbers of specific vibrations from the gas phase to solution.[78] Interestingly, we observed very large shifts of the I_2 vibration inside CBs relative to aqueous solution. The vibrational frequency of the CB7•I_2 complex is exceptionally low, that of the CB6•I_2 complex is exceptionally high, even higher than in the gas phase. In fact, for CB6•I_2 in 0.1 M Na_2SO_4 (Figure 4.5), the observed fundamental Raman mode of I_2 is as high as 219.54 cm^{-1}, a value much higher than that in the gas phase (~213 cm^{-1}), and clearly higher than any I_2 fundamental mode reported so far.[76, 79, 80] Moreover, it is also observed that for CB6•I_2, dissolved in the different aqueous salt solutions, the values of the I_2 vibration decrease slightly with increasing cation radius from the Na^+ (1.02 Å)[81] to Ru^+ (1.52 Å),[81] whereas there is no significant change upon changing from Ru^+ to Cs^+ (1.70 Å).[81] This situation agrees with the size restriction of the CB6 cavity, where smaller cations could be located close to the CB6 portals, in contrast to the larger cations. In contrast, no significant change of the iodine vibration modes inside CB7 was observed as the cation type was varied.

Important physical constants can be calculated from the observed high intensity overtone progressions in the Raman (or infrared absorption) spectra, for

example, the anharmonicity constants of the particular vibration. This has been done in the case of iodine by using Equation 1,[79]

$$\nu(\upsilon) = G(\upsilon) - G(0) = \upsilon\omega_e - (\upsilon^2 + \upsilon)\omega_e\chi_e + (\upsilon^3 + 3/2\upsilon^2 + 3/4\upsilon)\omega_e y_e + ... \qquad (1)$$

where $G(\upsilon)$ is the term value of the υth eigenvalue, ω_e is the harmonic frequency, $\omega_e\chi_e$ and $\omega_e y_e$ represent the first and second anharmonicity constants. We performed the calculation only for the first vibrational quantum numbers, and the wavenumbers of the overtone progression were therefore measured at the maxima of the observed bands. The plots of ν_{obs}/υ *vs* υ of the observed overtones for CBs•I_2 complexes are plotted as shown in Figure 4.7. The values of ν_{obs}/υ corresponding to the first few tones (υ = 1 to approximately 4 or 6) should lie along a straight line, and the slope of this line gives the value for $\omega_e\chi_e$. The known value for $\omega_e\chi_e$ can be used in Equation 1 to calculate the harmonic wavenumber ω_e by assuming the first-order linear approximation, neglecting the second term: this is a rough estimate since a more precise determination of ω_e requires the knowledge of $\omega_e y_e$ given by the deviation from the straight line. However, $\omega_e y_e$ in turn can only be precisely determined if intense and higher-order overtone progressions can be observed (up to at least υ = 14–20). Unfortunately, this is not possible if low concentrations of I2 are used, which is a limitation in water as solvent. The linear approximation is good at least for υ = 1-5 and provides an estimate for ω_e ($\omega_e = \nu_1 + 2\omega_e\chi_e$). Table 4.4 gives the calculated values of the spectroscopic constants for the $\nu_{I\text{---}I}$ vibration of molecular iodine, encapsulated inside CB6 and CB7.

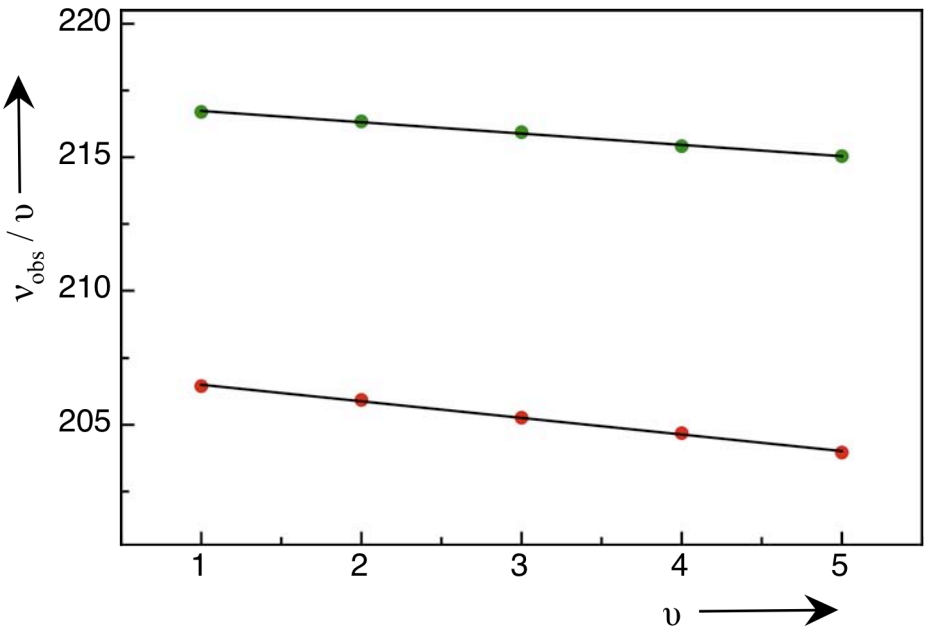

Figure 4.7: Determination of the first anharmonic constant ($\omega_e\chi_e$) of iodine for the systems CB6•I_2 (green) and CB7•I_2 (red) in 0.1 M Na_2SO_4. The solid lines represent the linear fit according to Equation 1 to determine $\omega_e\chi_e$.

In the case of CB7•I_2, where I_2 adapted the equatorial conformation inside CB7, and I---C distance is about 4.65 Å (calculated at HF/3-21G* level), the Raman shift is only 208.34 cm^{-1}. The observed wavenumber downshifts by 4 cm^{-1} with respect to iodine in the gas phase (213 cm^{-1}),[82] which reveals that there is less confinement in case of CB7 that presumably allows coupling with the ring–breathing modes of the CB7. This results in a stretching vibration with an overall increased reduced mass, which manifests itself in a dramatically lower harmonic frequency. In fact, the harmonic frequency value (208.34 cm^{-1}) falls at the lower end of those observed in any solvent, resembling the vibrational spectroscopy of I_2 in CS_2 as solvent.

Table 4.4: Spectroscopic constants of the iodine vibrational frequency in CB6 and CB7 measured at room temperature.

environment	CB6•I_2[a]		CB7•I_2[a]	
	ω_e [b] (cm^{-1})	$\omega_e \chi$ (cm^{-1})	ω_e [b] (cm^{-1})	$\omega_e \chi$ (cm^{-1})
H_2O	– [c]	– [c]	208.34	0.67 ± 0.02
Na_2SO_4	219.54	0.47 ± 0.08	207.62	0.61 ± 0.01
RuCl	217.74	0.42 ± 0.05	–	–
CsCl	217.8	0.45 ± 0.03	206.92	0.61 ± 0.01

[a] All measurements were performed at complexation degree more than 99% (0.1–0.5 mM I_2 and 3–4 mM CBs) and an excitation laser wavelength of 514 nm. [b] Values calculated according to ref.[79] [c] Raman signal could not be detected due to limited CB6 solubility in H_2O.

On the other hand, an unexpectedly large blue shift of the wavenumber of the I_2 vibration inside CB6 was observed. This might be, in part, due to the unique intermolecular interactions in the case of CB6, which become dominant depending both on the cavity size and the size–restricted encapsulation geometry of the guest molecule (I_2). This can be accounted for by considering the position of the almost axial iodine orientation inside CB6, with a very close I---O=C distance of 3.49 Å (see the crystal structure). Such interactions should then result either in an increase of the force constant or in the decrease of the reduced mass as can be seen from the following equation 2 for an equivalent isolated diatomic oscillator:

$$\nu = \frac{1}{2\pi}\sqrt{\frac{k_{eff}}{\mu_{eff}}} \qquad (2)$$

where ν is the vibrational wavenumber, μ_{eff} is the reduced mass, and k_{eff} is the force constant. With respect to the isolated I_2 oscillator (gas phase), the underlying reasons why k_{eff} or μ_{eff} increase and decrease for CB6 and CB7, respectively, are not trivial and open up an interesting fundamental question that can be looked at theoretically *via* perturbation theory or full *ab initio* treatment.[83]

4.5 Supramolecular Tandem Assays for Monitoring Peroxidase Activity

4.5.1 Supramolecular Tandem Assay

The need for monitoring the enzymatic reactions for biotechnological applications and for drug development is increasing and recently is of high demand in particular for "white biotechnology", where selective enzymes are chosen to initiate industrial processes with the minimum harm to the environment.[84][85] This requires the development of sensitive and fast monitoring techniques to respond to the vast advancements in these fields. The current methodologies to determine enzyme activities are mainly based on radioactively or fluorescently labeled substrates or antigen-antibody-based assays.[86, 87] Most of these methods have disadvantages, such as radio hazard contents, time consuming, economically expensive, and are not easily scalable for high–throughput screening. Hence, the need for a new methodology to overcome the drawbacks by the existing techniques is highly desirable.[88]

Supramolecular tandem assays have been introduced as an inexpensive and sensitive method for monitoring enzymatic reactions.[41] The method is based on the differential binding of a substrate and the corresponding product of an enzymatic reaction towards a macrocyclic host. A dye with complexation–dependent fluorescent emission response (enhancement or quenching) is used as a signal for the enzymatic conversion. During the course of the enzymatic reaction, the dye is displaced from the host cavity by a stronger binding product, or replaced into the cavity due to depletion of a stronger binding enzymatic substrate. Tandem assay can be considered as a time–resolved version of the indicator displacement assay, where the amount of the analyte, is either depleted (substrate) or produced (product). Employing the concept of tandem assays, the activity of various classes of enzymes have been successfully determined, for example decarboxylases,[41] diamine oxidase, arginase,[43] proteases,[42] potato apyrase,[89] and choline oxidase[90] have been successfully assayed.

Based on the preceding results for the encapsulation of molecular iodine inside CB7 and the ability of heme peroxidases to oxidize iodide ion to molecular iodine, here we introduce for the first time the applicability of supramolecular tandem assays to use an inorganic small ion (iodide) as a substrate, in contrast to the previously organic substrates used in enzymatic reactions.

4.5.2 Monitoring Heme Peroxidases Activity by Supramolecular Tandem Assays

Corresponds to:
El–Sheshtawy H. S., Nau W. M., "Fluorescence-Based Assay for Monitoring Peroxidase Activity *via* Molecular Iodine Encapsulation by Cucurbit[7]uril", in preparation.

Peroxidases, for example, myeloperoxidase (MPO), lactoperoxidase (LPO), and horseradish (HRP), are well known to oxidize iodide (I^-) in presence of hydrogen peroxide (H_2O_2) to produce molecular iodine (I_2). This process occurs through the formation of reactive intermediate Compound **I** (EO) and the production of the hypoiodous acid (HOI) according to equations 3 and 4.[91]

$$E + H_2O_2 \longrightarrow EO \xrightarrow{I^-} [EOI]^- \xrightarrow{H^+} E + HOI \qquad (3)$$

$$HOI + I^- + H^+ \longrightarrow I_2 + OH^- \qquad (4)$$

The enzymatic product from the oxidation of halides in presence of H_2O_2 (hypohalous acids), particularly in this work hypoiodous acid (HOI), is known for its wide effect as an anti–microbial agent.[92, 93] Herein, we are using the released molecular iodine to indirectly monitor the formation of HOI and peroxidases activity. The release of iodine as an enzymatic product could be monitored at low substrate concentrations in the μM range, another advantage offered by the sensitivity of our technique (see below).

Spectrophotometry has been widely used for the determination of the peroxidases activity.[94-97] They are essentially based on the oxidation of iodide to molecular iodine (I_2), which in presence of high concentration of iodide (I^-) forms a triiodide complex (I_3^-). As a result the activity of peroxidases were measured by recording the absorbance of the I_3^- complex at 350 nm (ε = 25 mM^{-1} cm^{-1}). However, the main drawback in this particular assay is that it gives quantitive results only when the concentration of both iodine and iodide exceeds 20 mM, which is required to form

a stable product (I_3^-).[97, 98] However, high concentration of iodide ion are known to inhibit both the activity[99] and the tyrosyl iodination ability of peroxidase.[100] Therefore, here we are introducing an alternative sensitive (in μM range) and rapid assay for the determination of peroxidases activity using supramolecular tandem assays.

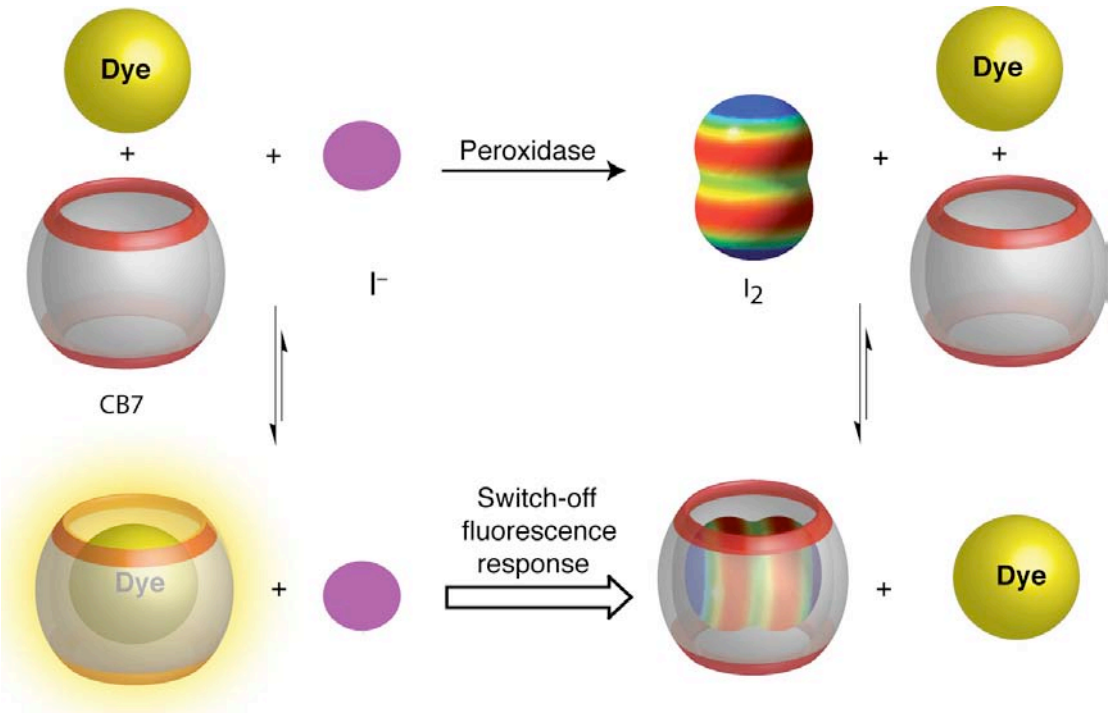

Scheme 4.7: Binding equilibria in a product–selective switch–off supramolecular tandem assay for peroxidases.

The underlying assay principal (Scheme 4.7) is based on the differential binding of iodide (weak competitor and enzymatic substrate) *versus* iodine (strong competitor and enzymatic product) as well as the competitive binding with 4′,6–diamidino–2–phenylindole (DAPI) to the macrocyclic (CB7). As we discussed in section 4.4.1, molecular iodine form an inclusion complex with CB7 ($5.6 \pm 0.1 \times 10^4$ M^{-1}), while no binding of iodide was observed in the concentration range used in our study. The fluorescent dye (DAPI) also forms an inclusion complex with CB7, which results in a strong binding and fluorescence enhancement of the dye.[101] We determined the binding constant of DAPI•CB7 to be $6.5 \pm 0.2 \times 10^6$ M^{-1} in 50 mM NaOAc buffer (Appendix III). In order to check the working principle, the desired

concentrations from both the host (CB7) and the guest (DAPI) were selected to be in the linear region from the host–guest titration curve to give a large fluorescence response.[42, 89] Subsequently, the reporter pair CB7/DAPI was titrated with I_2 to show the ability of I_2 molecule to displace the dye (Appendix III). The differential binding between molecular iodine and iodide to the CB7 host was used to monitor peroxidase activity.

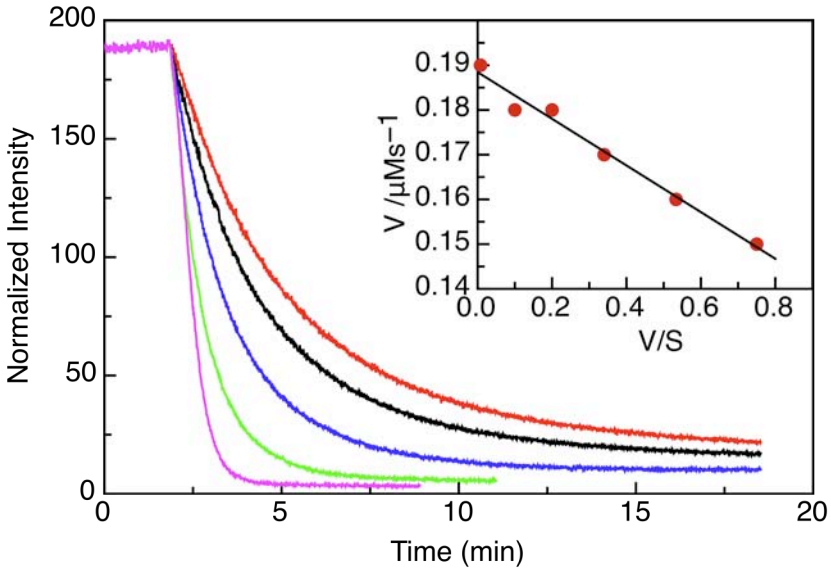

Figure 4.8: Continuous fluorescence enzyme assays for myeloperoxidase (in 10 mM NaOAc buffer at pH 5.0). The assays were performed with CB7/DAPI as reporter pair (1 nM enzyme, 75 μM H_2O_2, 0.2 μM DAPI, 0.3 μM CB7, λ_{exc} = 361 nm, λ_{em} = 467 nm). The inset shows the Eadie-Hofstee plot obtained for varying substrate concentrations (1 – 6 μM).

The assay was initiated by the addition of the required concentration of hydrogen peroxide (H_2O_2) to a solution containing the substrate, the host (CB7), the dye and the enzyme. A continuous decrease in fluorescence signal was observed until the complete conversion of the substrate to the product (Figure 4.8) had taken place. The formed product (I_2) has the ability to displace the fluorescent dye. Hence, we observed a plateau region at the complete conversion of the substrate, for example MPO (Figure 4.8). Continuous fluorescence assays for HRP and LPO are listed in Appendix III.

In order to investigate the enzyme kinetics we need first to determine the initial reaction rates.[42] For this reason, the observed fluorescence decay was correlated with the changes in absolute concentration of iodide.[89] Using different substrate concentrations, the initial reaction rates were determined and were used to

estimate the Michaelis–Menten constant using Eadie–Hofstee plot (equation 5).[102, 103]

$$V = -K_M \frac{V}{[S]} + V_{max} \qquad (5)$$

where V is the reaction velocity and S is the substrate concentration. A plot of V *vs* V/S will give the V_{max} at the intercept at the y–axis and the slope is $-K_M$ (Michaelis–Menten constant). From the determined parameters, the proteolytic constants (k_{cat}/K_M) for the different peroxidases were calculated (Table 4.5).

Table 4.5: Kinetics parameters for peroxidases activity in 50 mM NaOAc pH 5.5 at 25 ºC

enzyme	k_{cat}/K_M[a] (10^6 $s^{-1}M^{-1}$)	
	determined	reported
LPO	182	292[b]
MPO	92.0	–
HRP	0.7	7.4[c]

[a] k_{cat} is calculated using the enzyme concentration [E] ($k_{cat}= V_{max}/[E]$).
[b] From ref.[104] [c] From ref.[105]

Table 4.5 shows the peroxidases efficiency towards the oxidation of iodide by different peroxidases. The data reveals that LPO has the highest efficiency to oxidize iodide to molecular iodine compared to MPO and HRP.

4.5.3 Peroxidase Inhibition by Melatonin

Although the generation of oxidants by peroxidases is beneficial in terms of the immune response to invading pathogens, there is considerable evidence that inappropriate stimulation of oxidants formation by these enzymes can result in host tissue damage.[106] The excess production of oxidants is responsible for chronic inflammatory process, which is a direct reason for many diseases, for example atherosclerosis, systemic vasculitis, and autoimmune thyroid disease.[107-109] Therefore, there is increasing interest for screening the potent inhibitors for peroxidases.

Melatonin or *N*-acetyl-5-methoxytryptamine is a hormone secreted by the pineal gland of vertebrates, which controls several physiological functions related to circadian and seasonal rhythms.[110, 111] Its synthesis and release are stimulated by darkness and suppressed by light.[112, 113] Besides blood, melatonin was reported to be found and synthesized in a variety of tissues including bone marrow in relatively high concentrations.[114] Melatonin was reported to have important antioxidant effects[111] and play a vital role in immune system.[115]

Melatonin is oxidized by activated neutrophils (white blood cells), contain (MPO),[116][117] as well as by HRP,[116] and LPO to produce the oxidation product N^1–acetyl–N^2–formyl-5-methoxykynuramine as shown in Scheme 4.5.

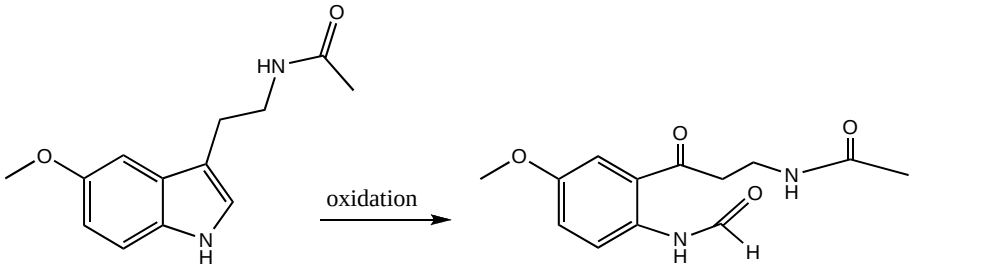

melatonin N^1-acetyl-N^2-formyl-5-methoxykynuramine (AFMK)

Scheme 4.5: Oxidation process of melatonin to N^1-acetyl-N^2-formyl-5-methoxykynuramine.

The inhibition of different peroxidases by melatonin was monitored using a supramolecular tandem assay principal. The substrate concentration (I^-) used was 5 μM and different concentrations of the second substrate (melatonin) were added. The addition of high concentrations of melatonin (20 μM) completely suppressed the

fluorescence response as can be seen for MPO (Figure 4.9) and for HRP and LPO in Appendix III, which indicates the efficient inhibition of peroxidases by melatonin. The initial rates decreases obtained from the fluorescence intensity with time were determined and employed to plot the corresponding dose–response curves. The dose–response curves were fitted using the Hill equation to give the respective IC_{50} values.[118]

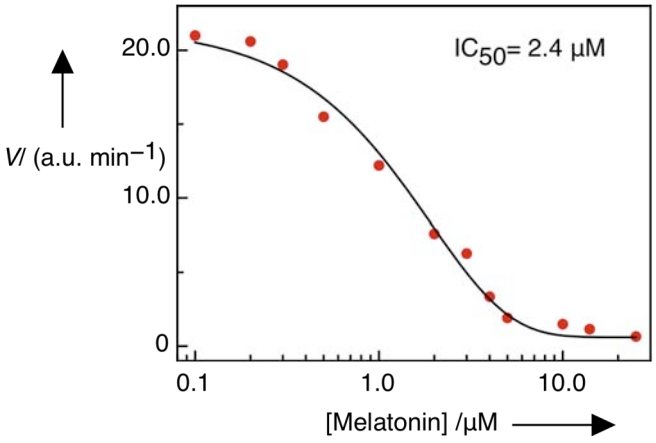

Figure 4.9: Determination of myeloperoxidase inhibition by melatonin at 25 ºC and the corresponding dose–response curve. The inhibition was determined in (1 nM enzyme, 0.2 µM DAPI, 0.3 µM CB7, and 5 µM I^-) in 50 mM NaOAc, pH 5.5.

IC_{50} values were then used to determine the inhibition constant K_i considering the concentration of the enzyme ($IC_{50} = K_i^{app} + ½[E]$).[118] The calculated K_i values are 2.4 ± 0.09 µM for MPO, 1.12 ± 0.06 µM for LPO, and 1.24 ± 0.08 µM for HRP. [119, 120] These results reveal that melatonin is a more potent inhibitor for LPO, than towards HRP or MPO. This conclusion is in agreement with the previous results obtained by different techniques.[119, 120]

4.6 Storage of CBs•I_2 in Gel Matrix

Molecular iodine has been used over years for wound treating and as disinfectant agent.[121] The early products of iodine caused irritation and skin discoloration, but the development of iodophores yielded safer and less painful products. Iodophores are chemical compounds, which have the ability to increase iodine solubility, for example polyvinylpyrrolidone (Povidone). CB6 and CB7 have the ability to encapsulate molecular iodine with extremely high binding constants (section 4.4.1). The CB7 encapsulation of iodine is accompanied by a large solubility enhancement, by factor of 3.2. Consequently, cucurbiturils serve as iodophores, carrying this reactive molecule into aqueous solution, where they can store it and, if required, released it in a controlled manner through a rapid host–guest equilibrium. Interestingly, the violet aqueous solution of CB7•I_2 complex did not change after preparing the complex in the gelrite matrix (Figure 4.10–b), suggesting its stability. This has been confirmed OD measurements, which show that a decrease of only 12.7% had taken place over a time interval of 20 h, in contrast to 36% decrease in aqueous solution (Figure 4.10–d). This effect can be manifested in the slow release of molecular iodine from the gelrite. This allows introducing the CB7•I_2 for use in creams and pastes, as they are routinely required. For example, in preparation of surgical procedures; there is no ambiguity of where the iodine in the hydrogel rests, because the highly characteristic violet color in the presence of CB7 signals its inclusion in the cavity (iodine hydrogels without macrocycles or with other macrocycles but CB7 are invariably brown in appearance).

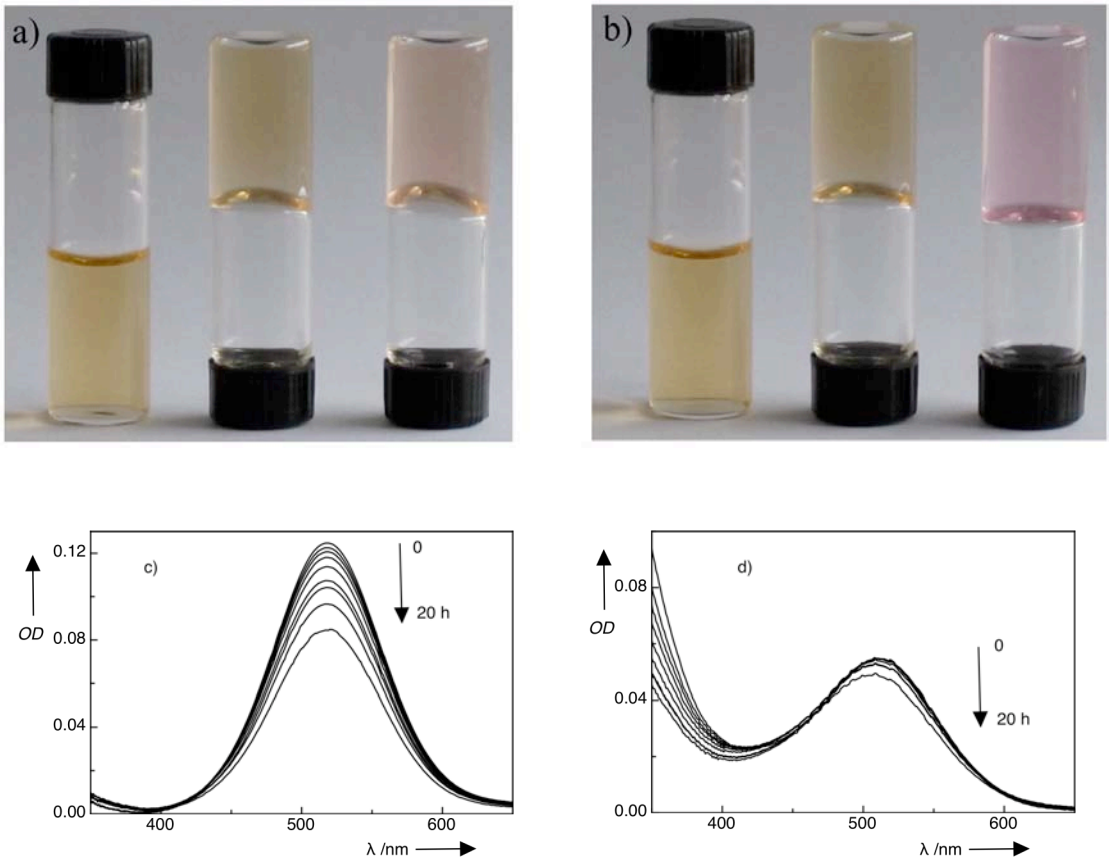

Figure 4.10: Inclusion of the CBs•I_2 complexes into gelrite matrix, the visible color change (photograph) of iodine in the absence (left vial) and presence of the host (right vial) for a) CB6•I_2 and b) CB7•I_2 complexes. The time effect on the absorption spectrum of CB7•I_2 complex in a) 0.1 M Na_2SO_4 aqueous solution and b) 0.1 M Na_2SO_4 aqueous solution prepared in gelrite matrix.

CB6 hydrogels can be similarly prepared, because solubility of the CB6•I_2 complex can be enhanced by addition of (earth) alkali cations without significantly affecting its stability (Figure 4.10–a). Keeping in mind that CBs do not show any detectable cellular or in *vivo* toxicity,[122] CBs•I_2 solutions and hydrogels be readily compared to contemporary medicinal aqueous formulations of iodine. Such examples include Povidone–iodine and Cadexomer iodine as opposed to the more toxic ethanolic solutions of Lugol's solution.

References

[1] J. W. Steed, J. L. Atwood, *Supramolecular Chemistry*, John Wiley & Sons Ltd: Chichester, England, **2000**.
[2] J. M. Lehn, *Supramolecular Chemistry: Concepts and Perspectives*, John Wiley & Sons Ltd: Chichester, England, **2000**.
[3] J. M. Lehn, *Pure Appl. Chem.* **1978**, *50*, 871.
[4] J. M. Lehn, *Angew. Chem.-Int. Edit.* **1988**, *27*, 89.
[5] D. Philp, J. F. Stoddart, *Angew. Chem.-Int. Edit.* **1996**, *35*, 1155.
[6] V. P. Fedin, V. Gramlich, M. Worle, T. Weber, *Inorg. Chem.* **2001**, *40*, 1074.
[7] X. Sun, B. Li, Q. Zhou, H. Zhang, G. Cheng, X. Zhou, *Cryst. Growth Des.* **2008**, *8*, 2970.
[8] Y. Lu, Y. Wang, Z. Xu, X. Yan, X. Luo, H. Jiang, W. Zhu, *J. Phys. Chem. B* **2009**, *113*, 12615.
[9] J. D. Watson, F. H. C. Crick, *Nature* **1953**, *171*, 737.
[10] H. Cong, C.-R. Li, S.-F. Xue, Z. Tao, Q.-J. Zhu, G. Wei, *Org. Biomol. Chem.* **2011**, *9*, 1041.
[11] A. Bondi, *J. Phys. Chem.* **1964**, *68*, 441.
[12] J. L. Syssa-Magale, K. Boubekeur, P. Palvadeau, A. Meerschaut, B. Schollhorn, *CrystEngComm* **2005**, *7*, 302.
[13] H. A. Benesi, J. H. Hildebrand, *J. Am. Chem. Soc.* **1949**, *71*, 2703.
[14] O. Hassel, *Science* **1970**, *170*, 497.
[15] G. Cavallo, S. Biella, J. Lu, P. Metrangolo, T. Pilati, G. Resnati, G. Terraneo, *J. Fluorine Chem.* **2010**, *131*, 1165.
[16] P. Metrangolo, C. Praesang, G. Resnati, R. Liantonio, A. C. Whitwood, D. W. Bruce, *Chem. Commun.* **2006**, 3290.
[17] P. Metrangolo, G. Resnati, T. Pilati, R. Liantonio, F. Meyer, *J. Polym. Sci., Part A: Polym. Chem.* **2007**, *45*, 1.
[18] A. R. Voth, P. S. Ho, *Curr. Top. Med. Chem.* **2007**, *7*, 1336.
[19] A. R. Voth, F. A. Hays, P. S. Ho, *Proc. Natl. Acad. Sci. USA* **2007**, *104*, 6188.
[20] C. J. Pederson, *J. Am. Chem. Soc.* **1967**, *89*, 2495.
[21] C. J. Pederson, *J. Am. Chem. Soc.* **1967**, *89*, 7017.
[22] E. Meyer, Inaugural Dissertation thesis, Heidelberg (Germany), **1904**.
[23] R. Behrend, E. Meyer, F. Rusche, *Justus Liebigs Ann. Chem.* **1905**, *339*, 1.
[24] W. A. Freeman, W. L. Mock, N.-Y. Shih, *J. Am.Chem. Soc.* **1981**, *103*, 7376.
[25] J. Kim, I. S. Jung, S. Y. Kim, E. Lee, J. K. Kang, S. Sakamoto, K. Yamaguchi, K. Kim, *J. Am. Chem. Soc.* **2000**, *122*, 540.
[26] A. I. Day, R. J. Blanch, A. P. Arnold, *PCT Int. Appl. WO 2000-2000 AU412 200005050. Periority: AU 99-232 19990507, Unisearch Limited, Australia* **2000**, *112*.
[27] C. Marquez, F. Huang, W. M. Nau, *IEEE Trans. Nanobiosci.* **2004**, *3*, 39.
[28] J. Lagona, P. Mukhopadhyay, S. Chakrabarti, L. Isaacs, *Angew. Chem.-Int. Edit.* **2005**, *44*, 4844.
[29] W. M. Nau, M. Florea, K. I. Assaf, *Isr. J. Chem.* **2011**, *51*, 559.
[30] S. Mecozzi, J. Rebek, *Chem.-Eur. J.* **1998**, *4*, 1016.
[31] N. Branda, R. Wyler, J. Rebek, *Science* **1994**, *263*, 1267.
[32] B. W. Purse, J. Rebek, *Proc. Natl. Acad. Sci. USA* **2006**, *103*, 2530.
[33] L. Garel, J. P. Dutasta, A. Collet, *Angew. Chem.-Int. Edit.* **1993**, *32*, 1169.
[34] A. V. Leontiev, A. W. Saleh, D. M. Rudkevich, *Org. Lett.* **2007**, *9*, 1753.

[35] O. Taratula, P. A. Hill, N. S. Khan, P. J. Carroll, I. J. Dmochowski, *Nat. Commun.* **2010**, *1*.
[36] I. W. Wyman, D. H. Macartney, *Org. Biomol. Chem.* **2008**, *6*, 1796.
[37] C. Kloeck, R. N. Dsouza, W. M. Nau, *Org. Lett.* **2009**, *11*, 2595.
[38] N. Saleh, A. L. Koner, W. M. Nau, *Angew. Chem.-Int. Edit.* **2008**, *47*, 5398.
[39] D. H. Macartney, *Isr. J. Chem.* **2011**, *51*, 600.
[40] D. M. Bailey, A. Hennig, V. D. Uzunova, W. M. Nau, *Chem.-Eur. J.* **2008**, *14*, 6069.
[41] A. Hennig, H. Bakirci, W. M. Nau, *Nat. Methods* **2007**, *4*, 629.
[42] G. Ghale, V. Ramalingam, A. R. Urbach, W. M. Nau, *J. Am. Chem. Soc.* **2011**, *133*, 7528.
[43] W. M. Nau, G. Ghale, A. Hennig, H. Bakirci, D. M. Bailey, *J. Am. Chem. Soc.* **2009**, *131*, 11558.
[44] J. E. Atwater, R. L. Sauer, J. R. Schultz, *J. Environ. Sci. Heal. A.* **1996**, *31*, 1965.
[45] W. Gottardi, *Arch. Pharm.* **1999**, *332*, 151.
[46] N. N. Kazantseva, A. Ernepesova, A. Khodjamamedov, O. A. Geldyev, B. S. Krumgalz, *Anal. Chim. Acta* **2002**, *456*, 105.
[47] M. Morrison, G. S. Bayse, A. W. Michaels, *Anal. Biochem.* **1971**, *42*, 195.
[48] D. J. Cram, *Nature* **1992**, *356*, 29.
[49] M. Florea, W. M. Nau, *Angew. Chem.-Int. Edit.* **2011**, *50*, 9338.
[50] J. P. Diard, E. Saintaman, D. Serve, *J. Electroanal. Chem.* **1985**, *189*, 113.
[51] L. Szente, E. Fenyvesi, J. Szejtli, *Environ. Sci. Technol.* **1999**, *33*, 4495.
[52] K. Tomono, H. Goto, T. Suzuki, H. Ueda, T. Nagai, J. Watanabe, *Drug Dev. Ind. Pharm.* **2002**, *28*, 1303.
[53] H.-J. Schneider, *Angew. Chem.-Int. Edit.* **2009**, *48*, 3924.
[54] C. Marquez, W. M. Nau, *Angew. Chem.-Int. Edit.* **2001**, *40*, 3155.
[55] P. Zhou, J. Lv, J. W. Zoo, F. F. Tian, Z. C. Shang, *J. Struct. Biol.* **2010**, *169*, 172.
[56] C. Ouvrard, J. Y. Le Questel, M. Berthelot, C. Laurence, *Acta Crystallogr. Sect. B-Struct. Sci.* **2003**, *59*, 512.
[57] D. M. Himmel, K. Das, A. D. Clark, S. H. Hughes, A. Benjahad, S. Oumouch, J. Guillemont, S. Coupa, A. Poncelet, I. Csoka, C. Meyer, K. Andries, C. H. Nguyen, D. S. Grierson, E. Arnold, *J. Med. Chem.* **2005**, *48*, 7582.
[58] J. Ghuman, P. A. Zunszain, I. Petitpas, A. A. Bhattacharya, M. Otagiri, S. Curry, *J. Mol. Biol.* **2005**, *353*, 38.
[59] M. Fourmigue, *Curr. Opin. Solid State Mat. Sci.* **2009**, *13*, 36.
[60] P. Auffinger, F. A. Hays, E. Westhof, P. S. Ho, *Proc. Natl. Acad. Sci. USA* **2004**, *101*, 16789.
[61] A. R. Voth, P. Khuu, K. Oishi, P. S. Ho, *Nat. Chem.* **2009**, *1*, 74.
[62] E. Parisini, P. Metrangolo, T. Pilati, G. Resnati, G. Terraneo, *Chem. Soc. Rev.* **2011**, *40*, 2267.
[63] J. Mohanty, W. M. Nau, *Angew. Chem.-Int. Edit.* **2005**, *44*, 3750.
[64] C. Reichardt, *Solvents and Solvent Effects in Organic Chemistry*, 3rd ed., Wiley-VCH, Weinheim, Germany, **2003**.
[65] M. A. Rankin, B. D. Wagner, *Supramol. Chem.* **2004**, *16*, 513.
[66] C. Marquez, W. M. Nau, *Angew. Chem.-Int. Edit.* **2001**, *40*, 4387.
[67] E. M. Voigt, *J. Phys. Chem.* **1968**, *72*, 3300.
[68] P. Spietz, J. Gomez Martin, J. P. Burrows, *Atmos. Chem. Phys.* **2006**, *6*, 2177.
[69] J. Ham, *J. Am. Chem. Soc.* **1954**, *76*, 3881.

[70] J. Mohanty, W. M. Nau, *Photochem. Photobiol. Sci.* **2004**, *3*, 1026.
[71] A. L. Lerosen, C. E. Reid, *J. Chem. Phys.* **1952**, *20*, 233.
[72] W. Brüll, W. Ellerbrock, *Z. Allgem. Anorg. Chemie* **1934**, *216*, 353.
[73] L. D. Gelb, K. E. Gubbins, R. Radhakrishnan, M. Sliwinska-Bartkowiak, *Rep. Prog. Phys.* **1999**, *62*, 1573.
[74] P. Xiu, B. Zhou, W. Qi, H. Lu, Y. Tu, H. Fang, *J. Am. Chem. Soc.* **2009**, *131*, 2840.
[75] G. Hummer, J. C. Rasaiah, J. P. Noworyta, *Nature* **2001**, *414*, 188.
[76] J. P. Zhai, H. F. Lee, I. L. Li, S. C. Ruan, Z. K. Tang, *Nanotechnology* **2008**, *19*.
[77] A. E. Johnson, A. B. Myers, *J. Phys. Chem.* **1996**, *100*, 7778.
[78] D. G. Cameron, S. C. Hsi, J. Umemura, H. H. Mantsch, *Can. J. Chem.-Rev. Can. Chim.* **1981**, *59*, 1357.
[79] W. Kiefer, Bernstei.Hj, *J. Mol. Spectrosc.* **1972**, *43*, 366.
[80] W. Guo, D. Wang, J. Hu, Z. K. Tang, S. Du, *Appl. Phys. Lett.* **2011**, *98*.
[81] R. Hoffmann, W. Knoche, C. Fenn, H. J. Buschmann, *J. Chem. Soc., Faraday Trans.* **1994**, *90*, 1507.
[82] R. J. Magana, J. S. Lannin, *Phys. Rev. B* **1985**, *32*, 3819.
[83] S. A. C. McDowell, A. D. Buckingham, *J. Chem. Soc., Faraday Trans.* **1993**, *89*, 4253.
[84] M. T. Reetz, *Angew. Chem.-Int. Edit.* **2011**, *50*, 138.
[85] A. Schmid, J. S. Dordick, B. Hauer, A. Kiener, M. Wubbolts, B. Witholt, *Nature* **2001**, *409*, 258.
[86] J. P. Goddard, J. L. Reymond, *Trends Biotechnol.* **2004**, *22*, 363.
[87] J. P. Goddard, J. L. Reymond, *Curr. Opin. Biotechnol.* **2004**, *15*, 314.
[88] J.-L. Reymond, V. S. Fluxa, N. Maillard, *Chem. Commun.* **2009**, 34.
[89] M. Florea, W. M. Nau, *Org. Biomol. Chem.* **2010**, *8*, 1033.
[90] D.-S. Guo, V. D. Uzunova, X. Su, Y. Liu, W. M. Nau, *Chem. Sci.* **2011**, *2*, 1722.
[91] S. Ohtaki, H. Nakagawa, M. Nakamura, I. Yamazaki, *J. Biol. Chem.* **1982**, *257*, 761.
[92] T. K. Davtyan, I. S. Hakobyan, R. E. Muradyan, H. G. Hovhannisyan, E. S. Gabrielyan, *J. Antimicrob. Chemother.* **2007**, *59*, 1114.
[93] C. Nathan, *Nat. Rev. Immunol.* **2006**, *6*, 173.
[94] C. D. Murphy, R. M. Moore, R. L. White, *J. Appl. Phycol.* **2000**, *12*, 507.
[95] T. Hosoya, I. Sato, Y. Hiyama, H. Yoshimura, H. Niimi, O. Tarutani, *J. Biochem.* **1985**, *98*, 637.
[96] J. Sakurada, S. Takahashi, T. Hosoya, *J. Biol. Chem.* **1987**, *262*, 4007.
[97] M. Huwiler, H. Kohler, *Eur. J. Biochem.* **1984**, *141*, 69.
[98] E. Verhaeghe, D. Buisson, E. Zekri, C. Leblanc, P. Potin, Y. Ambroise, *Anal. Biochem.* **2008**, *379*, 60.
[99] R. P. Magnusson, A. Taurog, M. L. Dorris, *J. Biol. Chem.* **1984**, *259*, 197.
[100] M. L. Coval, A. Taurog, *J. Biol. Chem.* **1967**, *242*, 5510.
[101] Z. Miskolczy, L. Biczok, M. Megyesi, I. Jablonkai, *J. Phys. Chem. B* **2009**, *113*, 1645.
[102] G. S. Eadie, *J. Biol. Chem.* **1942**, *146*, 85.
[103] B. H. J. Hofstee, *Nature* **1959**, *184*, 1296.
[104] R. P. Ferrari, E. M. Ghibaudi, S. Traversa, E. Laurenti, L. DeGioia, M. Salmona, *J. Inorg. Biochem.* **1997**, *68*, 17.
[105] S.-i. Ozaki, P. R. Ortiz de Montellano, *J. Am. Chem. Soc.* **1995**, *117*, 7056.

[106] M. J. Davies, *J. Clin. Biochem. Nutr.* **2011**, *48*, 8.
[107] E. A. Podrez, H. M. Abu-Soud, S. L. Hazen, *Free Radic. Biol. Med.* **2000**, *28*, 1717.
[108] S. J. Klebanoff, *J. Leukocyte Biol.* **2005**, *77*, 598.
[109] M. J. Davies, C. L. Hawkins, D. I. Pattison, M. D. Rees, *Antioxid. Redox Signaling* **2008**, *10*, 1199.
[110] J. A. Gastel, P. H. Roseboom, P. A. Rinaldi, J. L. Weller, D. C. Klein, *Science* **1998**, *279*, 1358.
[111] J. Arendt, *Melatonin and the Mammalian Pineal Gland*, 1st ed., Chapman &Hall, London, **1995**.
[112] R. J. Wurtman, J. Axelrod, L. S. Phillips, *Science* **1963**, *142*, 1071.
[113] G. M. Brown, *J. Psychiatry Neurosci.* **1994**, *19*, 345.
[114] D. X. Tan, L. C. Manchester, R. J. Reiter, W. B. Qi, M. Zhang, S. T. Weintraub, J. Cabrera, R. M. Sainz, J. C. Mayo, *Biochim. Biophys. Acta-Gen. Subj.* **1999**, *1472*, 206.
[115] S. Garcia–Maurino, M. G. Gonzalez–Haba, J. R. Calvo, M. Rafii–El–Idrissi, V. Sanchez–Margalet, R. Goberna, J. M. Guerrero, *J. Immunol.* **1997**, *159*, 574.
[116] S. de Oliveira Silva, V. F. Ximenes, L. H. Catalani, A. Campa, *Biochem. Biophys. Res. Commun.* **2000**, *279*, 657.
[117] S. O. Silva, S. R. Q. Carvalho, V. F. Ximenes, S. S. Okada, A. Campa, *Microbes Infect.* **2006**, *8*, 420.
[118] R. A. Copeland, *Anal. Biochem.* **2003**, *320*, 1.
[119] S. Galijasevic, I. Abdulhamid, H. M. Abu-Soud, *Biochemistry* **2008**, *47*, 2668.
[120] M. Sisecioglu, M. Cankaya, I. Gulcin, H. Ozdemir, *J. Enzyme Inhib. Med. Chem.* **2010**, *25*, 779.
[121] J. Davies, *Selections in Pathology and Surgery. Part II. London*, Longman, Orme, Browne, Greene and Longmans, **1839**.
[122] V. D. Uzunova, C. Cullinane, K. Brix, W. M. Nau, A. I. Day, *Org. Biomol. Chem.* **2010**, *8*, 2037.

Appendices

Appendix I

Appendix 1

1. Nanosecond Laser Flash Photolysis

The importance of reactive intermediates in understanding the mechanistic of modern organic chemistry has led to the enormous advances in the spectroscopic techniques required to monitor fast reactions. Therefore, monitoring the short live intermediates in photochemical reactions has been always of researchers interest to understand and illustrate the elemental reaction steps. Photochemical reactions play a key rule in many areas of modern chemistry such as combustion and atmospheric fields that involve the progression of free radicals, which have lifetime in millisecond to microsecond time scale.

The idea to use a flash lamp to study the transient phenomena came to G. Porter when he was a Radar scientist, using the electromagnetic radiation pulses, in the navy in World War II.[1] In 1945, Porter moved to Cambridge to work with R. G. W. Norrish as a graduate student. He introduced the flash–lamp in 1947 as an energy pulse to study the transient phenomena. Using the short energy pulses produced by flash lamps, Porter and Norrish were able to monitor the short–lifetime (in millisecond time scale) of reactive intermediates, such as free radicals and triplet states.[2-5] For this achievement, Porter and Norrish shared Noble Prize in 1967 with Eigen for is studies on fast reactions by relaxations methods. An example of a typical flash lamp is xenon lamp in a standard camera. In general, the pulse width of the light source must be much shorter than the half–life of the chemical reaction.

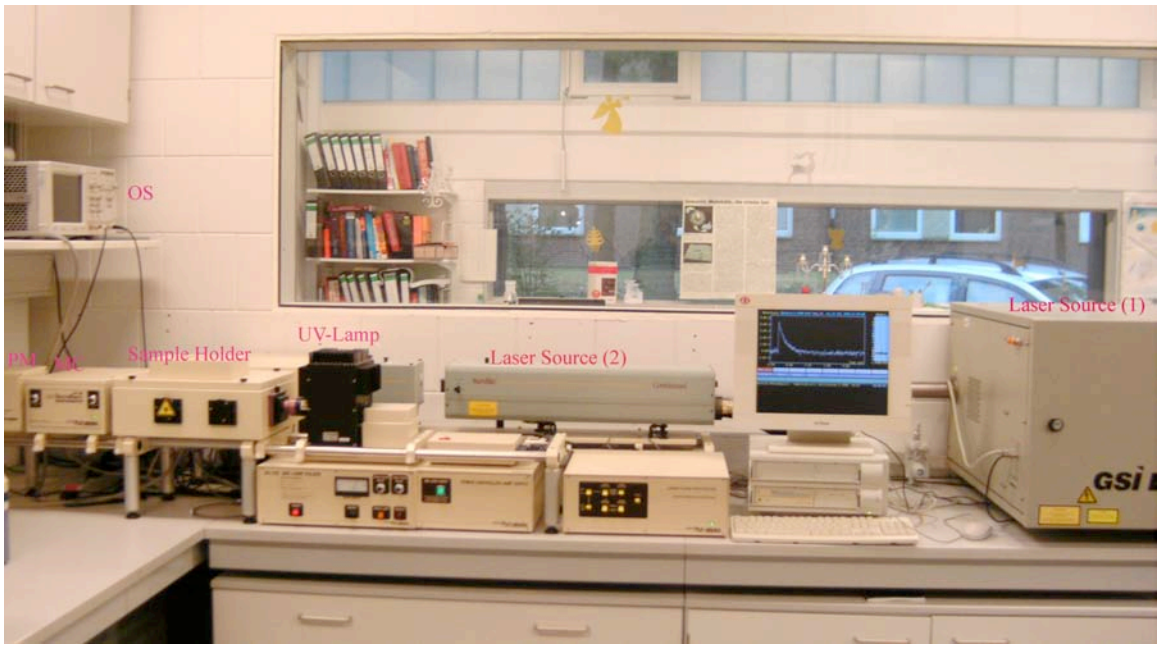

Figure A1–1: Nanosecond laser flash photolysis set up in Prof. Dr. Werner Nau's Lab at Jacobs University Bremen.

The pulse width of xenon flash lamps, such as those used in photography is in the microsecond time scale. For faster reactions, specially designed lasers must be used that have pulse widths in the nanosecond time scale or even shorter. The idea to use a laser beam to initiate the radical photolysis was suggested by Porter in his Nobel prize speech.[6] The huge breakthrough came after the inventions of laser in early 1960s and provided the opportunity for faster reactions. In 1966, Lindqvis introduced for the first time the laser flash photolysis by which he was able to monitor the triplet state of acridine.[7] This enormous step was succeeded by the immense improvements in the computer data acquisition.

In the laser flash photolysis system, the reactive intermediate is initiated using laser source (Figure A1–1). Nitrogen (337 nm) and ruby (694 nm) lasers played a key role in the early development of nanosecond laser flash photolysis. However, the fixed wavelength of these lasers is limiting their use for photochemical reactions initiation as the reactants can have a wide variety of different wavelengths, which are not accessible by a certain laser. Therefore, their role has gradually been taken over by the more

convenient excimer (laser source 1, Figure A1–1) and Nd/YAG (neodymium–yttrium aluminum garnet) (laser source 2, Figure A1–1) lasers.

Excimer lasers has emerged as an important laser sources since their early development in 1970. The term excimer comes from excited dimer. The first excimer beam generation has been obtained by high current electron beam to excite liquid Xe.[8] Today the name of excimer lasers is used only by convention since now excited complexes (exciplexes) of rare gas monohalides rather than excited dimers form the active medium. The exciplexes are formed by the complexation of Ar, Kr, or Xe with F or Cl. Excimer lasers are gas lasers that emit pulses of light with duration of 10 ns to several 10 ns in the ultraviolet (UV) spectral range. The most important are ArF; 193 nm, KrF; 248 nm, and XeCl; 308 nm.[9]

Nd/YAG lasers produce a fundamental single beam with 1064 nm, which can generate different wavelengths (532, 355, and 266 nm) by generation of harmonics from the fundamental wavelength.

The monitoring beam (Figure 1, UV–Lamp) is usually consists of a Xenon lamp, which can give a high voltage pulse for a few millisecond. Although the pulsed xenon lamps improve the signal to noise ratio, they are suffering from the lamp–lifetime, which can be solved by using the ceramic lamps that operates without pulsing due to the high efficiency. In all lasers setup, the detection system consists of a monochromator (MC) and photomultiplier (PM), which can monitor the transient species absorbing from 200 nm to near IR region. Finally, the electronic signal from the photomultiplier is digitized by the very fast digital oscilloscope (OS).

In my thesis, I have performed all the experiments, documented in chapter 2 and chapter 3 using laser–flash photolysis, consists of an LKS.60 set–up (Applied Photophysics). A XeCl excimer laser (GSI Lumonics Pulsemaster 846, λ_{exc} = 308 nm, fwhm *ca*. 10 ns, pulse energy *ca*. 80 mJ) has also been used for excitation.

Table A1–1: Concentration C/(mM) of oxygen in *n*–hexane and acetonitrile at different temperatures at atmospheric pressure (0.1 MPa).

T /°C	*n*–hexane[10]	acetonitrile[11]
15	16.77	9.09
20	16.11	8.79
25	15.16	8.49
30	13.19	8.19
35	12.70	7.89
40	11.56	7.59
45	10.41	7.28
55	8.22	6.68

2. Dibenzylketone Photolysis

Dibenzyl ketone (Fluka) was purified by sublimation, and the aryl–substituted benzyl ketones (*p*–MeO, *p*–Me, *p*–Cl, and *p*–CF_3) were synthesized according to the reported procedures[12-14]. Oxygen concentrations (2±0.039, 5±0.1, 10±0.2) vol% were supplied by AIR LIQUIDE Deutschland GmbH. Exact oxygen concentrations in acetonitrile and *n*–hexane at different temperatures were calculated according to the reported solubility from Table A1–1).

Irradiation of dibenzylketone gives a singlet–exited species with a lifetime of around 3 ns,[15] which undergoes intersystem crossing to give a triplet state species (Scheme A1–1).[16] The photocleavage of the triplet state (Norrish Type I cleavage) occurs very fast to give phenacetyl and benzyl radicals,[17] However, the decarbonylation process is slow (100–500 ns) and further produces another equivalent of benzyl radical and one equivalent of carbon monoxide.[18] Nau and Zhang[19] studied the effect of solvents on the decarbonylation of different substituted phenacetyl radicals reporting higher rate constants in *n*–hexane than in acetonitrile, and both electron donating as well

as electron–withdrawing groups were shown to accelerate the decarbonylation process. In the presence of molecular oxygen, substituted benzylperoxy radicals are formed very fast at diffusion–controlled rate (Scheme A1–1).

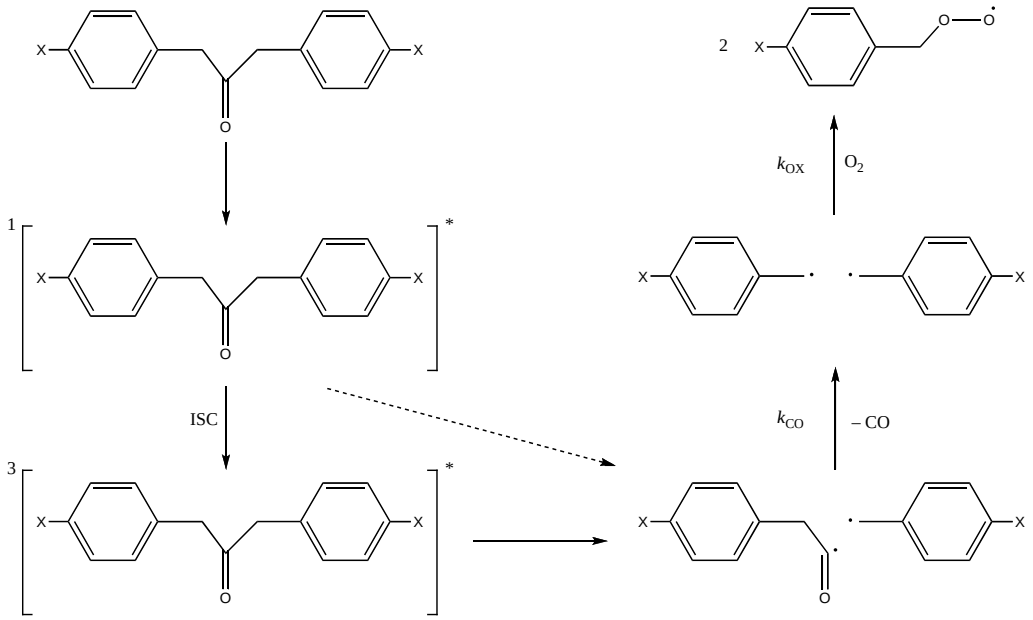

Scheme A1–1: The pathways for dibenzylketone photolysis.

3. Computational Methods

All quantum chemical calculations were performed using Gaussian03 software.[20] Optimizations of the structures to obtain the potential energy surface were performed at the B3LYP level of the theory with a 6-311G(2d,p) basis set. During the calculation of the potential energy surface, the C–OO bond length was kept fixed in–between 1.5 to 3.0 Å. All geometries were optimized at C_s symmetry. Transition state and minimum geometry optimization were performed under no constrains. Analytical frequency calculations were performed at the same level of the theory, in order to determine the zero–point vibrational energy (ZPVE). And to verify the stationary points on the potential energy surface, one imaginary frequency for the transition state and only positive frequencies for the minimum energy state were confirmed. Frequency calculations were followed by intrinsic reaction coordinate (IRC) calculations to track the reaction path from the transition state to products as well as to the reactants. Thermodynamic parameters (ΔG, ΔH, and $T\Delta S$) were calculated.

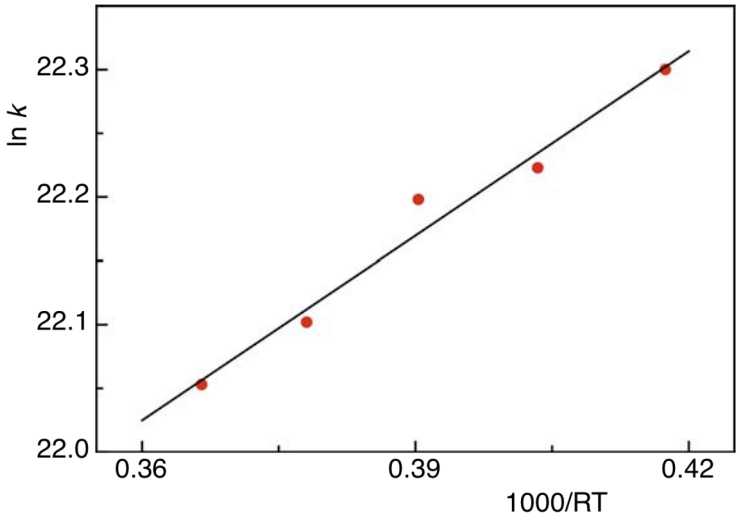

Figure A1–2: Arrhenius plot for *p*–methoxybenzyl radical of the measured rate constants over a temperature range from 288 to 318 K.

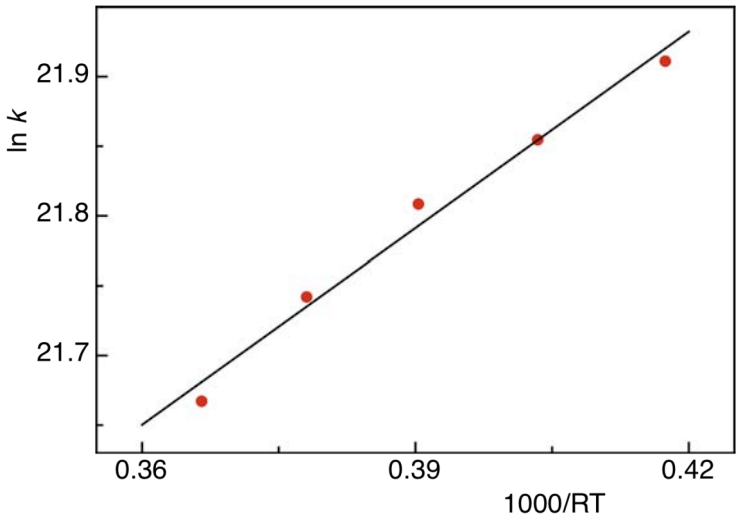

Figure A1–3: Arrhenius plot for *p*–methylbenzyl radical of the measured rate constants over a temperature range from 288 to 318 K.

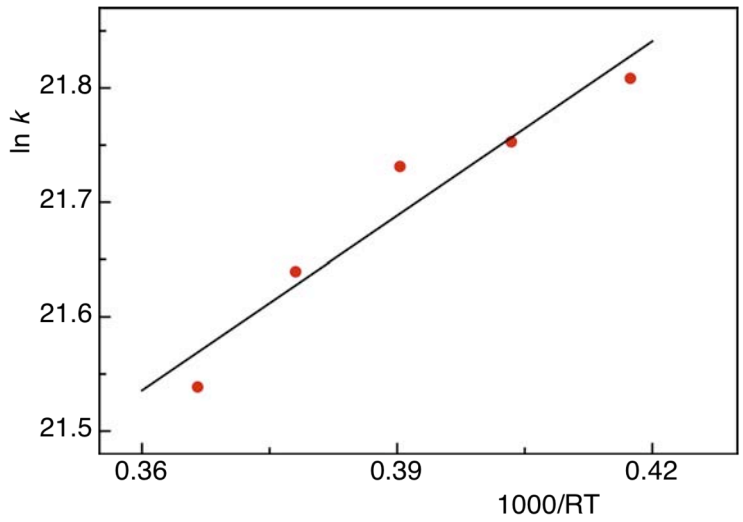

Figure A1–4: Arrhenius plot for *p*–chlorobenzyl radical of the measured rate constants over a temperature range from 288 to 318 K.

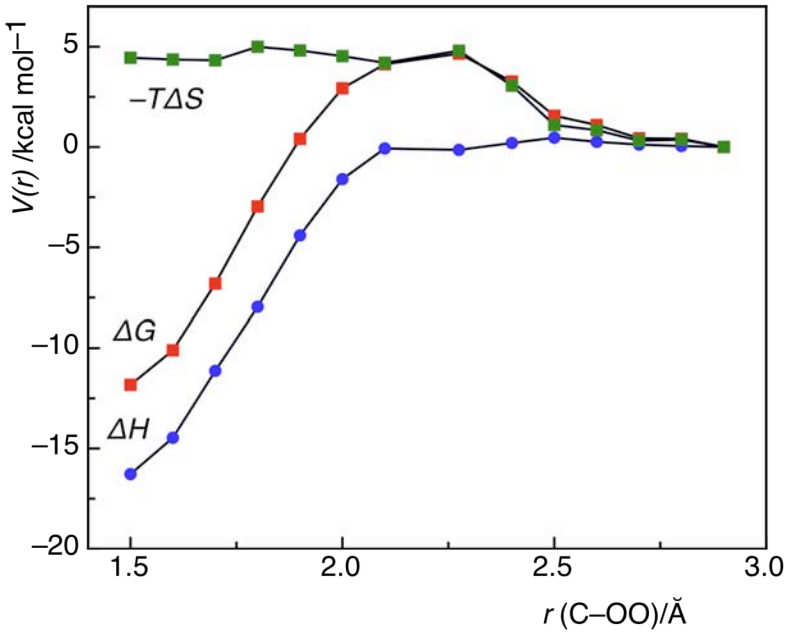

Figure A1–5: Potential energy profile for *p*–methylbenzyl radical calculated at UB3LYP with 6–311G(2d,p) basis set.

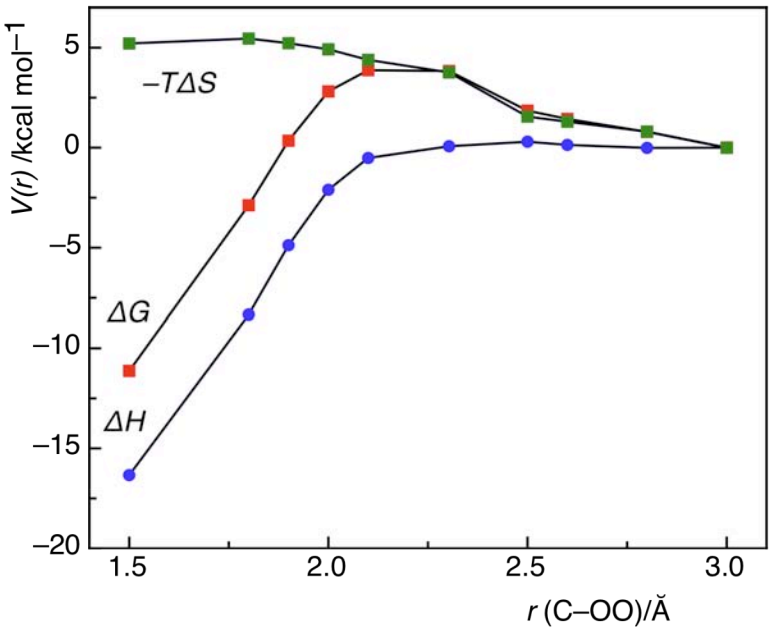

Figure A1–6: Potential energy profile for *p*–methoxybenzyl radical calculated at UB3LYP with 6–311G(2d,p) basis set.

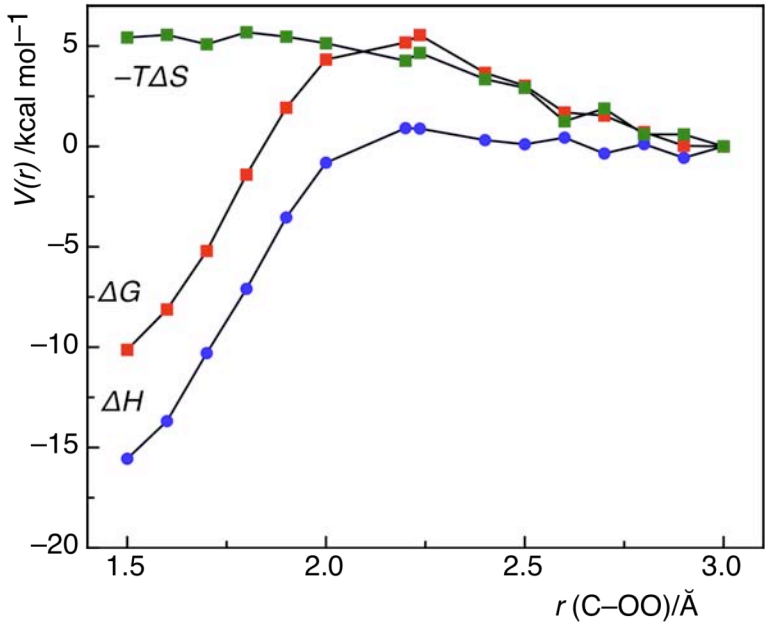

Figure A1–7: Potential energy profile for *p*–chlorobenzyl radical calculated at UB3LYP with 6–311G(2d,p) basis set.

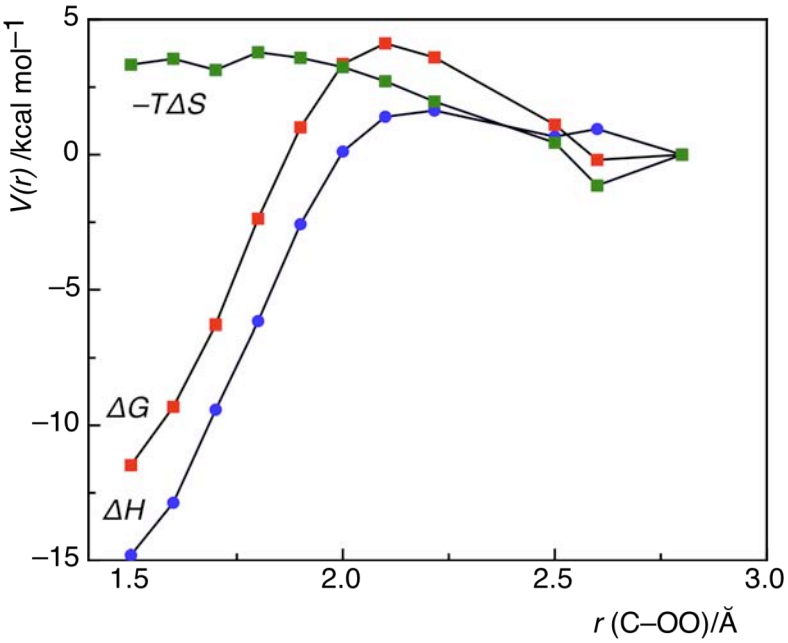

Figure A1–8: Potential energy profile for *p*–trifluorobenzyl radical calculated at UB3LYP with 6–311G(2d,p) basis set.

3. Transition States of Aryl–Substituted Benzyl–OO Radicals

Table A1–2: Calculated energies and optimized transition state structure for benzyl radical.

HF= -421.3666971
Zero-point correction= 0.119599 (Hartree/Particle)
Thermal correction to Energy= 0.128034
Thermal correction to Enthalpy= 0.128978
Thermal correction to Gibbs Free Energy= 0.083733
Sum of electronic and zero-point Energies= -421.247098
Sum of electronic and thermal Energies= -421.238663
Sum of electronic and thermal Enthalpies= -421.237719
Sum of electronic and thermal Free Energies= -421.282965

C	0.005033	-0.001607	-0.000034
C	0.005174	-0.002802	1.395069
C	1.215413	-0.001630	2.089066
C	2.413243	0.001850	1.400222
C	2.437470	0.006222	-0.014153
C	1.198392	0.001873	-0.696595
C	3.661107	-0.016494	-0.723102
O	4.143588	-2.209799	-1.002667
O	5.194361	-2.414479	-1.611469
H	1.216378	-0.003479	3.172699

H	3.352600	0.000335	1.941394
H	1.196105	0.000377	-1.780685
H	-0.934584	-0.003437	-0.539832
H	-0.932147	-0.004573	1.938133
H	3.675889	0.097273	-1.797563
H	4.600600	0.097255	-0.201524

Table A1–3: Calculated energies and optimized transition state structure for *p*–methylbenzyl radical

HF= -460.696687
Zero-point correction= 0.146726 (Hartree/Particle)
Thermal correction to Energy= 0.157065
Thermal correction to Enthalpy= 0.158010
Thermal correction to Gibbs Free Energy= 0.107553
Sum of electronic and zero-point Energies= -460.549961
Sum of electronic and thermal Energies= -460.539621
Sum of electronic and thermal Enthalpies= -460.538677
Sum of electronic and thermal Free Energies= -460.589134

C	0.000000	0.000000	0.000000
C	0.000000	0.000000	1.399824
C	1.179786	0.000000	2.117274
C	2.432270	0.001947	1.461384
C	2.423454	-0.005259	0.046409
C	1.237560	-0.006223	-0.657923
C	3.642671	-0.023926	2.188283
C	-1.287106	0.029141	-0.779110
O	4.133383	-2.224871	2.486077
O	5.179383	-2.420254	3.107426
H	-0.946587	-0.002100	1.929524
H	1.153852	-0.005291	3.201159
H	3.368614	-0.014777	-0.484751
H	1.261088	-0.013661	-1.742559
H	4.590944	0.084863	1.681829
H	3.641233	0.087849	3.263025
H	-2.127571	-0.315493	-0.174833
H	-1.519948	1.044715	-1.116327
H	-1.227931	-0.599465	-1.670255

Table A1–4: Calculated energies and optimized transition state structure for *p*–methoxybenzyl radical

HF= -535.927024
Zero-point correction= 0.151993 (Hartree/Particle)
Thermal correction to Energy= 0.163042

Thermal correction to Enthalpy= 0.163986
Thermal correction to Gibbs Free Energy= 0.112371
Sum of electronic and zero-point Energies= -535.775031
Sum of electronic and thermal Energies= -535.763982
Sum of electronic and thermal Enthalpies= -535.763038
Sum of electronic and thermal Free Energies= -535.814653

C	-0.001984	-0.019824	-0.007845
C	0.000833	-0.009022	1.411482
C	1.173748	0.000481	2.125302
C	2.409451	0.002516	1.459046
C	2.440733	-0.005417	0.060031
C	1.255382	-0.015196	-0.652016
H	-0.946740	-0.007316	1.937990
H	1.175976	0.007306	3.208101
O	3.506122	0.011520	2.257228
H	3.381021	-0.003577	-0.473303
H	1.288780	-0.018047	-1.735561
C	4.790659	0.020482	1.649177
H	5.506692	0.030829	2.467852
H	4.948970	-0.874253	1.040032
H	4.932442	0.912073	1.031539
C	-1.205101	-0.002672	-0.740475
H	-1.197839	-0.110556	-1.815431
H	-2.156826	-0.107259	-0.240127
O	-1.732525	2.215516	-1.064047
O	-2.800553	2.390554	-1.655107

Table A1–5: Calculated energies and optimized transition state structure for *p*–chlorobenzyl radical

HF= -880.992770
Zero-point correction= 0.111223 (Hartree/Particle)
Thermal correction to Energy= 0.121296
Thermal correction to Enthalpy= 0.122240
Thermal correction to Gibbs Free Energy= 0.072713
Sum of electronic and zero-point Energies= -880.870468
Sum of electronic and thermal Energies= -880.860395
Sum of electronic and thermal Enthalpies= -880.859451
Sum of electronic and thermal Free Energies= -880.908978

C	0.000000	0.000000	0.000000
C	0.000000	0.000000	1.380486
C	1.207826	0.000000	2.116141
C	2.419422	0.007278	1.386746
C	2.426569	0.007454	0.006278

C	1.215056	0.003258	-0.680763
H	-0.929007	-0.002329	-0.554433
H	-0.943362	0.000160	1.913900
H	3.359992	0.013119	1.925037
H	3.358430	0.010829	-0.543339
C	1.204089	0.027280	3.529874
H	0.281120	-0.096113	4.077781
H	2.124953	-0.090504	4.082539
Cl	1.219600	0.000857	-2.434548
O	1.196027	2.196252	4.071798
O	1.191499	2.403414	5.286260

Table A1–6: Calculated energies and optimized transition state structure for *p*–triflurobenzyl radical

HF= -758.518659
Zero-point correction= 0.125520 (Hartree/Particle)
Thermal correction to Energy= 0.137910
Thermal correction to Enthalpy= 0.138854
Thermal correction to Gibbs Free Energy= 0.083278
Sum of electronic and zero-point Energies= -758.382246
Sum of electronic and thermal Energies= -758.369856
Sum of electronic and thermal Enthalpies= -758.368912
Sum of electronic and thermal Free Energies= -758.424488

C	0.000000	0.000000	0.000000
C	0.000000	0.000000	1.381179
C	1.207863	0.000000	2.078081
C	2.418835	-0.001321	1.381201
C	2.421511	-0.000579	0.002239
C	1.210486	0.004150	-0.728123
H	-0.940213	-0.005261	-0.538625
H	-0.933527	-0.005129	1.927404
H	3.352672	-0.009196	1.928494
H	3.362148	-0.006436	-0.535635
C	1.211840	-0.024122	-2.144325
H	2.134292	0.101162	-2.692885
H	0.290069	0.100301	-2.694258
O	1.214588	-2.179653	-2.659234
O	1.228041	-2.399881	-3.870257
C	1.224996	0.044196	3.579364
F	0.049847	-0.335626	4.115759
F	2.180315	-0.757559	4.093521
F	1.481618	1.290021	4.038233

References

[1] M. W. Windsor, *Photochem. Photobiol. Sci.* **2003**, *2*, 455.
[2] R. G. W. Norrish, G. Porter, *Discuss. Faraday Soc.* **1947**, *2*, 97.
[3] M. I. Christie, G. Porter, *Proc. R. Soc. London, Ser. A* **1952**, *212*, 390.
[4] K. Knox, R. G. W. Norrish, G. Porter, *J. Chem. Soc.* **1952**, 1477.
[5] R. G. W. Norrish, G. Porter, B. A. Thrush, *Nature* **1952**, *169*, 582.
[6] G. Porter, *Science* **1968**, *160*, 1299.
[7] L. Lindqvis, *C. R. Hebd. Seances Acad. Sci. Ser. C* **1966**, *263*, 852.
[8] N. G. Basov, V. A. Danilych, Y. M. Popov, D. D. Khodkevi, *Jetp Letters-Ussr* **1970**, *12*, 329.
[9] D. Basting, U. Stamm, *Z. Phys. Chemie-Int. J. Res. Phys. Chem. Chem. Phys.* **2001**, *215*, 1575.
[10] A. M. A. Dias, R. P. Bonifacio, I. M. Marrucho, A. A. H. Padua, M. F. Costa Gomes, *Phys. Chem. Chem. Phys.* **2003**, *5*, 543.
[11] S. Horstmann, A. Grybat, R. Kato, *J. Chem. Thermodyn.* **2004**, *36*, 1015.
[12] R. A. Pascal, W. D. McMillan, D. Vanengen, R. G. Eason, *J. Am. Chem. Soc.* **1987**, *109*, 4660.
[13] R. P. Lesperance, D. Vanengen, R. Dayal, R. A. Pascal, *J. Org. Chem.* **1991**, *56*, 688.
[14] S. Chiavarelli, G. Settimj, A. H. Magalhaes, *Gazz. Chim. Ital.* **1957**, *87*, 109.
[15] M. Lipson, T. H. Noh, C. E. Doubleday, J. M. Zaleski, N. J. Turro, *J. Phys. Chem.* **1994**, *98*, 8844.
[16] T. H. Noh, E. Step, N. J. Turro, *J. Photochem. Photobiol. A-Chem.* **1993**, *72*, 133.
[17] P. S. Engel, *J. Am. Chem. Soc.* **1970**, *92*, 6074.
[18] L. Lunazzi, K. U. Ingold, J. C. Scaiano, *J. Phys. Chem.* **1983**, *87*, 529.
[19] X. Y. Zhang, W. M. Nau, *J. Phys. Org. Chem.* **2000**, *13*, 634.
[20] M. J. Frisch, G. W. Trucks, H. B. Schlegel, G. E. Scuseria, M. A. Robb, J. R. Cheeseman, J. A. Montgomery, T. V. Jr., K. N. Kudin, J. C. Burant, J. M. Millam, S. S. Iyengar, J. Tomasi, V. Barone, B. Mennucci, M. Cossi, G. Scalmani, N. Rega, G. A. Petersson, H. Nakatsuji, M. Hada, M. Ehara, K. Toyota, R. Fukuda, J. Hasegawa, M. Ishida, T. Nakajima, Y. Honda, O. Kitao, H. Nakai, M. Klene, X. Li, J. E. Knox, H. P. Hratchian, J. B. Cross, V. Bakken, C. Adamo, J. Jaramillo, R. Gomperts, R. E. Stratmann, O. Yazyev, A. J. Austin, R. Cammi, C. Pomelli, J. W. Ochterski, P. Y. Ayala, K. Morokuma, G. A. Voth, P. Salvador, J. J. Dannenberg, V. G. Zakrzewski, S. Dapprich, A. D. Daniels, M. C. Strain, O. Farkas, D. K. Malick, A. D. Rabuck, K. Raghavachari, J. B. Foresman, J. V. Ortiz, Q. Cui, A. G. Baboul, S. Clifford, J. Cioslowski, B. B. Stefanov, G. Liu, A. Liashenko, P. Piskorz, I. Komaromi, R. L. Martin, D. J. Fox, T. Keith, M. A. Al-Laham, C. Y. Peng, A. Nanayakkara, M. Challacombe, P. M. W. Gill, B. Johnson, W. Chen, M. W. Wong, C. Gonzalez, J. A. Pople, *Gaussian 03 Revision E.01*, Gaussian.

Appendix II

Solvent Polarity Affects H Atom Abstractions from C–H Donors

Hamdy S. El-Sheshtawy,[†] Uwe Pischel,[‡,]* Werner M. Nau[†,]*

School of Engineering and Science, Jacobs University Bremen, Campus Ring 1, D-28759 Bremen (Germany), and Centro de Investigación en Química Sostenible (CIQSO), Universidad de Huelva, Campus de El Carmen, E-21071 Huelva (Spain)

w.nau@jacobs-university.de; uwe.pischel@diq.uhu.es

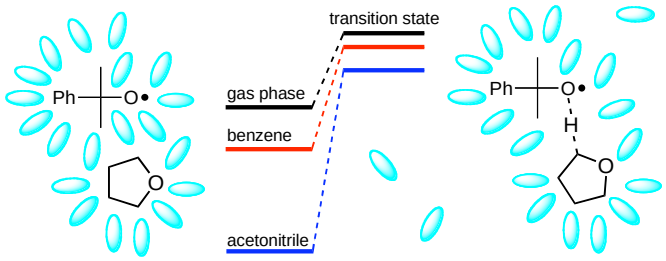

Kinetic solvent effects on hydrogen abstractions involving C–H donors (dienes, ethers, alkylbenzenes) have been corroborated by experiment and theory (UB3LYP/6-311++G**, polarized continuum model). To single out the effect of solvent polarity, rate constants for scavenging of the cumyloxyl radical and fluorescence quenching of 2,3-diazabicyclo[2.2.2]oct-2-ene were obtained in binary aprotic mixtures of ethylacetate and acetonitrile. Polar solvents result in a selective stabilization of the reactants, which results in slower rate constants.

This work corresponds to: H. S. El-Sheshtawy, U. Pischel, W. N. Nau, *Org. Lett.* **2011**, 13, 2694. Pages from 102-121 are not displayed here because of the copyright restrictions.

Appendix III

Appendix III

1. Materials and Methods

1.1 Synthesis of Cucurbit[7]uril

The CB7 synthesis has been performed according to the standard procedures in the literature.[1-3] However, the modification for the synthesis developed by our group has been followed in order to have high CB7 yield (Figure A3–1).[2] This procedure has undergone modifications and improvements, as listed below:

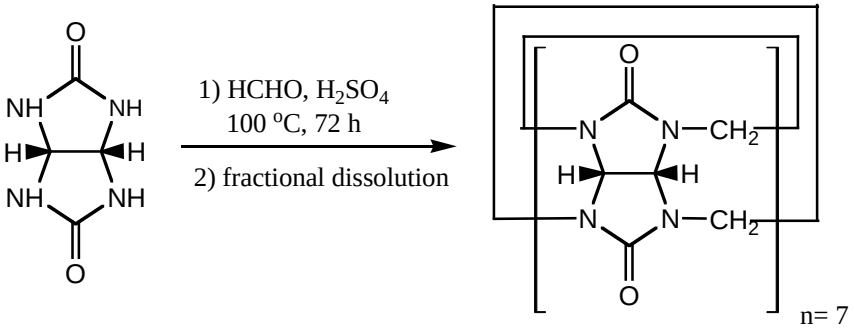

Figure A3–1. Synthesis and isolation of CB7

All reagents for synthesis were purchased from Fluka, glycouril (≥98%) was from Aldrich and acetone was from Applichem. Formaldehyde (20 ml of 37 % aqueous solution) was mixed with sulphoric acid (60 ml of 9 M aqueous solution) and the magnetically stirred mixture was cooled down to 2–5 °C, using an ice bath. Glycoluril (11.46 g, 80 mmol), was added in small portions during 2 hours. Then the temperature was increased to 95 °C using an oil bath. As a result the formed viscous gel redissolved. Heating was continued for 72 hours. The reaction mixture was then poured into 200 ml of deionized water. Then 800 ml of acetone were added. This produced white precipitate, which contained all of the CBn oligomers. The suspension was let to settle down and filtered using a large frit and washed with 250 ml mixture of acetone and water (8:2 v/v).

In order to remove the concentrated acid the filtrate was collected and decanted with I liter of acetone and water mixture (8:2 v/v) on small portions. Then the precipitate was filtered using a glass frit and the filtrate was dissolved in 400 ml deionized water. This dissolved all the oligomers except CB6, which is insoluble in water (solubility in water ca. 20 μM) and was filtered away. This was done twice to ensure that no CB6 is present in the filtrate. 300 ml of acetone were added to the filtrate, which precipitated mainly the CB7 homolouge. The precipitate was immediately filtered and kept in an oven at 75 °C for three days. The product was characterized by ^{1}H NMR (400 MHz, D_2O) δ TMS: 4.14 (d, 14H), 5.39 (s, 14H), 5.65 (d, 14H).

1.2 Solutions

All used solvents in this study unless mentioned are a spectroscopic grade with high purity and purchased from Sigma–Aldrich (Germany) and used without further purification. Iodine (Sigma-Aldrich) concentration was determined from its absorbance at 460 nm using extinction coefficient of 740 M^{-1}. The fluorescent dye, 4′,6-diamidino-2-phenylindole (DAPI), was purchased from Sigma-Aldrich and the concentration was determined using the molar absorption coefficient of 27 x 10^3 $M^{-1}cm^{-1}$ at 340 nm.[4] The concentration of horse radish peroxidase (HRP) (Sigma-Aldrich), lactoperoxidase, (Sigma-Aldrich), and myeloperoxidase (MPO) (Planta Natural Products, Austria) were determined from the UV peaks at 403 nm, 412 nm, and 430 nm using an extinction coefficient of 91, 114, and 91 mM, respectively.[5-7] Hydrogen peroxide obtained from 30% solution (Sigma-Aldrich), was diluted and the concentration determined from the absorbance at 240 nm, where the extinction coefficient is 39.4 molar.[8] 1–adamantanecarboxylic acid and potassium iodide were purchased from Sigma-Aldrich, Germany and used without further purification. Absorption measurements were performed with a Varian Cary 4000 spectrophotometer. For fluorescence measurements, a Varian Ecllipse fluorimeter was used for intensities and time courses at ambient temperature (for the titration) or at 25.0 ± 0.1 °C (using an external Peltier thermostate,

only for the enzyme assay). The pH of the solution was adjusted (± 0.2) using a pH meter (WTW 330i equipped with a combined Sen Tix Mic pH glass electrode).

1.3 Computational Methods

All quantum chemical calculations were performed with Gaussian 03W,[9] and CBs geometries were adopted the symmetry structure; CB5 (C_{2v}), CB6 (D_{6h}), CB7 (C_{2v}), and CB8 (D_{8h}). In order to determine the favorable conformation of I_2 inside CBs, the $CB_n \bullet I_2$ structure were optimized under fixed CB_n geometry (HF/3-21G*), while for the energy calculations no constrain has been applied. A single point energy calculations was performed with MP2/3-21G* to further refine the calculated energy. The molecular volume of I_2 was obtained with the Quantitative Structure–Activity Relationship (QSAR) module of Hyperchem package after conducting a semi–empirical AM1 geometry optimization.

Table A3–1: Calculated relative energies for different $CBs \bullet I_2$ conformations.

	Method	Axial	Equatorial	Axi-Equ kcal M^{-1}
CB6	B3LYP/3-21G*	–17371.57586	–17371.56194	–8.73
	HF/3-21G*	–17345.29666	–17345.27509	–13.54
	MP2/3-21G*	–17352.48908	–17352.48915	+ 0.04
CB7	B3LYP/3-21G*	–17970.33153	–17970.33100	–0.33
	HF/3-21G*	–17940.49547	–17940.49164	–2.40
	MP2/3-21G*	–17948.94349	–17948.94920	+3.59

1.4 Cucurbit[6]uril• I_2 Single–Crystal X–Ray Analysis

X-ray crystallography. A purple block of **CB6• I_2** with dimensions 0.17 x 0.15 x 0.08 mm^3 was mounted on a Hampton cryo-loop for indexing and intensity data collection at 173 K on a Bruker KAPPA APEX II CCD using Mo-Kα radiation (λ = 0.71073 Å). Lorentz and polarization corrections were applied, and an absorption correction was performed using the SADABS program (G. M. Sheldrick, Siemens Analytical X-ray Instrument Division: Madison, WI, 1995). Direct methods were used to locate the electron density peaks (SHELXS-97). Then the atoms were named and refined using successive Fourier maps (SHELXL-97). Due to low amount of data, all heavy atoms were refined isotropically and the hydrogen atoms were calculated in a constrained refinement using a riding model, in order to reduce the amount variable parameters. The crystallographic data for **CB6• I_2** are summarized in Table A3–2, followed by the CIF file.

Table A3–2. Crystal data for CB6•I_2 crystal.

Compound	CB6•I_2
Empirical formula	C36H44I2N24O22
Formula weight, g/mol	1418.75
Crystal system	Orthorhombic
Space group	$Cmc2_1$
a, Å	19.3748(10)
b, Å	16.0589(10)
c, Å	16.0249(11)
α , °	90
β , °	90
Γ , °	90
Volume, $Å^3$	4986.0(5)
Z	4
D_{calc}, g/cm^3	1.890
Absorption coefficient	1.371
F(000)	2840
Crystal size, mm	0.17 x 0.15 x 0.08
Theta range for data collection, °	3.40 - 21.97
Reflections collected	25924
Independent reflections	3153
R(int)	0.0800
Observed ($I > 2\sigma(I)$)	2716
Goodness-of-fit on F2	1.000
$R_1[I > 2\sigma(I)]$[a]	0.0738
wR_2 (all data)[b]	0.2163

[a] $R = \Sigma||F_o| - |F_c||/\Sigma|F_o|$. [b] $R_w = [\Sigma w(F_o^2 - F_c^2)^2/\Sigma w(F_o^2)^2]^{1/2}$.

CIF file for CB6• I_2 crystal: data_wn4

```
_audit_creation_method            SHELXL-97
_chemical_name_systematic
;
 ?
;
_chemical_name_common             ?
_chemical_melting_point           ?
_chemical_formula_moiety          ?
_chemical_formula_sum
 'C36 H44 I2 N24 O22'
_chemical_formula_weight          1418.75

loop_
 _atom_type_symbol
 _atom_type_description
 _atom_type_scat_dispersion_real
 _atom_type_scat_dispersion_imag
 _atom_type_scat_source
 'C'  'C'   0.0033   0.0016
 'International Tables Vol C Tables 4.2.6.8 and 6.1.1.4'
 'H'  'H'   0.0000   0.0000
 'International Tables Vol C Tables 4.2.6.8 and 6.1.1.4'
 'N'  'N'   0.0061   0.0033
 'International Tables Vol C Tables 4.2.6.8 and 6.1.1.4'
 'O'  'O'   0.0106   0.0060
 'International Tables Vol C Tables 4.2.6.8 and 6.1.1.4'
 'I'  'I'  -0.4742   1.8119
 'International Tables Vol C Tables 4.2.6.8 and 6.1.1.4'

_symmetry_cell_setting            Orthorhombic
_symmetry_space_group_name_H-M    Cmc2(1)

loop_
 _symmetry_equiv_pos_as_xyz
 'x, y, z'
 '-x, -y, z+1/2'
 'x, -y, z+1/2'
 '-x, y, z'
 'x+1/2, y+1/2, z'
 '-x+1/2, -y+1/2, z+1/2'
 'x+1/2, -y+1/2, z+1/2'
 '-x+1/2, y+1/2, z'

_cell_length_a                    19.3748(10)
_cell_length_b                    16.0589(10)
_cell_length_c                    16.0249(11)
_cell_angle_alpha                 90.00
_cell_angle_beta                  90.00
_cell_angle_gamma                 90.00
_cell_volume                      4986.0(5)
_cell_formula_units_Z             4
```

```
_cell_measurement_temperature     173(2)
_cell_measurement_reflns_used     3705
_cell_measurement_theta_min       2.54
_cell_measurement_theta_max       19.92

_exptl_crystal_description        block
_exptl_crystal_colour             purple
_exptl_crystal_size_max           0.17
_exptl_crystal_size_mid           0.15
_exptl_crystal_size_min           0.08
_exptl_crystal_density_meas       ?
_exptl_crystal_density_diffrn     1.890
_exptl_crystal_density_method     'not measured'
_exptl_crystal_F_000              2840
_exptl_absorpt_coefficient_mu     1.371
_exptl_absorpt_correction_type    multi-scan
_exptl_absorpt_correction_T_min   0.8024
_exptl_absorpt_correction_T_max   0.8982
_exptl_absorpt_process_details    SADABS

_exptl_special_details
;
 ?
;

_diffrn_ambient_temperature       173(2)
_diffrn_radiation_wavelength      0.71073
_diffrn_radiation_type            MoK\a
_diffrn_radiation_source          'fine-focus sealed tube'
_diffrn_radiation_monochromator   graphite
_diffrn_measurement_device_type   'Bruker APEX-II CCD'
_diffrn_measurement_method        '\f and \w scans'
_diffrn_detector_area_resol_mean  ?
_diffrn_reflns_number             25924
_diffrn_reflns_av_R_equivalents   0.0800
_diffrn_reflns_av_sigmaI/netI     0.0465
_diffrn_reflns_limit_h_min        -19
_diffrn_reflns_limit_h_max        20
_diffrn_reflns_limit_k_min        -16
_diffrn_reflns_limit_k_max        16
_diffrn_reflns_limit_l_min        -16
_diffrn_reflns_limit_l_max        16
_diffrn_reflns_theta_min          3.40
_diffrn_reflns_theta_max          21.97
_diffrn_measured_fraction_theta_max    0.995
_diffrn_reflns_theta_full              21.97
_diffrn_measured_fraction_theta_full   0.995
_reflns_number_total              3153
_reflns_number_gt                 2716
_reflns_threshold_expression      >2sigma(I)

_computing_data_collection        'Bruker APEX2'
_computing_cell_refinement        'Bruker SAINT'
_computing_data_reduction         'Bruker SAINT'
```

```
_computing_structure_solution     'SHELXS-97 (Sheldrick, 2008)'
_computing_structure_refinement   'SHELXL-97 (Sheldrick, 2008)'
_computing_molecular_graphics     'Bruker SHELXTL'
_computing_publication_material   'Bruker SHELXTL'

_refine_special_details
;
 Refinement of F^2^ against ALL reflections.  The weighted R-factor
wR and
 goodness of fit S are based on F^2^, conventional R-factors R are
based
 on F, with F set to zero for negative F^2^. The threshold
expression of
 F^2^ > 2sigma(F^2^) is used only for calculating R-factors(gt) etc.
and is
 not relevant to the choice of reflections for refinement.  R-
factors based
 on F^2^ are statistically about twice as large as those based on F,
and R-
 factors based on ALL data will be even larger.
;

_refine_ls_structure_factor_coef  Fsqd
_refine_ls_matrix_type            full
_refine_ls_weighting_scheme       calc
_refine_ls_weighting_details
 'calc w=1/[\s^2^(Fo^2^)+(0.1400P)^2^+70.0000P] where
P=(Fo^2^+2Fc^2^)/3'
_atom_sites_solution_primary      direct
_atom_sites_solution_secondary    difmap
_atom_sites_solution_hydrogens    geom
_refine_ls_hydrogen_treatment     mixed
_refine_ls_extinction_method      none
_refine_ls_extinction_coef        ?
_refine_ls_abs_structure_details
 'Flack H D (1983), Acta Cryst. A39, 876-881'
_refine_ls_abs_structure_Flack    0.01(5)
_refine_ls_number_reflns          3153
_refine_ls_number_parameters      198
_refine_ls_number_restraints      1
_refine_ls_R_factor_all           0.0864
_refine_ls_R_factor_gt            0.0738
_refine_ls_wR_factor_ref          0.2163
_refine_ls_wR_factor_gt           0.2034
_refine_ls_goodness_of_fit_ref    1.000
_refine_ls_restrained_S_all       1.000
_refine_ls_shift/su_max           0.000
_refine_ls_shift/su_mean          0.000
_refine_diff_density_max    0.787
_refine_diff_density_min   -2.226
_refine_diff_density_rms    0.154

loop_
 _atom_site_label
```

```
 _atom_site_type_symbol
 _atom_site_fract_x
 _atom_site_fract_y
 _atom_site_fract_z
 _atom_site_U_iso_or_equiv
 _atom_site_adp_type
 _atom_site_occupancy
 _atom_site_symmetry_multiplicity
 _atom_site_calc_flag
 _atom_site_refinement_flags
 _atom_site_disorder_assembly
 _atom_site_disorder_group
C1 C 0.1844(5) 0.2006(6) 0.0835(6) 0.014(2) Uiso 1 1 d . . .
C2 C 0.2591(5) 0.1209(6) 0.1752(6) 0.018(2) Uiso 1 1 d . . .
H2A H 0.3089 0.1313 0.1838 0.021 Uiso 1 1 calc R . .
H2B H 0.2547 0.0804 0.1289 0.021 Uiso 1 1 calc R . .
C3 C 0.1811(5) 0.3661(6) 0.2602(6) 0.015(2) Uiso 1 1 d . . .
C4 C 0.0000 -0.0719(8) 0.3327(8) 0.014(3) Uiso 1 2 d S . .
C5 C 0.0408(5) 0.4149(6) 0.0444(6) 0.015(2) Uiso 1 1 d . . .
H5A H 0.0595 0.4546 0.0021 0.018 Uiso 1 1 calc R . .
C6 C 0.0413(5) -0.0318(6) 0.4642(6) 0.014(2) Uiso 1 1 d . . .
H6A H 0.0602 -0.0735 0.5046 0.017 Uiso 1 1 calc R . .
C7 C 0.1275(5) -0.0728(6) 0.3524(6) 0.012(2) Uiso 1 1 d . . .
H7A H 0.1518 -0.1029 0.3976 0.014 Uiso 1 1 calc R . .
H7B H 0.1253 -0.1102 0.3034 0.014 Uiso 1 1 calc R . .
C8 C 0.2574(5) 0.2671(6) 0.3361(6) 0.017(2) Uiso 1 1 d . . .
H8A H 0.2517 0.3080 0.3819 0.021 Uiso 1 1 calc R . .
H8B H 0.3074 0.2577 0.3282 0.021 Uiso 1 1 calc R . .
C9 C 0.1258(5) 0.0754(6) 0.5125(6) 0.011(2) Uiso 1 1 d . . .
H9A H 0.1485 0.0270 0.5391 0.014 Uiso 1 1 calc R . .
H9B H 0.1230 0.1203 0.5548 0.014 Uiso 1 1 calc R . .
C10 C 0.1247(5) 0.3075(6) -0.0028(6) 0.012(2) Uiso 1 1 d . . .
H10A H 0.1460 0.3547 -0.0331 0.014 Uiso 1 1 calc R . .
H10B H 0.1203 0.2606 -0.0425 0.014 Uiso 1 1 calc R . .
C11 C 0.2071(5) 0.0469(6) 0.3905(6) 0.013(2) Uiso 1 1 d . . .
H11A H 0.2382 0.0096 0.4234 0.016 Uiso 1 1 calc R . .
C12 C 0.0000 0.2855(8) 0.0041(8) 0.012(3) Uiso 1 2 d S . .
C13 C 0.0000 0.0977(8) 0.5074(8) 0.012(3) Uiso 1 2 d S . .
C14 C 0.2488(5) 0.2782(6) 0.1753(6) 0.016(2) Uiso 1 1 d . . .
H14A H 0.2995 0.2859 0.1664 0.019 Uiso 1 1 calc R . .
C15 C 0.1816(5) 0.1854(6) 0.4286(6) 0.011(2) Uiso 1 1 d . . .
C16 C 0.2073(5) 0.3369(6) 0.1206(6) 0.016(2) Uiso 1 1 d . . .
H16A H 0.2383 0.3754 0.0889 0.019 Uiso 1 1 calc R . .
C17 C 0.2492(5) 0.1078(6) 0.3342(6) 0.013(2) Uiso 1 1 d . . .
H17A H 0.3000 0.1018 0.3441 0.016 Uiso 1 1 calc R . .
C18 C 0.1853(5) 0.0172(6) 0.2523(6) 0.017(2) Uiso 1 1 d . . .
C19 C 0.0000 0.4576(9) 0.1767(9) 0.016(3) Uiso 1 2 d S . .
C20 C 0.1265(5) 0.4576(7) 0.1580(7) 0.024(2) Uiso 1 1 d . . .
H20A H 0.1235 0.4934 0.2082 0.029 Uiso 1 1 calc R . .
H20B H 0.1524 0.4887 0.1148 0.029 Uiso 1 1 calc R . .
N1 N 0.2272(4) 0.1972(5) 0.1503(5) 0.0179(19) Uiso 1 1 d . . .
N2 N 0.2288(4) 0.3020(5) 0.2599(6) 0.0186(18) Uiso 1 1 d . . .
N3 N 0.1670(4) 0.0004(5) 0.3305(5) 0.0160(19) Uiso 1 1 d . . .
N4 N 0.1711(4) 0.2823(5) 0.0651(5) 0.0177(19) Uiso 1 1 d . . .
```

```
N5 N 0.0576(4) 0.4410(5) 0.1277(5) 0.017(2) Uiso 1 1 d . . .
N6 N 0.2311(4) 0.0827(5) 0.2512(5) 0.0168(18) Uiso 1 1 d . . .
N7 N 0.1643(4) 0.3825(5) 0.1789(5) 0.0180(19) Uiso 1 1 d . . .
N8 N 0.0571(4) 0.0520(5) 0.4893(5) 0.0131(19) Uiso 1 1 d . . .
N9 N 0.1686(4) 0.1037(5) 0.4448(5) 0.0142(18) Uiso 1 1 d . . .
N10 N 0.2249(4) 0.1885(5) 0.3607(5) 0.0160(19) Uiso 1 1 d . . .
N11 N 0.0570(4) -0.0538(5) 0.3801(5) 0.0111(17) Uiso 1 1 d . . .
N12 N 0.0576(4) 0.3315(5) 0.0238(5) 0.0161(18) Uiso 1 1 d . . .
O1 O 0.1645(3) 0.1404(4) 0.0411(4) 0.0206(16) Uiso 1 1 d . . .
O2 O 0.1606(3) 0.2453(4) 0.4678(4) 0.0207(17) Uiso 1 1 d . . .
O3 O 0.1604(4) 0.4030(5) 0.3209(4) 0.0260(18) Uiso 1 1 d . . .
O4 O 0.0000 0.4877(6) 0.2460(6) 0.026(2) Uiso 1 2 d S . .
O5 O 0.0000 0.1705(6) 0.5351(6) 0.017(2) Uiso 1 2 d S . .
O6 O 0.0000 -0.1002(5) 0.2624(6) 0.015(2) Uiso 1 2 d S . .
O7 O 0.1675(3) -0.0220(4) 0.1892(4) 0.0244(17) Uiso 1 1 d . . .
O8 O 0.0000 0.2153(6) -0.0256(6) 0.022(2) Uiso 1 2 d S . .
I1 I 0.0000 0.10948(19) 0.20516(18) 0.0580(9) Uiso 0.60 2 d SP . .
I2 I 0.0000 0.24935(14) 0.29794(15) 0.0638(7) Uiso 0.80 2 d SP . .
I1A I 0.0299(4) 0.1186(4) 0.2045(4) 0.0546(14) Uiso 0.20 1 d P . .
I2A I 0.0328(7) 0.2417(7) 0.2900(9) 0.057(2) Uiso 0.10 1 d P . .
O1W O 0.1643(5) 0.4436(6) 0.4871(6) 0.050(2) Uiso 1 1 d . . .
O2WA O -0.0910(9) 0.6469(12) 0.2904(13) 0.054(5) Uiso 0.50 1 d P . .
O2WB O -0.0696(10) 0.6119(12) 0.3396(13) 0.056(5) Uiso 0.50 1 d P .
.
O3WA O -0.0779(8) 0.7810(10) 0.1804(10) 0.035(4) Uiso 0.50 1 d P . .
O3WB O -0.0842(7) 0.7504(8) 0.2419(9) 0.024(3) Uiso 0.50 1 d P . .
O4WA O -0.0777(7) -0.3222(8) 0.0893(9) 0.023(3) Uiso 0.50 1 d P . .
O4WB O -0.0559(9) -0.3483(12) 0.0321(12) 0.048(5) Uiso 0.50 1 d P .
.
O5WI O 0.0000 0.4148(12) 0.3976(12) 0.087(5) Uiso 1 2 d S . .

_geom_special_details
;
 All esds (except the esd in the dihedral angle between two l.s.
planes)
 are estimated using the full covariance matrix.  The cell esds are
taken
 into account individually in the estimation of esds in distances,
angles
 and torsion angles; correlations between esds in cell parameters
are only
 used when they are defined by crystal symmetry.  An approximate
(isotropic)
 treatment of cell esds is used for estimating esds involving l.s.
planes.
;

loop_
 _geom_bond_atom_site_label_1
 _geom_bond_atom_site_label_2
 _geom_bond_distance
 _geom_bond_site_symmetry_2
 _geom_bond_publ_flag
C1 O1 1.243(12) . ?
```

```
C1 N1 1.354(13) . ?
C1 N4 1.369(14) . ?
C2 N1 1.429(13) . ?
C2 N6 1.468(13) . ?
C3 O3 1.208(12) . ?
C3 N7 1.368(13) . ?
C3 N2 1.383(13) . ?
C4 O6 1.213(15) . ?
C4 N11 1.372(11) . ?
C4 N11 1.372(11) 4 ?
C5 N12 1.417(14) . ?
C5 N5 1.436(13) . ?
C5 C5 1.58(2) 4 ?
C6 N11 1.427(13) . ?
C6 N8 1.438(13) . ?
C6 C6 1.599(19) 4 ?
C7 N3 1.445(13) . ?
C7 N11 1.469(12) . ?
C8 N2 1.453(13) . ?
C8 N10 1.464(13) . ?
C9 N8 1.432(12) . ?
C9 N9 1.439(13) . ?
C10 N12 1.421(13) . ?
C10 N4 1.468(13) . ?
C11 N3 1.444(13) . ?
C11 N9 1.465(13) . ?
C11 C17 1.561(14) . ?
C12 O8 1.224(17) . ?
C12 N12 1.374(12) 4 ?
C12 N12 1.374(12) . ?
C13 O5 1.250(16) . ?
C13 N8 1.360(11) . ?
C13 N8 1.360(11) 4 ?
C14 N1 1.426(13) . ?
C14 N2 1.461(13) . ?
C14 C16 1.518(14) . ?
C15 O2 1.218(11) . ?
C15 N9 1.361(12) . ?
C15 N10 1.375(13) . ?
C16 N4 1.432(13) . ?
C16 N7 1.450(13) . ?
C17 N6 1.434(12) . ?
C17 N10 1.444(13) . ?
C18 O7 1.240(12) . ?
C18 N3 1.330(13) . ?
C18 N6 1.376(13) . ?
C19 O4 1.210(17) . ?
C19 N5 1.390(12) . ?
C19 N5 1.390(12) 4 ?
C20 N5 1.447(14) . ?
C20 N7 1.450(14) . ?
I1 I1A 0.597(7) 4 ?
I1 I1A 0.597(7) . ?
I1 I2A 2.601(13) . ?
```

```
I1 I2A 2.601(13) 4 ?
I1 I2 2.694(4) . ?
I2 I2A 0.660(13) 4 ?
I2 I2A 0.660(13) . ?
I2 I1A 2.644(7) 4 ?
I2 I1A 2.644(7) . ?
I1A I1A 1.157(14) 4 ?
I1A I2A 2.407(13) . ?
I1A I2A 2.695(13) 4 ?
I2A I2A 1.27(3) 4 ?
I2A I1A 2.695(13) 4 ?
O2WA O2WB 1.05(2) . ?
O3WA O3WB 1.11(2) . ?
O4WA O4WB 1.09(2) . ?

loop_
 _geom_angle_atom_site_label_1
 _geom_angle_atom_site_label_2
 _geom_angle_atom_site_label_3
 _geom_angle
 _geom_angle_site_symmetry_1
 _geom_angle_site_symmetry_3
 _geom_angle_publ_flag
O1 C1 N1 126.2(9) . . ?
O1 C1 N4 124.6(9) . . ?
N1 C1 N4 108.9(8) . . ?
N1 C2 N6 115.5(8) . . ?
O3 C3 N7 126.4(9) . . ?
O3 C3 N2 126.1(9) . . ?
N7 C3 N2 107.5(8) . . ?
O6 C4 N11 126.4(6) . . ?
O6 C4 N11 126.4(6) . 4 ?
N11 C4 N11 107.2(11) . 4 ?
N12 C5 N5 116.2(8) . . ?
N12 C5 C5 103.2(5) . 4 ?
N5 C5 C5 103.0(5) . 4 ?
N11 C6 N8 116.7(8) . . ?
N11 C6 C6 102.3(5) . 4 ?
N8 C6 C6 102.3(5) . 4 ?
N3 C7 N11 113.4(8) . . ?
N2 C8 N10 113.2(8) . . ?
N8 C9 N9 115.0(8) . . ?
N12 C10 N4 114.4(8) . . ?
N3 C11 N9 116.4(8) . . ?
N3 C11 C17 102.8(7) . . ?
N9 C11 C17 102.7(8) . . ?
O8 C12 N12 125.7(6) . 4 ?
O8 C12 N12 125.7(6) . . ?
N12 C12 N12 108.6(11) 4 . ?
O5 C13 N8 125.5(6) . . ?
O5 C13 N8 125.5(6) . 4 ?
N8 C13 N8 109.0(11) . 4 ?
N1 C14 N2 115.0(8) . . ?
N1 C14 C16 104.4(8) . . ?
```

```
N2 C14 C16 103.5(8) . . ?
O2 C15 N9 126.9(9) . . ?
O2 C15 N10 125.7(9) . . ?
N9 C15 N10 107.4(8) . . ?
N4 C16 N7 115.4(8) . . ?
N4 C16 C14 103.8(8) . . ?
N7 C16 C14 104.2(8) . . ?
N6 C17 N10 116.4(8) . . ?
N6 C17 C11 103.4(8) . . ?
N10 C17 C11 102.8(7) . . ?
O7 C18 N3 126.3(9) . . ?
O7 C18 N6 123.8(9) . . ?
N3 C18 N6 109.8(8) . . ?
O4 C19 N5 126.5(6) . . ?
O4 C19 N5 126.5(6) . 4 ?
N5 C19 N5 106.7(11) . 4 ?
N5 C20 N7 113.0(8) . . ?
C1 N1 C14 111.4(8) . . ?
C1 N1 C2 121.4(8) . . ?
C14 N1 C2 125.2(8) . . ?
C3 N2 C8 122.6(8) . . ?
C3 N2 C14 112.0(8) . . ?
C8 N2 C14 125.3(7) . . ?
C18 N3 C11 112.3(8) . . ?
C18 N3 C7 122.3(8) . . ?
C11 N3 C7 122.9(8) . . ?
C1 N4 C16 111.2(8) . . ?
C1 N4 C10 122.6(8) . . ?
C16 N4 C10 126.2(8) . . ?
C19 N5 C5 113.6(8) . . ?
C19 N5 C20 121.1(9) . . ?
C5 N5 C20 125.1(8) . . ?
C18 N6 C17 111.2(8) . . ?
C18 N6 C2 124.6(8) . . ?
C17 N6 C2 124.2(7) . . ?
C3 N7 C20 120.0(8) . . ?
C3 N7 C16 112.3(8) . . ?
C20 N7 C16 124.2(8) . . ?
C13 N8 C9 124.0(8) . . ?
C13 N8 C6 113.0(8) . . ?
C9 N8 C6 121.1(8) . . ?
C15 N9 C9 123.7(8) . . ?
C15 N9 C11 113.1(8) . . ?
C9 N9 C11 123.0(8) . . ?
C15 N10 C17 113.6(8) . . ?
C15 N10 C8 120.4(8) . . ?
C17 N10 C8 123.6(8) . . ?
C4 N11 C6 113.8(8) . . ?
C4 N11 C7 122.6(8) . . ?
C6 N11 C7 122.3(8) . . ?
C12 N12 C5 112.0(8) . . ?
C12 N12 C10 121.9(9) . . ?
C5 N12 C10 122.4(8) . . ?
I1A I1 I1A 151.6(15) 4 . ?
```

```
I1A I1 I2A 92.7(8) 4 . ?
I1A I1 I2A 64.7(8) . . ?
I1A I1 I2A 64.7(8) 4 4 ?
I1A I1 I2A 92.7(8) . 4 ?
I2A I1 I2A 28.3(6) . 4 ?
I1A I1 I2 78.8(8) 4 . ?
I1A I1 I2 78.8(8) . . ?
I2A I1 I2 14.2(3) . . ?
I2A I1 I2 14.2(3) 4 . ?
I2A I2 I2A 149(2) 4 . ?
I2A I2 I1A 62.2(12) 4 4 ?
I2A I2 I1A 87.4(12) . 4 ?
I2A I2 I1A 87.4(12) 4 . ?
I2A I2 I1A 62.2(12) . . ?
I1A I2 I1A 25.3(3) 4 . ?
I2A I2 I1 74.9(12) 4 . ?
I2A I2 I1 74.9(12) . . ?
I1A I2 I1 12.79(15) 4 . ?
I1A I2 I1 12.79(15) . . ?
I1 I1A I1A 14.2(8) . 4 ?
I1 I1A I2A 102.3(9) . . ?
I1A I1A I2A 91.4(4) 4 . ?
I1 I1A I2 88.4(8) . . ?
I1A I1A I2 77.36(15) 4 . ?
I2A I1A I2 14.0(3) . . ?
I1 I1A I2A 74.5(8) . 4 ?
I1A I1A I2A 63.2(3) 4 4 ?
I2A I1A I2A 28.1(6) . 4 ?
I2 I1A I2A 14.1(3) . 4 ?
I2 I2A I2A 15.5(12) . 4 ?
I2 I2A I1A 103.8(13) . . ?
I2A I2A I1A 88.6(4) 4 . ?
I2 I2A I1 90.9(12) . . ?
I2A I2A I1 75.9(3) 4 . ?
I1A I2A I1 12.95(19) . . ?
I2 I2A I1A 78.5(12) . 4 ?
I2A I2A I1A 63.2(3) 4 4 ?
I1A I2A I1A 25.4(3) . 4 ?
I1 I2A I1A 12.77(15) . 4 ?
```

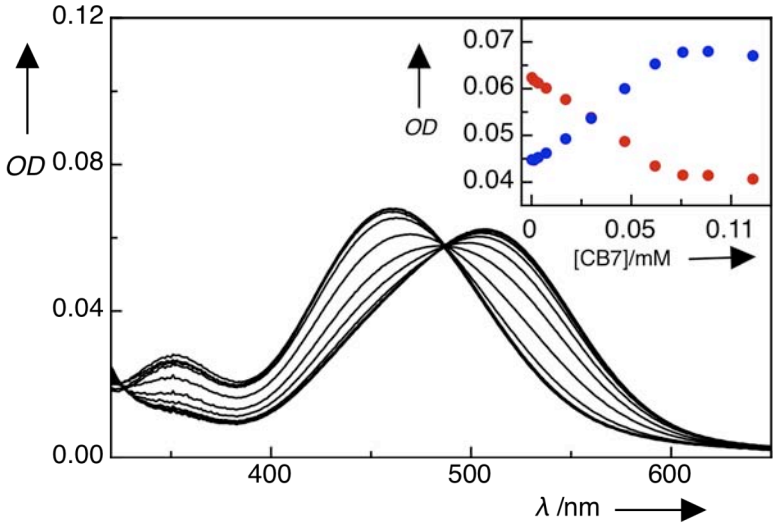

Figure A3–2: UV–Vis absorbance change of 90 μM I_2 and 170 μM CB7 aqueous solution upon addition of successive concentration of 1–adamantanecarboxylic acid (60 μM) at pH 3.3.

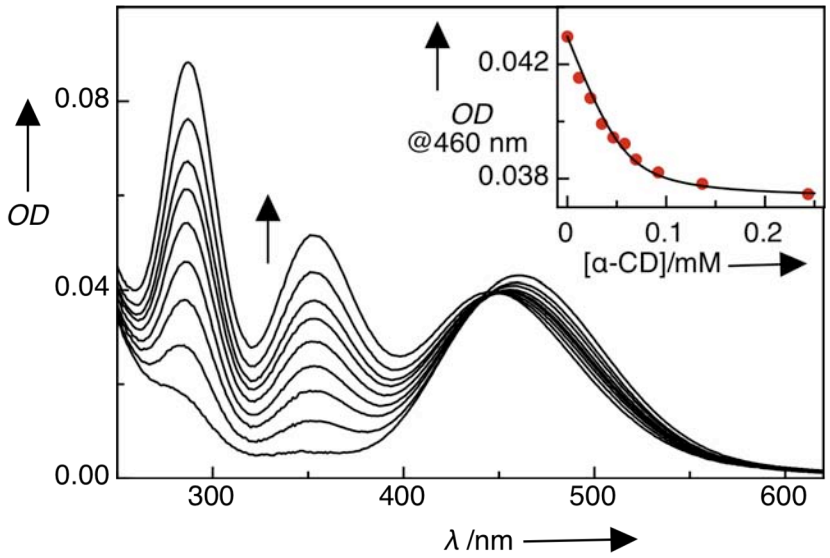

Figure A3–3: UV–Vis titrations of iodine (50 μM) upon addition of α–CD in aqueous solution. The insets show the titration curves fitted according to 1:1 binding model.

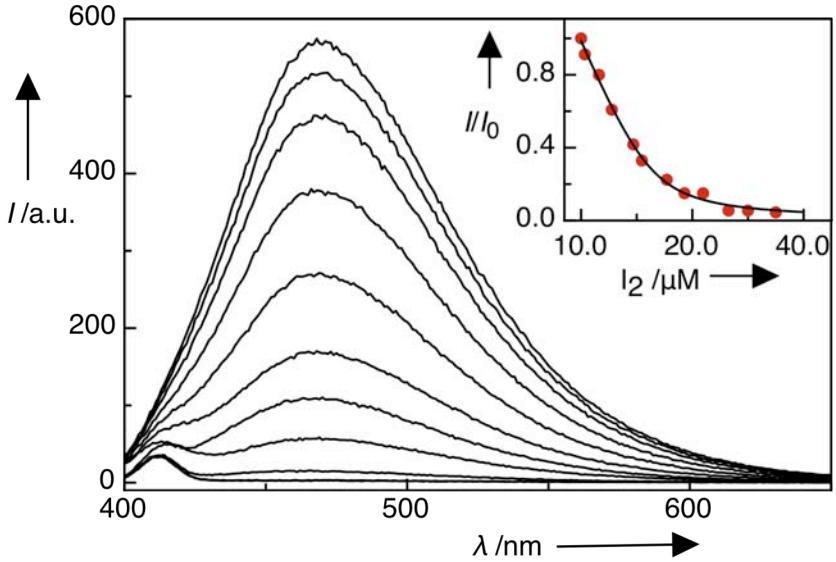

Figure A3–4: Changes in fluorescence intensity and spectra of DAPI/CB7 reporter pair (0.2 μM DAPI, 0.3 μM CB7 λ_{exc} = 361 nm, λ_{em} = 467 nm) upon displacement by I_2 in H_2O, pH 3. The data were fitted according to 1:1 complexation (inset).

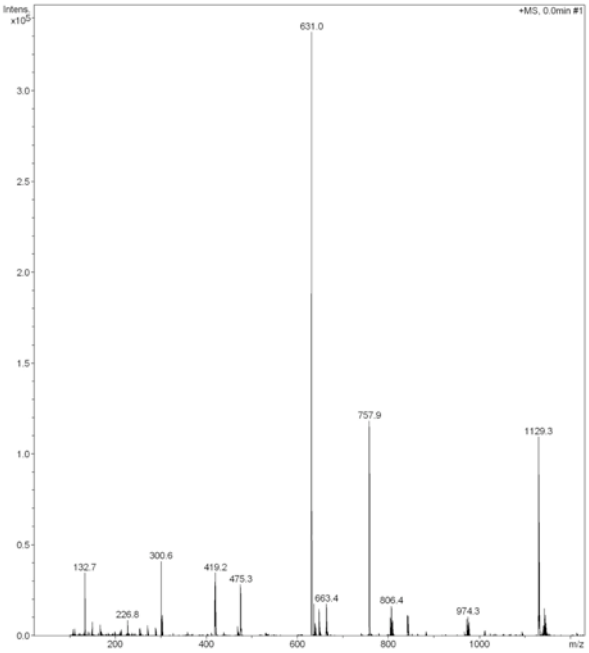

Figure A3–5: Electron spray mass spectrum of CB6•2Cs^+ with two Cs^+ ions on the portal (m/z = 631.0) and CB6•I_2•2Cs^+ molecular complex with I_2 encapsulated inside CB6 and two Cs^+ (m/z = 757.9) are attached on the portals as "lids".

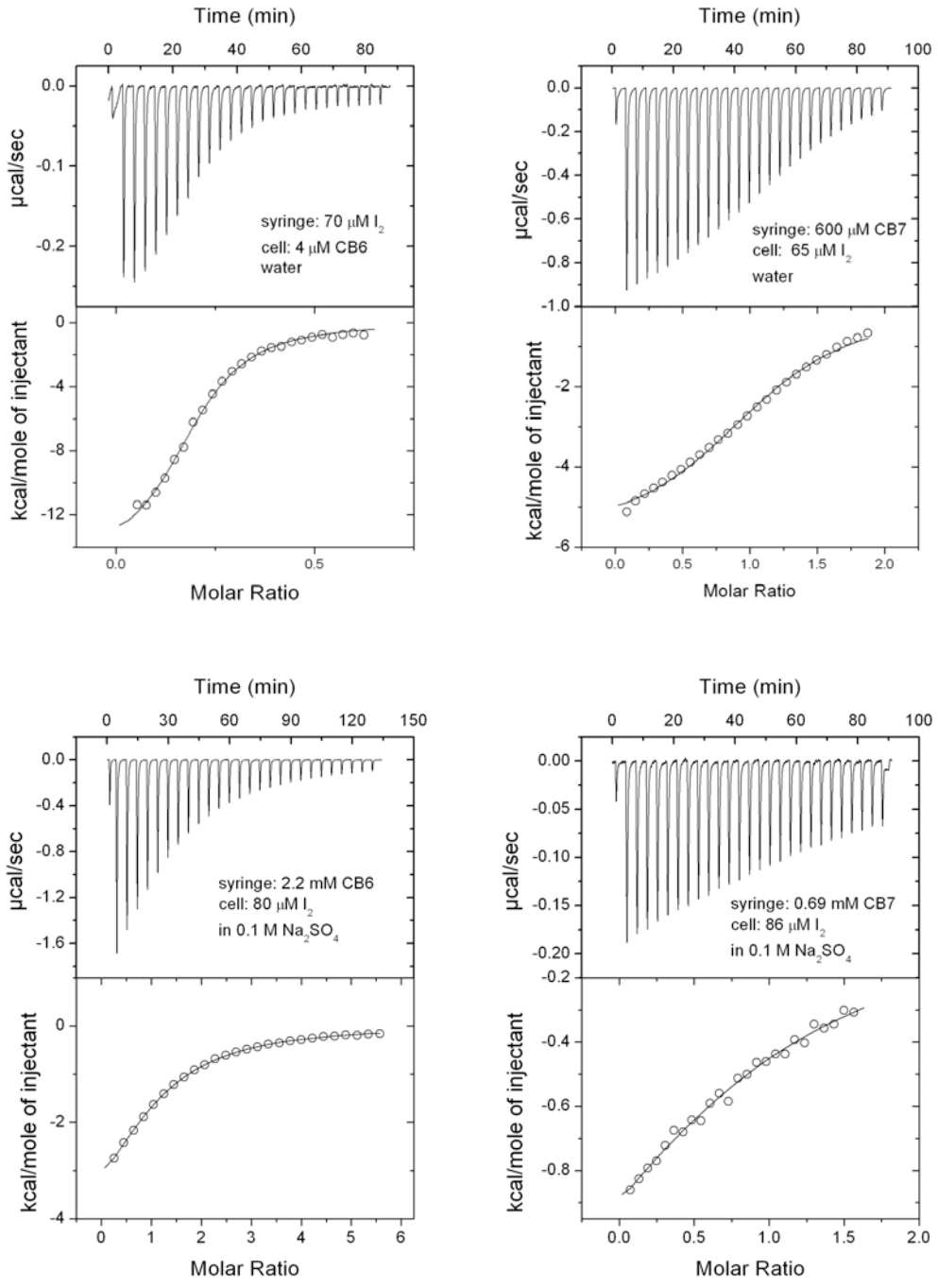

Figure A3–6: Microcalorimetric titration of CB6 and CB7 with I_2 in aqueous solution (pH 3.3) at 298.15 k.

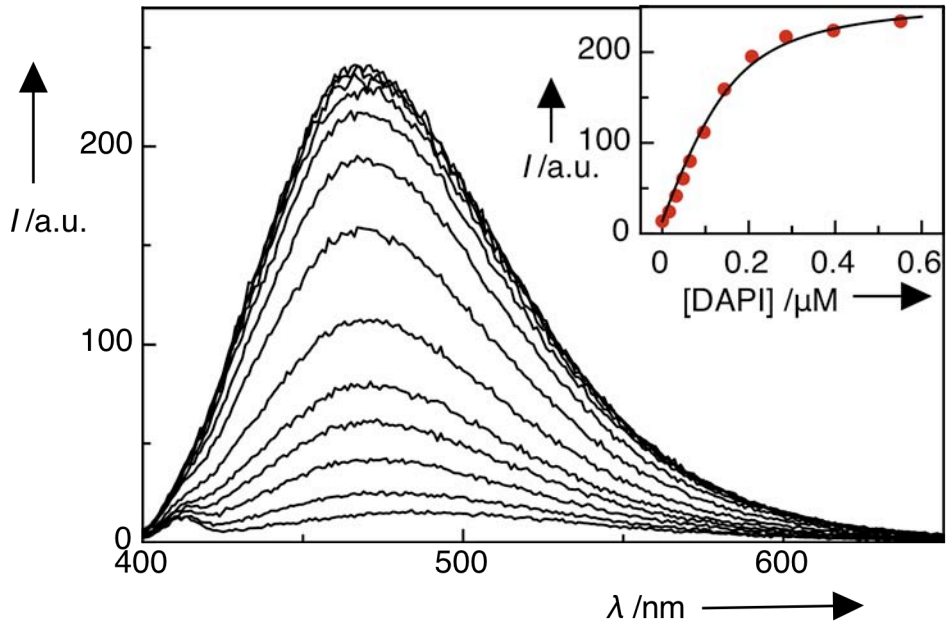

Figure A3–7: Changes in fluorescence intensity and spectra of 0.2 μM DAPI upon addition of successive amount of CB7 pH 3. The data were fitted according to 1:1 complexation (inset).

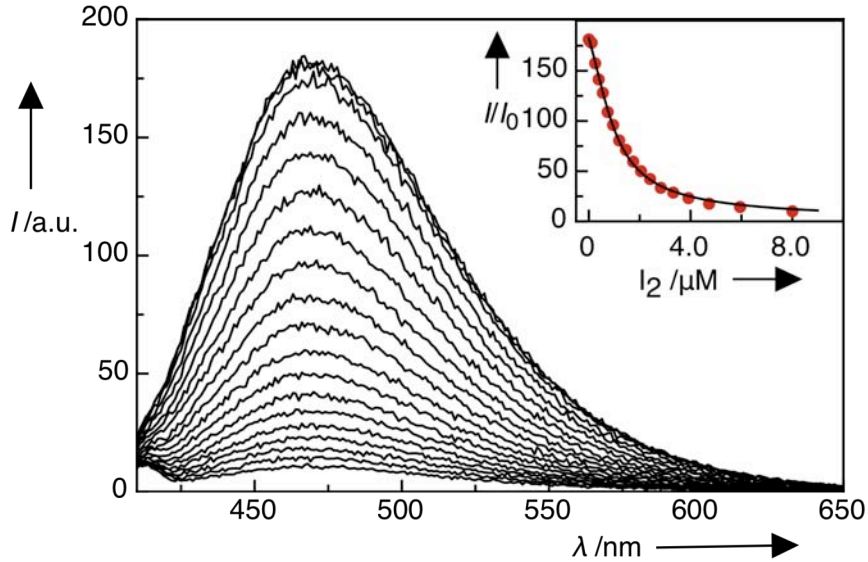

Figure A3–8: Changes in fluorescence intensity and spectra of DAPI/CB7 reporter pair (0.2 μM DAPI, 0.3 μM CB7 λ_{exc} = 361 nm, λ_{em} = 467 nm) upon displacement by I_2 in 50 mM NaOAc pH 5.5. The data were fitted according to 1:1 complexation (inset).

1.6 Supramolecular tandem assays

All the stock solutions required for the enzyme assay, iodide, the fluorescent dye (DAPI), the macrocycle (CB7), hydrogen peroxide, and the required concentrations of the enzyme were prepared as a fresh solutions in 10 mM sodium acetate buffer, pH 5.5 immediately before use. The respective concentrations of the enzyme assay contents except the substrate (iodide) were taken in 1.4 mL quartz cuvettes (Starna, Type 29-F/Q/10 mm) and the fluorescence intensity were recorded to examine the stability of the host-guest fluorescence in presence of the other additives. The actual tandem assay experiment were performed by taking the calculated volumes from the stock solutions in 1.4 mL cuvette and the enzymatic reaction was initiated by the addition of the desired concentration of hydrogen peroxide.

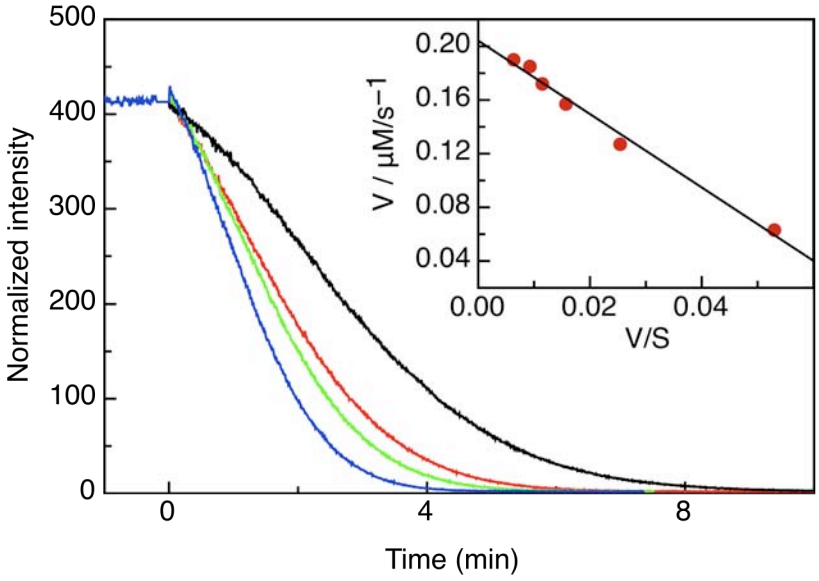

Figure A3–9: Continuous fluorescence enzyme assays for horseradish peroxidase, (in 10 mM NaOAc buffer at pH 5.0). The assays are performed with the CB7/DAPI reporter pair (10 nM enzyme, 60 μM H_2O_2, 0.2 μM DAPI, 0.3 μM CB7, λ_{exc} = 361 nm, λ_{em} = 467 nm). The inset shows the Eadie-Hofstee plot obtained for varying substrate concentrations (10 – 25 μM).

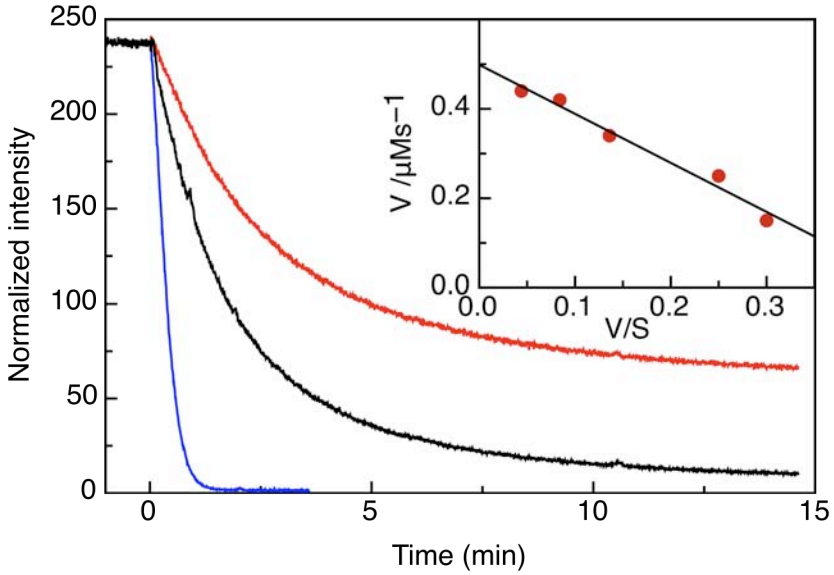

Figure A3–10: Continuous fluorescence enzyme assays for lactoperoxidase (in 10 mM NaOAc buffer at pH 5.0). The assays are performed with the CB7/DAPI reporter pair (2.5 nM enzyme, 75 μM H_2O_2, 0.2 μM DAPI, 0.3 μM CB7, λ_{exc} = 361 nm, λ_{em} = 467 nm). The inset shows the Eadie-Hofstee plot obtained for varying substrate concentrations (1-15 μM).

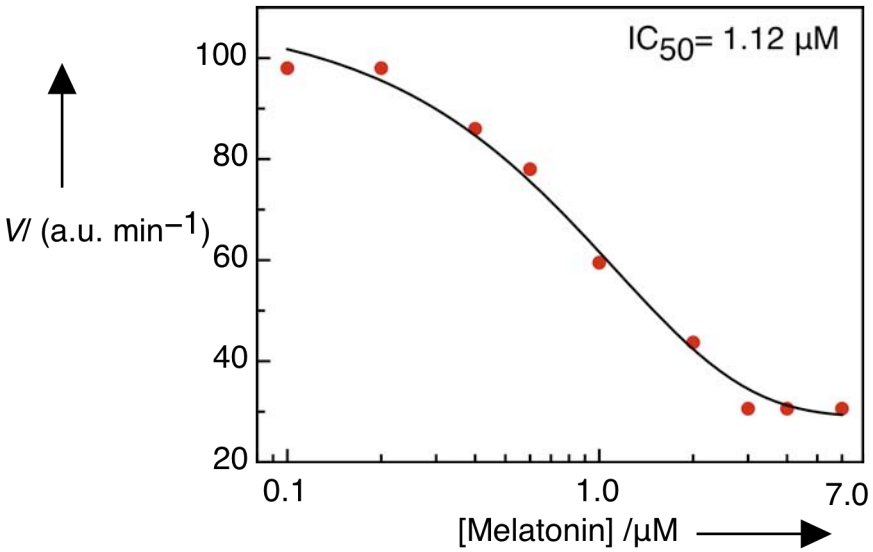

Figure A3–11: Determination of lactoperoxidase inhibition by melatonin at 25 ºC and corresponding dose–response curve. The inhibition was determined in (2.5 nM enzyme, 0.2 μM DAPI, 0.3 μM CB7, and 5 μM I^-) in 50 mM NaOAc, pH 5.5.

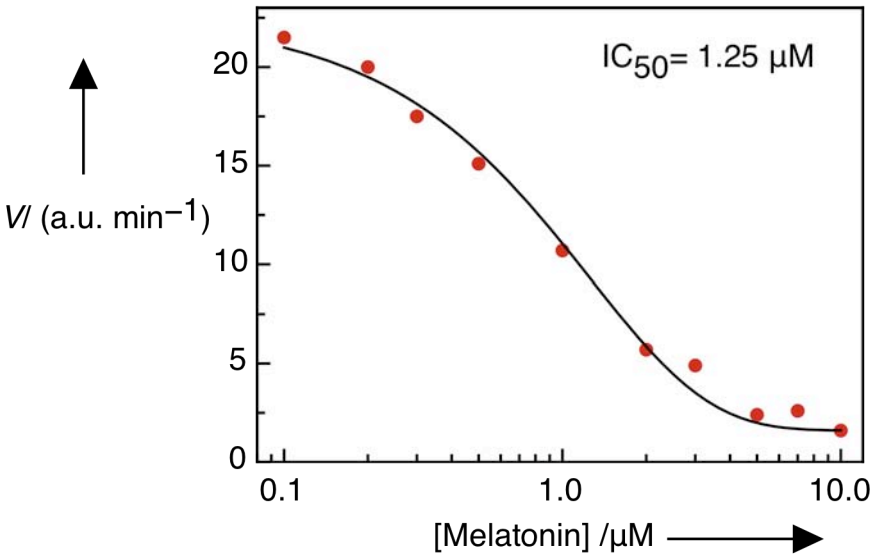

Figure A3–12: Determination of horseradish peroxidase inhibition by melatonin at 25 ºC and corresponding dose–response curve. The inhibition was determined in (10 nM enzyme, 0.2 µM DAPI, 0.3 µM CB7, and 5 µM I^-) in 50 mM NaOAc, pH 5.5.

3. Preparation of Gelrite–CBs•I_2 Hydrogel

Appropriate quantities of gelrite (10 mg) were dispersed in ultrapure deionized water (5 ml) containing 0.1 M Na_2SO_4. The dispersion was heated to 90°C for 20 min while stirring. The hot solution was added to a solution of CBs•I_2 prepared in 0.1 M Na_2SO_4 and the solutions were allowed to cool at room temperature for nearly one hour to obtain the hydrogel.

Table A3–3: Optimized geometry of the axial CB6•I_2 complexes under D_{6h} symmetry

HF= -17345.2966636

MP2=-17352.4890835

Center Number	Atomic Number	Atomic Type	Coordinates (Angstroms) X	Y	Z
1	7	0	1.745080	4.129091	1.225831
2	6	0	0.602017	3.968422	1.955838
3	7	0	-0.442603	4.461612	1.225851
4	6	0	-0.014916	5.091859	0.006843
5	6	0	1.524285	4.857754	0.006808
6	7	0	1.745029	4.129088	-1.212191
7	6	0	0.601949	3.968407	-1.942167
8	7	0	-0.442656	4.461599	-1.212159
9	8	0	0.532343	3.512667	3.091836
10	8	0	0.532249	3.512643	-3.078160
11	6	0	-1.784560	4.559217	-1.746122
12	7	0	-2.703641	3.576635	-1.212104
13	6	0	-3.135940	2.505386	-1.942099
14	7	0	-4.084357	1.847430	-1.212088
15	6	0	-4.416850	2.532336	0.006925
16	6	0	-3.445519	3.749078	0.006926
17	7	0	-2.703597	3.576602	1.225906
18	6	0	-3.135855	2.505341	1.955907
19	7	0	-4.084305	1.847391	1.225934
20	8	0	-2.775283	2.217989	3.091898
21	8	0	-2.775423	2.218047	-3.078110

22	6	0	-4.840549	0.734150	1.759943
23	7	0	-4.449201	-0.553796	1.225914
24	6	0	-4.969431	-1.109623	0.006926
25	6	0	-4.402287	-2.558582	0.006906
26	7	0	-3.642961	-2.613606	1.225886
27	6	0	-3.737850	-1.463042	1.955883
28	7	0	-4.449278	-0.553793	-1.212094
29	6	0	-3.737958	-1.463077	-1.942110
30	7	0	-3.643064	-2.613637	-1.212108
31	8	0	-3.308721	-1.295066	-3.078132
32	8	0	-3.308540	-1.295002	3.091872
33	6	0	-4.840633	0.734200	-1.746076
34	6	0	-3.056027	-3.825011	1.759881
35	7	0	-1.745025	-4.129087	1.225853
36	6	0	-0.601939	-3.968399	1.955819
37	7	0	0.442663	-4.461576	1.225797
38	6	0	0.014943	-5.091833	0.006807
39	6	0	-1.524261	-4.857752	0.006825
40	7	0	0.442635	-4.461570	-1.212191
41	6	0	-0.601984	-3.968389	-1.942186
42	7	0	-1.745053	-4.129081	-1.212194
43	8	0	-0.532224	-3.512658	3.091820
44	8	0	-0.532296	-3.512642	-3.078187
45	6	0	-1.784494	4.559180	1.759893
46	6	0	-3.056078	-3.825008	-1.746169
47	6	0	3.056034	3.824995	-1.746204
48	7	0	3.642950	2.613588	-1.212195
49	6	0	3.737817	1.463010	-1.942174
50	7	0	4.449174	0.553747	-1.212168

51	6	0	4.969379	1.109609	0.006815
52	6	0	4.402227	2.558566	0.006787
53	7	0	3.642956	2.613614	1.225799
54	6	0	3.737884	1.463068	1.955819
55	7	0	4.449249	0.553801	1.225826
56	8	0	3.308636	1.295060	3.091837
57	8	0	3.308517	1.294968	-3.078167
58	6	0	4.840651	-0.734134	1.759840
59	7	0	4.084402	-1.847393	1.225874
60	6	0	4.416916	-2.532317	0.006877
61	6	0	3.445616	-3.749084	0.006899
62	7	0	2.703728	-3.576636	1.225903
63	6	0	3.135980	-2.505368	1.955898
64	7	0	4.084368	-1.847411	-1.212122
65	6	0	3.135945	-2.505387	-1.942108
66	7	0	2.703697	-3.576652	-1.212107
67	8	0	2.775384	-2.218035	-3.078102
68	8	0	2.775427	-2.218014	3.091895
69	6	0	4.840517	-0.734222	-1.746144
70	6	0	1.784676	-4.559247	1.759917
71	6	0	3.056016	3.825023	1.759780
72	6	0	1.784524	-4.559169	-1.746195
73	53	0	0.000010	-0.000005	1.316800
74	53	0	-0.000080	0.000021	-1.383594
75	1	0	-5.798253	0.879039	1.566974
76	1	0	-4.729773	0.717344	2.743938
77	1	0	-0.234035	6.066003	0.006836
78	1	0	-2.021872	-5.723690	0.006829
79	1	0	-3.660903	-4.581522	1.566897

80	1	0	-2.986086	-3.737493	2.743878
81	1	0	-4.729906	0.717409	-2.730077
82	1	0	-5.798327	0.879091	-1.553057
83	1	0	-3.660955	-4.581512	-1.553159
84	1	0	-2.986179	-3.737513	-2.730171
85	1	0	-2.137692	5.461521	1.566914
86	1	0	-1.743646	4.454876	2.743890
87	1	0	-5.135999	-3.235587	0.006920
88	1	0	-5.370065	2.830408	0.006946
89	1	0	-3.945884	4.613141	0.006946
90	1	0	-5.967763	-1.110565	0.006949
91	1	0	-1.743766	4.454925	-2.730123
92	1	0	-2.137731	5.461562	-1.553112
93	1	0	5.798350	-0.879010	1.566832
94	1	0	4.729926	-0.717324	2.743841
95	1	0	2.021900	5.723690	0.006800
96	1	0	0.234078	-6.065974	0.006802
97	1	0	2.137898	-5.461575	1.566922
98	1	0	1.743859	-4.454949	2.743916
99	1	0	4.729762	-0.717446	-2.730142
100	1	0	5.798217	-0.879121	-1.553161
101	1	0	2.137709	-5.461513	-1.553204
102	1	0	1.743699	-4.454869	-2.730194
103	1	0	3.660874	4.581540	1.566760
104	1	0	2.986118	3.737535	2.743782
105	1	0	3.946004	-4.613134	0.006899
106	1	0	5.967711	1.110557	0.006794
107	1	0	5.135936	3.235574	0.006735
108	1	0	5.370138	-2.830364	0.006866

109	1	0	2.986099	3.737474	-2.730201
110	1	0	3.660925	4.581495	-1.553222

Table A3–4: Optimized geometry of the equatorial CB6•I_2 complexes under D_{6h} symmetry

HF=-17345.2750868

MP2=-17352.4891522

Center Number	Atomic Number	Atomic Type	Coordinates (Angstroms) X	Y	Z
1	7	0	4.312494	1.212841	1.218983
2	6	0	3.472718	2.006060	1.949002
3	7	0	3.207035	3.130146	1.219018
4	6	0	3.966055	3.188947	0.000021
5	6	0	4.743682	1.840732	0.000004
6	7	0	4.312508	1.212857	-1.218999
7	6	0	3.472722	2.006082	-1.949000
8	7	0	3.207030	3.130151	-1.218993
9	8	0	3.073649	1.776161	3.084999
10	8	0	3.073653	1.776202	-3.085001
11	6	0	2.445325	4.239353	-1.752996
12	7	0	1.103356	4.343712	-1.218989
13	6	0	-0.002735	4.013996	-1.948979
14	7	0	-1.108642	4.344287	-1.218971
15	6	0	-0.780446	5.032200	0.000025
16	6	0	0.775554	5.031789	0.000006
17	7	0	1.103386	4.343691	1.218997

18	6	0	-0.002696	4.013978	1.949002
19	7	0	-1.108613	4.344286	1.219015
20	8	0	-0.002808	3.552974	3.085000
21	8	0	-0.002861	3.552999	-3.084981
22	6	0	-2.450637	4.240632	1.753021
23	7	0	-3.212929	3.131838	1.219008
24	6	0	-3.971913	3.191046	0.000009
25	6	0	-4.750269	1.843252	-0.000005
26	7	0	-4.319448	1.215123	1.218992
27	6	0	-3.479239	2.007882	1.949015
28	7	0	-3.212914	3.131854	-1.218983
29	6	0	-3.479197	2.007924	-1.948988
30	7	0	-4.319410	1.215147	-1.218989
31	8	0	-3.080247	1.777814	-3.084984
32	8	0	-3.080319	1.777758	3.085018
33	6	0	-2.450674	4.240625	-1.752956
34	6	0	-4.899788	0.001277	1.752974
35	7	0	-4.320125	-1.212883	1.218973
36	6	0	-3.480352	-2.006119	1.948980
37	7	0	-3.214664	-3.130187	1.218971
38	6	0	-3.973676	-3.188961	-0.000032
39	6	0	-4.751304	-1.840747	-0.000022
40	7	0	-3.214657	-3.130165	-1.219031
41	6	0	-3.480341	-2.006082	-1.949020
42	7	0	-4.320118	-1.212861	-1.219003
43	8	0	-3.081295	-1.776232	3.084983
44	8	0	-3.081278	-1.776174	-3.085017
45	6	0	2.445363	4.239315	1.752981
46	6	0	-4.899761	0.001319	-1.752981

47	6	0	4.892177	-0.001300	-1.753001
48	7	0	4.311853	-1.215149	-1.219010
49	6	0	3.471639	-2.007915	-1.949018
50	7	0	3.205341	-3.131847	-1.219021
51	6	0	3.964332	-3.191052	-0.000025
52	6	0	4.742700	-1.843264	-0.000026
53	7	0	4.311876	-1.215139	1.218972
54	6	0	3.471655	-2.007894	1.948985
55	7	0	3.205344	-3.131825	1.218991
56	8	0	3.072716	-1.777782	3.084984
57	8	0	3.072693	-1.777809	-3.085016
58	6	0	2.443043	-4.240618	1.752991
59	7	0	1.101011	-4.344244	1.218997
60	6	0	0.772808	-5.032138	-0.000008
61	6	0	-0.783192	-5.031717	0.000014
62	7	0	-1.110988	-4.343645	1.219029
63	6	0	-0.004884	-4.013956	1.949013
64	7	0	1.100976	-4.344199	-1.218997
65	6	0	-0.004949	-4.013884	-1.948969
66	7	0	-1.111023	-4.343610	-1.218957
67	8	0	-0.004844	-3.552864	-3.084960
68	8	0	-0.004733	-3.552976	3.085021
69	6	0	2.443049	-4.240649	-1.753016
70	6	0	-2.452947	-4.239292	1.753062
71	6	0	4.892214	-0.001295	1.752958
72	6	0	-2.452976	-4.239382	-1.753035
73	53	0	-1.308765	0.000333	-0.000004
74	53	0	1.345807	-0.000385	-0.000001
75	1	0	-2.935417	5.079766	1.560048

76	1	0	-2.394654	4.143596	2.737018
77	1	0	4.590260	3.967783	0.000026
78	1	0	-5.738349	-1.991454	-0.000028
79	1	0	-5.868785	0.001556	1.559965
80	1	0	-4.787801	0.001236	2.736975
81	1	0	-2.394706	4.143598	-2.736955
82	1	0	-2.935459	5.079753	-1.559969
83	1	0	-5.868760	0.001592	-1.559980
84	1	0	-4.787766	0.001303	-2.736981
85	1	0	2.930591	5.078188	1.560001
86	1	0	2.389343	4.142309	2.736979
87	1	0	-5.737229	1.994517	-0.000010
88	1	0	-1.143203	5.962295	0.000042
89	1	0	1.138802	5.961691	0.000011
90	1	0	-4.595706	3.970212	0.000010
91	1	0	2.389301	4.142369	-2.736996
92	1	0	2.930551	5.078224	-1.560003
93	1	0	2.927811	-5.079751	1.559984
94	1	0	2.387067	-4.143605	2.736991
95	1	0	5.730723	1.991464	0.000005
96	1	0	-4.597890	-3.967791	-0.000049
97	1	0	-2.938179	-5.078160	1.560068
98	1	0	-2.396895	-4.142320	2.737061
99	1	0	2.387070	-4.143638	-2.737016
100	1	0	2.927827	-5.079776	-1.560009
101	1	0	-2.938213	-5.078244	-1.560032
102	1	0	-2.396947	-4.142395	-2.737035
103	1	0	5.861213	-0.001575	1.559955
104	1	0	4.780221	-0.001255	2.736959

105	1	0	-1.146447	-5.961617	0.000011
106	1	0	4.588118	-3.970224	-0.000024
107	1	0	5.729658	-1.994539	-0.000029
108	1	0	1.135558	-5.962235	-0.000022
109	1	0	4.780182	-0.001268	-2.737001
110	1	0	5.861177	-0.001555	-1.560000

Table A3–5: Optimized geometry of the axial CB7•I_2 complexes under D_{7h} symmetry

HF= -17940.4954674

MP2=-17948.9434913

Center Number	Atomic Number	Atomic Type	Coordinates (Angstroms) X	Y	Z
1	7	0	1.295291	5.096229	-1.221607
2	6	0	0.983776	5.782898	0.008404
3	6	0	-0.581421	5.837572	0.008416
4	7	0	-0.940508	5.173403	-1.221592
5	6	0	0.166080	4.812986	-1.981614
6	7	0	-0.940489	5.173377	1.238416
7	6	0	0.166110	4.812944	1.998413
8	7	0	1.295310	5.096188	1.238405
9	6	0	-2.270075	5.164605	1.803430
10	7	0	-3.176835	4.190333	1.238443
11	6	0	-3.659331	3.130564	1.998453
12	7	0	-4.630796	2.489987	1.238475
13	6	0	-4.926705	3.184935	0.008475

14	6	0	-3.908025	4.374730	0.008454
15	7	0	-4.630845	2.489985	-1.221535
16	6	0	-3.659410	3.130560	-1.981553
17	7	0	-3.176884	4.190331	-1.221563
18	6	0	-5.452914	1.444674	1.803486
19	7	0	-5.256200	0.129432	1.238476
20	6	0	-4.729335	-0.908110	1.998456
21	7	0	-4.834850	-2.067758	1.238448
22	6	0	-5.561414	-1.865955	0.008458
23	6	0	-5.857384	-0.327864	0.008464
24	7	0	-4.834884	-2.067754	-1.221553
25	6	0	-4.729390	-0.908104	-1.981561
26	7	0	-5.256234	0.129435	-1.221564
27	6	0	-4.529423	-3.363185	1.803437
28	7	0	-3.378593	-4.029117	1.238424
29	6	0	-2.238695	-4.263869	1.998421
30	7	0	-1.397864	-5.069053	1.238414
31	6	0	-2.008532	-5.511413	0.008419
32	6	0	-3.395484	-4.783956	0.008442
33	7	0	-1.397905	-5.069052	-1.221596
34	6	0	-2.238762	-4.263866	-1.981574
35	7	0	-3.378634	-4.029116	-1.221539
36	6	0	-0.195456	-5.637955	1.803408
37	7	0	1.044021	-5.153224	1.238406
38	6	0	1.938584	-4.408482	1.998403
39	7	0	3.091958	-4.252673	1.238406
40	6	0	3.056654	-5.006790	0.008410
41	6	0	1.623262	-5.637735	0.008412
42	7	0	3.091961	-4.252686	-1.221593

43	6	0	1.938590	-4.408502	-1.981591
44	7	0	1.044025	-5.153236	-1.221589
45	6	0	4.286507	-3.668107	1.803408
46	7	0	4.680048	-2.397518	1.238412
47	6	0	4.655377	-1.233379	1.998422
48	7	0	5.253221	-0.234166	1.238421
49	6	0	5.820603	-0.732097	0.008415
50	6	0	5.419523	-2.245864	0.008427
51	7	0	5.253183	-0.234175	-1.221577
52	6	0	4.655315	-1.233393	-1.981552
53	7	0	4.680010	-2.397527	-1.221535
54	6	0	5.540420	1.064593	1.803427
55	7	0	4.792019	2.163942	1.238431
56	6	0	5.134743	2.836617	0.008441
57	6	0	4.201793	4.094515	0.008444
58	7	0	3.458630	3.960349	1.238430
59	6	0	3.867081	2.870373	1.998428
60	7	0	3.458661	3.960377	-1.221562
61	6	0	3.867131	2.870419	-1.981576
62	7	0	4.792041	2.163955	-1.221582
63	8	0	3.522270	2.615249	-3.106580
64	6	0	5.540449	1.064621	-1.786597
65	6	0	2.621801	4.995243	-1.786555
66	6	0	2.621739	4.995182	1.803434
67	8	0	3.522195	2.615182	3.123420
68	8	0	4.240693	-1.123504	3.123425
69	8	0	4.240597	-1.123527	-3.106543
70	6	0	4.286459	-3.668118	-1.786520
71	8	0	1.765315	-4.016023	3.123404

72	8	0	1.765317	-4.016040	-3.106590
73	6	0	-0.195456	-5.637963	-1.786588
74	8	0	-2.038850	-3.884395	3.123422
75	8	0	-2.038954	-3.884391	-3.106581
76	6	0	-4.529491	-3.363195	-1.786511
77	8	0	-4.307595	-0.827442	3.123453
78	8	0	-4.307681	-0.827433	-3.106569
79	6	0	-5.452960	1.444681	-1.786562
80	8	0	-3.332846	2.851668	3.123448
81	8	0	-3.332970	2.851663	-3.106561
82	6	0	-2.270150	5.164604	-1.786590
83	8	0	0.151866	4.384301	3.123415
84	8	0	0.151818	4.384352	-3.106618
85	53	0	-0.000032	0.000032	1.302383
86	53	0	-0.000103	0.000015	-1.398140
87	1	0	-2.710620	6.164786	1.699431
88	1	0	-2.161960	4.916656	2.858430
89	1	0	-6.509462	1.724600	1.699494
90	1	0	-5.191909	1.375510	2.858482
91	1	0	-4.312715	-3.201278	2.858433
92	1	0	-5.407386	-4.014047	1.699436
93	1	0	-0.185842	-5.367390	2.858408
94	1	0	-0.233307	-6.729670	1.699406
95	1	0	5.116285	-4.378317	1.699406
96	1	0	4.080861	-3.491548	2.858406
97	1	0	5.274324	1.013013	2.858423
98	1	0	6.612999	1.270771	1.699451
99	1	0	2.496113	4.755334	2.858429
100	1	0	3.129389	5.962430	1.699453

101	1	0	1.446950	6.777442	0.008406
102	1	0	-0.975297	6.861600	0.008416
103	1	0	-4.396595	5.357634	0.008455
104	1	0	-5.972834	3.515893	0.008486
105	1	0	-6.930150	-0.097445	0.008470
106	1	0	-6.472557	-2.478015	0.008465
107	1	0	-4.244713	-5.478636	0.008440
108	1	0	-2.098557	-6.604822	0.008414
109	1	0	1.636747	-6.734778	0.008422
110	1	0	3.855518	-5.759499	0.008416
111	1	0	6.285963	-2.919232	0.008407
112	1	0	6.906790	-0.576086	0.008393
113	1	0	6.201506	3.095018	0.008465
114	1	0	4.756705	5.040960	0.008455
115	1	0	-2.162068	4.916645	-2.841592
116	1	0	-2.710698	6.164782	-1.682586
117	1	0	-6.509505	1.724606	-1.682544
118	1	0	-5.191980	1.375522	-2.841565
119	1	0	-5.407443	-4.014068	-1.682482
120	1	0	-4.312820	-3.201282	-2.841514
121	1	0	-0.233314	-6.729676	-1.682580
122	1	0	-0.185841	-5.367403	-2.841589
123	1	0	5.116240	-4.378327	-1.682532
124	1	0	4.080794	-3.491561	-2.841515
125	1	0	6.613027	1.270786	-1.682582
126	1	0	5.274370	1.013071	-2.841599
127	1	0	2.496201	4.755434	-2.841561
128	1	0	3.129463	5.962479	-1.682526

Table A3–6: Optimized geometry of the equatorial CB7•I_2 complexes under D_{7h} symmetry

HF=-17940.4916385

MP2=-17948.9492043

Center Number	Atomic Number	Atomic Type	Coordinates (Angstroms) X	Y	Z
1	7	0	5.097118	-1.220826	1.230036
2	6	0	5.560132	-1.816783	0.000020
3	6	0	4.881202	-3.227816	-0.000006
4	7	0	4.126207	-3.236886	1.229997
5	6	0	4.321151	-2.089902	1.990036
6	7	0	4.126195	-3.236835	-1.230001
7	6	0	4.321131	-2.089820	-1.989995
8	7	0	5.097096	-1.220785	-1.229999
9	6	0	3.500242	-4.410855	-1.795011
10	7	0	2.216259	-4.759921	-1.230015
11	6	0	1.054253	-4.694965	-1.990010
12	7	0	0.035283	-5.258019	-1.230008
13	6	0	0.513325	-5.842013	-0.000022
14	6	0	2.040310	-5.493950	-0.000035
15	7	0	0.035316	-5.258068	1.230000
16	6	0	1.054305	-4.695046	1.989998
17	7	0	2.216291	-4.759971	1.229969
18	6	0	-1.272709	-5.500069	-1.795005
19	7	0	-2.345745	-4.714132	-1.229987
20	6	0	-3.019792	-3.765156	-1.989976
21	7	0	-4.094810	-3.319211	-1.229969

22	6	0	-4.254765	-4.057238	0.000021
23	6	0	-3.029714	-5.034174	-0.000003
24	7	0	-4.094790	-3.319247	1.230030
25	6	0	-3.019759	-3.765214	1.990007
26	7	0	-2.345724	-4.714168	1.229979
27	6	0	-5.099856	-2.448257	-1.794960
28	7	0	-5.154926	-1.119260	-1.229961
29	6	0	-4.832995	-0.000247	-1.989971
30	7	0	-5.155043	1.118735	-1.229964
31	6	0	-5.830998	0.782685	0.000047
32	6	0	-5.830904	-0.783315	0.000031
33	7	0	-5.154987	1.118711	1.230033
34	6	0	-4.832904	-0.000286	1.990003
35	7	0	-5.154869	-1.119284	1.229986
36	6	0	-5.100112	2.447736	-1.794968
37	7	0	-4.095158	3.318797	-1.229979
38	6	0	-3.020187	3.764853	-1.989988
39	7	0	-2.346239	4.713901	-1.230002
40	6	0	-3.030247	5.033890	-0.000004
41	6	0	-4.255199	4.056830	0.000017
42	7	0	-2.346237	4.713952	1.230006
43	6	0	-3.020184	3.764934	1.990032
44	7	0	-4.095157	3.318848	1.230043
45	6	0	-1.273285	5.499949	-1.795022
46	7	0	0.034732	5.258038	-1.230025
47	6	0	1.053761	4.695089	-1.990025
48	7	0	2.215759	4.760169	-1.230030
49	6	0	2.039730	5.494180	-0.000040
50	6	0	0.512712	5.842099	-0.000043

51	7	0	2.215769	4.760234	1.229987
52	6	0	1.053776	4.695194	1.989995
53	7	0	0.034741	5.258103	1.229973
54	6	0	3.499780	4.411236	-1.795025
55	7	0	4.125855	3.237283	-1.230012
56	6	0	4.880860	3.228345	-0.000015
57	6	0	5.559953	1.817390	0.000006
58	7	0	5.096998	1.221335	-1.229985
59	6	0	4.320937	2.090263	-1.990005
60	7	0	5.097005	1.221374	1.230018
61	6	0	4.320948	2.090326	1.990015
62	7	0	4.125851	3.237301	1.230004
63	8	0	3.934976	1.903298	3.115019
64	6	0	3.499764	4.411255	1.795006
65	6	0	5.624097	0.000422	1.795036
66	6	0	5.624083	0.000360	-1.794959
67	8	0	3.934957	1.903210	-3.115002
68	8	0	0.958779	4.277058	-3.115015
69	8	0	0.958804	4.277223	3.115008
70	6	0	-1.273271	5.500058	1.794962
71	8	0	-2.753178	3.429854	-3.114986
72	8	0	-2.753163	3.429970	3.115038
73	6	0	-5.100109	2.447807	1.795066
74	8	0	-4.404012	-0.000217	-3.114978
75	8	0	-4.403869	-0.000278	3.114990
76	6	0	-5.099781	-2.448288	1.794968
77	8	0	-2.752815	-3.430143	-3.114978
78	8	0	-2.752754	-3.430221	3.115008
79	6	0	-1.272684	-5.500131	1.794953

80	8	0	0.959233	-4.276962	-3.115007
81	8	0	0.959310	-4.277072	3.115008
82	6	0	3.500280	-4.410928	1.794968
83	8	0	3.935119	-1.902823	-3.114991
84	8	0	3.935151	-1.902953	3.115043
85	53	0	-1.247971	-0.000103	-0.000014
86	53	0	1.445843	0.000025	-0.000034
87	1	0	4.181278	-5.264829	-1.691021
88	1	0	3.331230	-4.198844	-2.850007
89	1	0	-1.515650	-6.565084	-1.691025
90	1	0	-1.212718	-5.236050	-2.850001
91	1	0	-4.855866	-2.330239	-2.849960
92	1	0	-6.084831	-2.922306	-1.690945
93	1	0	-4.856105	2.329742	-2.849967
94	1	0	-6.085138	2.921684	-1.690972
95	1	0	-1.516359	6.564934	-1.691038
96	1	0	-1.213274	5.235932	-2.850018
97	1	0	3.330782	4.199209	-2.850020
98	1	0	4.180731	5.265278	-1.691045
99	1	0	5.353099	0.000317	-2.849963
100	1	0	6.717083	0.000439	-1.690962
101	1	0	6.656134	-1.868742	0.000012
102	1	0	5.605236	-4.052785	-0.000020
103	1	0	2.682356	-6.382917	-0.000058
104	1	0	0.320377	-6.922022	-0.000029
105	1	0	-3.323663	-6.090188	-0.000017
106	1	0	-5.218737	-4.579288	0.000015
107	1	0	-6.840880	-1.212373	0.000059
108	1	0	-6.841024	1.211623	0.000078

109	1	0	-5.219234	4.578763	0.000008
110	1	0	-3.324306	6.089873	-0.000030
111	1	0	0.319647	6.922087	-0.000062
112	1	0	2.681684	6.383213	-0.000057
113	1	0	5.604799	4.053398	-0.000023
114	1	0	6.655949	1.869469	0.000008
115	1	0	3.331277	-4.198958	2.849974
116	1	0	4.181314	-5.264898	1.690939
117	1	0	-1.515634	-6.565141	1.690942
118	1	0	-1.212674	-5.236147	2.849957
119	1	0	-6.084761	-2.922334	1.690982
120	1	0	-4.855754	-2.330282	2.849961
121	1	0	-6.085133	2.921759	1.691070
122	1	0	-4.856090	2.329839	2.850065
123	1	0	-1.516327	6.565043	1.690938
124	1	0	-1.213263	5.236080	2.849968
125	1	0	4.180696	5.265308	1.690991
126	1	0	3.330795	4.199247	2.850010
127	1	0	5.353111	0.000415	2.850040
128	1	0	6.717096	0.000498	1.691025

References

[1] J. Kim, I. S. Jung, S. Y. Kim, E. Lee, J. K. Kang, S. Sakamoto, K. Yamaguchi, K. Kim, *J. Am. Chem. Soc.* **2000**, *122*, 540.

[2] C. Marquez, F. Huang, W. M. Nau, *IEEE Trans. Nanobiosci.* **2004**, *3*, 39.

[3] A. Day, A. P. Arnold, R. J. Blanch, B. Snushall, *J. Org. Chem.* **2001**, *66*, 8094.

[4] J. Kapuscinski, B. Skoczylas, *Nucleic Acids Res.* **1978**, *5*, 3775.

[5] T. Odajima, I. Yamazaki, *Biochim. Biophys. Acta* **1970**, *206*, 71.

[6] M. Morrison, H. B. Hamilton, E. Stotz, *J. Biol. Chem.* **1957**, *228*, 767.
[7] B. C. Saunders, A. G. Holmes-Siedle, B. P. Stark, *Peroxidase, AVersatile Enzyme*, Butterworths: London, **1964**.
[8] D. P. Nelson, L. A. Kiesow, *Anal. Biochem.* **1972**, *49*, 474.
[9] M. J. Frisch, G. W. Trucks, H. B. Schlegel, G. E. Scuseria, M. A. Robb, J. R. Cheeseman, J. A. Montgomery, T. V. Jr., K. N. Kudin, J. C. Burant, J. M. Millam, S. S. Iyengar, J. Tomasi, V. Barone, B. Mennucci, M. Cossi, G. Scalmani, N. Rega, G. A. Petersson, H. Nakatsuji, M. Hada, M. Ehara, K. Toyota, R. Fukuda, J. Hasegawa, M. Ishida, T. Nakajima, Y. Honda, O. Kitao, H. Nakai, M. Klene, X. Li, J. E. Knox, H. P. Hratchian, J. B. Cross, V. Bakken, C. Adamo, J. Jaramillo, R. Gomperts, R. E. Stratmann, O. Yazyev, A. J. Austin, R. Cammi, C. Pomelli, J. W. Ochterski, P. Y. Ayala, K. Morokuma, G. A. Voth, P. Salvador, J. J. Dannenberg, V. G. Zakrzewski, S. Dapprich, A. D. Daniels, M. C. Strain, O. Farkas, D. K. Malick, A. D. Rabuck, K. Raghavachari, J. B. Foresman, J. V. Ortiz, Q. Cui, A. G. Baboul, S. Clifford, J. Cioslowski, B. B. Stefanov, G. Liu, A. Liashenko, P. Piskorz, I. Komaromi, R. L. Martin, D. J. Fox, T. Keith, M. A. Al-Laham, C. Y. Peng, A. Nanayakkara, M. Challacombe, P. M. W. Gill, B. Johnson, W. Chen, M. W. Wong, C. Gonzalez, J. A. Pople, *Gaussian 03 Revision E.01*, Gaussian.

Appendix IV

Curriculum Vitae

Hamdy Saad El–Sheshtawy
School of Engineering and Science
Jacobs University Bremen
Campus Ring 1
D-28759 Bremen
Germany

h.elsheshtawy@jacobs-university.de

Skills

Languages: English: very good in spoken and writing
Arabic: mother tongue
German: basic knowledge

Education

09/2007-09/2009 Master's degree in Nanomolecular Science, September 2009, Jacobs University Bremen, Germany.

01/2001-3/2003 Master's degree in chemistry (with specialization in Physical Chemistry) from South Valley University, Egypt.

09/1994-07/1998 Bachelor's degree in Chemistry.

Instrumental Expertise

Nanosecond time-resolved laser flash photolysis (Applied Photophysics), eximer laser (Lumonics), Nd-YAG laser (Continuum), UV spectrophotometer (JASCO, Carry), fluorescence spectrometer (Perkin Elmer, Cary Eclipse, Edinburgh Instruments), nanosecond & picosecond time-resolved single photon counting spectrometer (IBH, Applied Photophysics, Edinburgh Instruments), CD dichrograph (JASCO), NMR (400 MHz, JEOL), photoreactors (Luzchem).

List of Publication

1- Charge-Transfer Complexes of Mercaptobenzimidazoles with σ- and π - Electron Acceptors, H. M. A. Salman, M. M. Abu-Krisha and H.S. El-Sheshtawy *Can. J. Anal. Sci. Spectrosc.* **2004**, 49, 282-289.

2- Solvent Polarity Affects H Atom Abstractions from C–H Donors, El–Sheshtawy H. S., Pischel U., Nau W. M., *Org. Lett.* **2011**, 13, 2694–2697.

3- Molecular Complexes of Some 2-Mercaptobenzothiazoles with σ- and π-Electron Acceptors, Salman H. M. A., Abu El-Wafa M. H., and El-Sheshtawy H. S., *Can. J. Anal. Sci. Spectrosc*. Submitted.

4- Oxygen Scavenging of Aryl–Substituted Benzyl Radicals, El–Sheshtawy H. S., Nau, W. M., in preparation.

5- Iodine by the Barrel–On the Macrocyclic Recognition of an Element El–Sheshtawy H. S., Bassil B., Gesing T. M., Kortz U., Nau W. M., in preparation.

6- Raman Spectroscopy of Iodine Molecules Trapped in Cucurbiturils, El–Sheshtawy H. S., Donfack P., Materny A., Nau W. M., in preparation.

7- Fluorescence-Based Assay for Monitoring Peroxidase Activity *via* Molecular Iodine Encapsulation by Cucurbit[7]uril, El–Sheshtawy H. S., Nau W. M., in preparation.

List of Attended Conferences

1- A peroxidase Enzyme Assay Based on Molecular Iodine Encapsulation by Cucurbit[*n*]urils, H. El–Sheshtawy, W. M. Nau, IV joint International Symposium on Macrocyclic & Supramolecular Chemistry'', June **2009**, Maastricht, Netherlands.

2- Oxygen Scavenging of Aryl-Substituted Benzyl Radicals, H. El–Sheshtawy, W. M.

Nau, XXIV International Conference on Photochemistry'', July **2009**, Toledo, Spain.

3- Fluorescence-based Assay for Monitoring Peroxidase Activity *via* Molecular Iodine Encapsulation by Cucurbit[7]uril, H. El–Sheshtawy, W. M. Nau, XXIIIrd IUPAC Symposium in Photochemistry, Ferrara, Italy, July **2010**.

4- Fluorescence-based Assay for Monitoring Peroxidase Activity *via* Molecular Iodine Encapsulation by Cucurbit[7]uril, H. El–Sheshtawy, W. M. Nau, 22th Lecture Conference of the GDCh-Division of Photochemistry, Erlangen, Germany, September **2010**.

5- Fluorescence-based Assay for Monitoring Peroxidase Activity *via* Molecular Iodine Encapsulation by Cucurbit[7]uril, H. El–Sheshtawy, W. M. Nau, ICCB 2011, Cambridge, United Kingdom, June **2011**.

Oral Presentation

1- Fluorescence-based Assay for Monitoring Peroxidase Activity *via* Molecular Iodine Encapsulation by Cucurbit[7]uril, H. El–Sheshtawy, W. M. Nau, NanoFun Center and Nanomole Graduate Program Retreat, Schedule, 12–14 January **2011**